Pull Strength Evaluation of Sn-Pb Solder Joints Made to Au-Pt-Pd and Au Thick Film Structures on Low-Temperature Co-Fired Ceramic – Final Report for the MC4652 Crypto-Coded Switch (W80)

Paul T. Vianco, Fernando Uribe, and Gary L. Zender

Sandia National Laboratories

Pull Strength Evaluation of Sn-Pb Solder Joints Made to Au-Pt-Pd and Au Thick Film Structures on Low-Temperature Co-Fired Ceramic – Final Report for the MC4652 Crypto-Coded Switch (W80)

Paul T. Vianco
Microsystem Materials and Mechanical Behavior Department

Fernando Uribe
Thin Film Vacuum and Packaging Department

Gary L. Zender
Materials Characterization Department

Sandia National Laboratories
P.O. Box 5800
Albuquerque, NM 87185

Abstract

A study was performed that examined the microstructure and mechanical properties of 63Sn-37Pb (wt.%, Sn-Pb) solder joints made to thick film layers on low-temperature co-fired (LTCC) substrates. The thick film layers were combinations of the Dupont™ 4596 (Au-Pt-Pd) conductor and Dupont™ 5742 (Au) conductor, the latter having been deposited between the 4596 layer and LTCC substrate. Single (1x) and triple (3x) thicknesses of the 4596 layer were evaluated. Three footprint sizes were evaluated of the 5742 thick film. The solder joints exhibited excellent solderability of both the copper (Cu) lead and thick film surface. In all test sample configurations, the 5742 thick film prevented side wall cracking of the vias. The pull strengths were in the range of 3.4 – 4.0 lbs, which were only slightly lower than historical values for alumina (Al_2O_3) substrates.

General (qualitative) observations: (a) The pull strength was maximized when the total number of thick film layers was between two and three. Fewer that two layers did not develop as strong of a bond at the thick film/LTCC interface; more than three layers and of increased footprint area, developed higher residual stresses at the thick film/LTCC interface and in the underlying LTCC material that weakened the joint. (b) Minimizing the area of the weaker 4596/LTCC interface (e.g., larger 5742 area) improved pull strength. *Specific observations*: (a) In the presence of vias and the need for the 3x 4596 thick film, the preferred 4596:5742 ratio was 1.0:0.5. (b) For those LTCC components that require the 3x 4596 layer, but do not have vias, it is preferred to refrain from using the 5742 layer. (c) In the absence of vias, the highest strength was realized with a 1x thick 5742 layer, a 1x thick 4596 layer, and a footprint ratio of 1.0:1.0.

Acknowledgements

(This page was intentionally left blank)

1. Introduction

The long-term reliability of hybrid microcircuit (HMC) assemblies is determined to a large extent by the integrity of the soldered interconnections. Hybrid microcircuit assemblies use ceramic base materials in place of the traditional, organic laminate-based, printed circuit boards. Instead of a built-up copper (Cu) layer to serve as the conductive traces and solder pads, HMC assemblies utilize either thick film or thin film layers (or, in some cases, a combination of the two layer technologies) to create the conductor paths between resistors, integrated circuits, capacitors, and other components, as well as the bond pads used to solder these components to the ceramic base material. This report addresses an application that used thick film technology. Therefore, a brief introduction below describes thick film conductors.

Thick film traces and solder pads are formed on the ceramic base material by the print-dry-fire process using the thick film paste (or "ink"). The paste is comprised of the conductor metal, the glassy phase that bonds the metal to the ceramic, and thixiotropic additions for printability. The desired pattern of traces and pads is created on the ceramic surface by spreading or printing the thick film paste over a stencil having openings that allow the paste to be deposited on the ceramic with the desired pattern. Then, the assembly is placed through a (low temperature) drying step to remove the volatiles from the paste. Next, the assembly is subjected to the high-temperature firing process. The typical firing temperature is 850°C and time periods range from 5 – 20 min; 15 min is typical for the thick film composition used in this study. During the firing process, which is performed in air, the glassy phase migrates to the conductor metal/ceramic interface where it serves as the "glue" that binds the metal to the ceramic. The metal particles are left behind; they sinter together to form a continuous, albeit porous, conductive layer. Multiple print-dry-fire steps can be used to build up the thickness of the conductor – 1x, 2x or even 3x thickness are routine.

Nuclear weapons applications that utilize thick film HMC components – whether for war reserve (WR) stockpile or for joint test assemblies (JTAs) – have traditionally been constructed with 96% alumina (Al_2O_3) substrate material and the 76Au-21Pt-3Pd (wt.%, abbreviated Au-Pt-Pd) thick film conductor. The Au-Pt-Pd thick film is referred to by its DuPont™ product number, *4596*. This thick film composition was selected for nuclear weapons HMC applications because of its resistance to leaching by the molten solder. Therefore, multiple soldering process cycles can be performed on these components, such as would be required by initial assembly, repair, and rework activities without unacceptable loss of the conductor layer.

The functionality of HMC assemblies can be significantly increased by changing the substrate material from alumina to low-temperature co-fired ceramic (LTCC). The improvement comes about because, like advanced organic laminate circuit board, the LTCC substrate can be constructed with multiple internal layers for the routing of electrical signals between components on either side of the substrate. Vias provide the means for connecting between the different layers and LTCC surfaces. The multi-layer LTCC substrate is built-up by combining layers of "green tape" material that have been patterned to provide the internal conductor layers as well as the via connections between layers. These layers of green tape are then pressed together at high temperatures to form a contiguous structure. The 4596 thick film traces and bond pads are added to the LTCC surfaces by the same print-dry-fire sequence described above. The surface conductors are connected to the internal layers by the via structures.

The Au-Pt-Pd or 4596 thick film technology on LTCC has been successfully evaluated for the HMC assemblies of both WR and JTA applications [1]. However, a defect did appear in those development programs that could potentially detract from the long-term performance of future, more complex LTCC assemblies. The defect was observed when 4596 thick film pads were placed over a filled via. A crack was observed in the LTCC material adjacent to the via side walls as shown by the scanning electron microscopy/secondary electron (SEM/SE) photographs in Fig. 1. Considering that the photographs in Fig. 1 originated from the metallographic cross section of a single plane of the via, the crack actually extended about the circumference of the via.

Subsequent investigations determined that a contributing factor in those cracks was the diffusion of bismuth (Bi) from the glassy phase of the 4596 thick film layer into the vias [2]. A residual stress state contributed the driving force for the fracture. The initiation point of the crack often had a void nearby to it. Also, it was observed that the Au-based via fill material became denser near that point of origin. The cause-and-effect relationship, if any, between Bi diffusion, voids, and via fill material densification, as well as the origin of the residual stress needed to generate the crack, are not completely understood at this time.
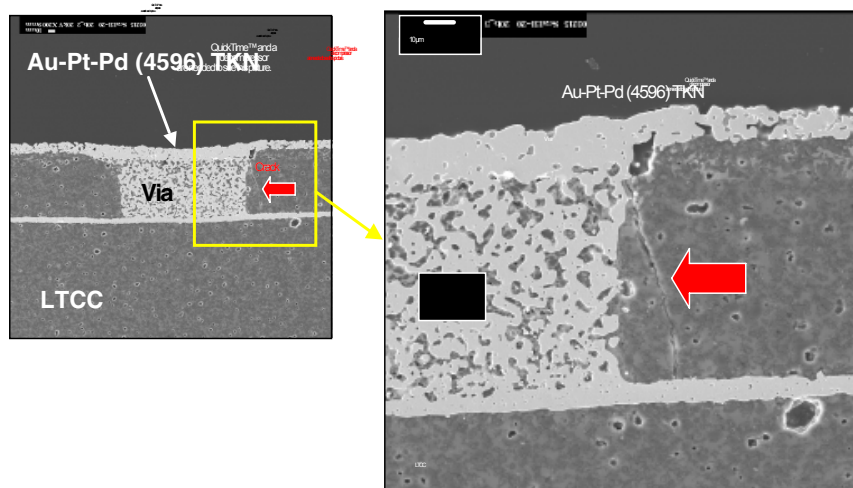
Fig. 1 SEM/SE image of the a crack in the sidewall of a via over which, was deposited Au-Pt-Pd (4596) a thick film pad.

In terms of long-term reliability, the primary concern was not structural failure of the via, per se, but rather, the extension of the crack through nearby internal conductor layers, which would cause an electrical open in the circuitry. The potential for such a scenario is evident even in Fig. 1, given the crack's path an proximity of the internal layer. Therefore, a mitigation strategy was required to eliminate the formation of such cracks.

One such approach was to introduce a second thick film composition between the LTCC substrate (which included the via) and the 4596 thick film. The second layer would serve as a barrier against Bi diffusion into the via material. The selected material was the Au-based thick film designated by its DuPont™ product number as *5742*. This thick film is essentially 100% Au metal component and, as such, could not be used by itself as a pad due to the rapid leaching of Au by Sn-based solders. The cited studies confirmed that the 4596/5742 thick film combination prevented cracks from forming in the via sidewall.

As noted above, the 5742 thick film layer was located between the 4596 layer and the LTCC. Therefore, the 4596 thick film remained as the solderable layer. The presence of the 5742 layer was not expected to affect pad solderability, at least, not directly. On the other hand, it became necessary to determine whether the addition of the 5742 thick film layer impacted the *mechanical strength* of the soldered interconnection on LTCC base material.

A study was undertaken, the objective of which, was to determine the mechanical strength of the soldered interconnections made to pads constructed of 4596 and 5742 thick film layers. The DuPont™ pull test procedure was used to assess the solder joint strength. Several test vehicles were constructed to determine the effect of multiple 4596 print-dry-fire sequences, as well as the role had by the dimensions of the 5742 layer, on the solder joint strength. This report describes the results of the study, which were based upon pull strength (load) and failure mode analyses, the latter having been made using both stereo microscopy (visual inspection) and metallographic cross sections combined with SEM photography.

2. Experimental Procedures

2.1 Test vehicles

The test vehicles were LTCC substrates built from DuPont™ 951AX green tape. A schematic diagram of the LTCC substrate is shown in Fig. 2a. The substrate measured 1.0 x 1.0 x 0.036 in. A total of four (4) green tape layers were used to construct each specimen. Each layer was 0.010 in.; the total layer thickness before firing was 0.040 in. After the green tape layers were pressed and fired to build up the LTCC substrate, a pattern of nine (9) solder pads were placed onto one surface by the print-dry-fire (so-called "post-process") steps. The pads were comprised of combinations of 4596 and 5742 thick films. Each bond pad measured 0.080 x 0.080 in. The 4596 thick film was fired at 850°C. The hold time at temperature was 15 – 20 min. Multiple 4596 layers, as well as the inclusion of the 5742 layer, were deposited by a succession of print-dry-fire cycles. The vias were made with the Au-based Dupont 5738 ink. When there were vias under the bond pad, there were three such vias per pad, arranged in a triangular pattern about the middle of the pad.
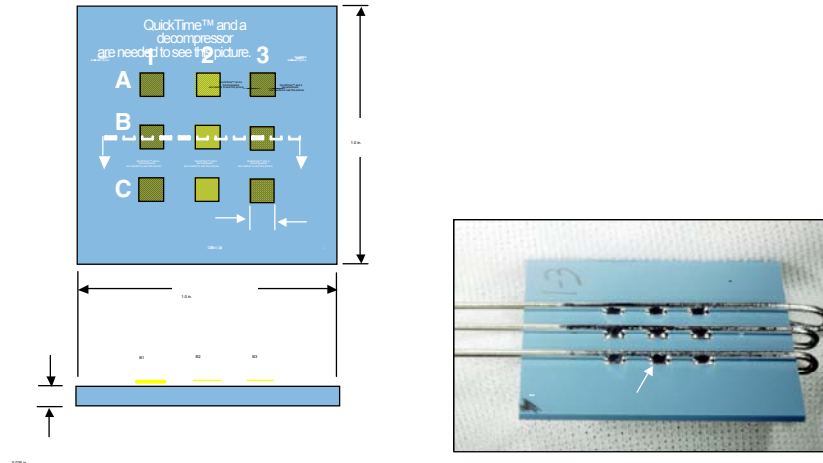
Fig. 2 (a) Schematic diagram showing the geometry of the LTCC pull test substrate. (b) Stereo photograph of the test specimen after soldering, but prior to cutting the leads for pull testing.

The matrix of the thick film layers was comprised of the combinations listed below. Schematic diagrams of the conditions are provided in Fig. 3.

1. Single print-dry-fire (1x), 4596; no vias *(Fig. 3a)*
2. Triple print-dry-fire (3x), 4596; no vias *(Fig. 3a)*
3. **[**Single print-dry-fire (1x), 5742; single print-dry-fire (1x) 4596**]**; no vias; the 5742 and 4596 footprints were of equal area (1.0:1.0); *(Fig. 3b)*
4. **[**Single print-dry-fire (1x), 5742; triple print-dry-fire (3x) 4596**]**; the 5742 and 4596 footprints were of equal area (1.0:1.0); no vias *(Fig. 3b)*

5. Single print-dry-fire (1x), 4596; over vias *(Fig. 3c)*
6. Single print-dry-fire (1x), 5742; over vias *(Fig. 3d)*

In the cases below, the ratio of the 4596 thick film annulus to the 5742 annulus was noted in parentheses: (1.0:1.0), (1.0:0.5), or (1.0:0.2).

7. **(1.0:1.0)[**Single print-dry-fire (1x), 5742; single print-dry-fire (1x), 4596**]**; over vias *(Fig. 3e)*
8. **(1.0:0.5)[**Single print-dry-fire (1x), 5742; single print-dry-fire (1x), 4596**]**; over vias *(Fig. 3f)*
9. **(1.0:0.2)[**Single print-dry-fire (1x), 5742; single print-dry-fire (1x), 4596**]**; over vias *(Fig. 3g)*

10. **(1.0:1.0)[**Single print-dry-fire (1x), 5742; triple print-dry-fire (3x), 4596**]**; over vias *(Fig. 3e)*

11. **(1.0:0.5)[**Single print-dry-fire (1x), 5742; triple print-dry-fire (3x), 4596**]**; over vias *(Fig. 3f)*

12. **(1.0:0.2)[**Single print-dry-fire (1x), 5742; triple print-dry-fire (3x), 4596**]**; over vias *(Fig. 3g)*
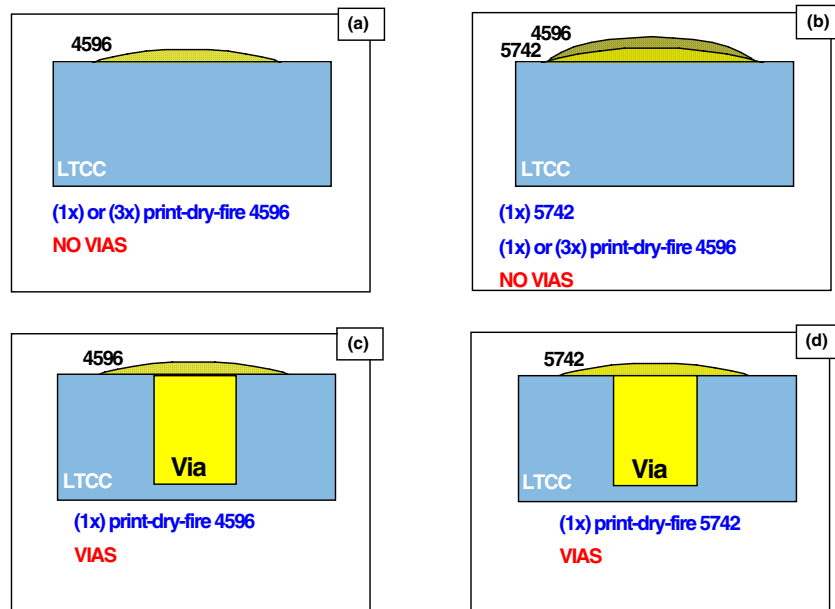
Fig. 3 Schematic diagram showing each of the different 4596 and 5742 thick film combinations and pad geometries. Note that the annular widths defined the ratios of the thick film footprints, which were expressed as (4596/5742):1.0:1.0, 1.0:0.5, and 1.0/0.2. *(con't)*
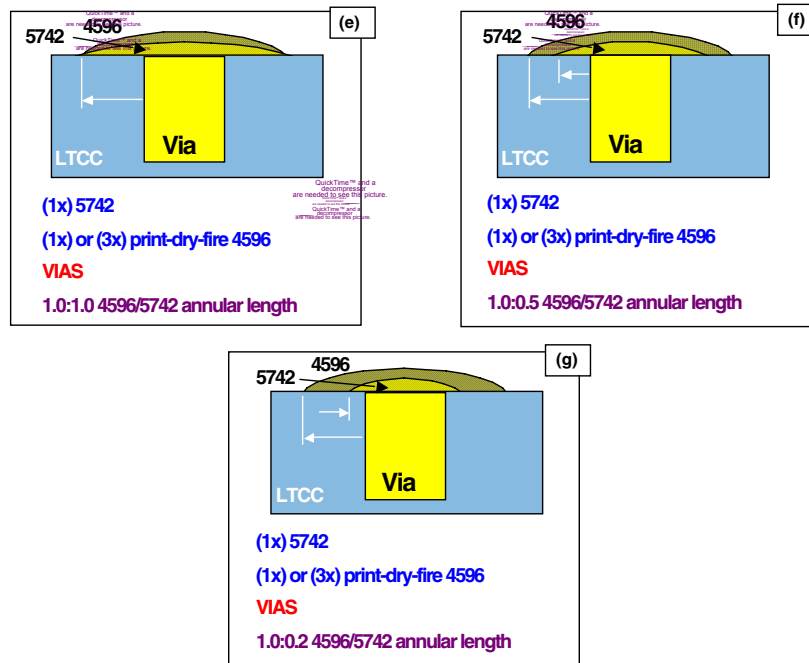
Fig. 3 Schematic diagrams showing the different 4596 and 5742 thick film combinations and pad geometries. Note that the annular widths defined the ratios of the thick film footprints, which were expressed as (4596/5742):1.0:1.0, 1.0:0.5, and 1.0/0.2.

A brief explanation will be made of the twelve (12) conditions of pad geometries. Conditions 1 and 2 established the baseline data for the 4596 thick film on LTCC; the resulting pull strengths could also be compared to historical data. Conditions 3 and 4 determined the performance of the combination of 5742 and 4596 thick film layers in the absence of vias. The conditions 5 and 6 examined the strength of the 5742 and 4596 layers by themselves, when placed over a via, to determine the compatibility of the via with these thick film combinations. The conditions 7 – 9 and 10 – 12 were used to determine the effect of different sizes of the 5742 thick film footprint between the 4596 thick film pad and the via. Two thicknesses of 4596 layer were evaluated: the single 4596 layer designated "1x" (7 – 9) or the triple 4596 layer designated "3x" (10 – 12), the latter having been made by a succession of three print-dry-fire cycles.

2.2 Solder joint fabrication

The 63Sn-37Pb (wt.%) eutectic alloy (Sn-Pb) was used to make all of the solder joints except for the case of the stand-alone 5742 (which will be discussed below). The solder joints were made by the following process. A length of hot-Sn-Pb solder dipped AWG #20 (0.030 in diameter) copper (Cu) wire was located over each of three of the nine

13

bond pads. One end of each wire was clipped and bent around the edge of LTCC plate to secure the length in place. (The bend caused the wire to look like a shepard's hook; hence, the name, "shepard's hook test," came to describe this pull test procedure as well as the more seasoned "Dupont pull test" terminology.) After the three wires had been placed on the LTCC substrate, the solder joint areas were coated with flux and the entire assembly was immersed edge-on into a bath of molten Sn-Pb solder (260°C) and held there 5 s to complete a solder joints. The soldered test specimen appeared as shown in the stereo photograph in Fig. 2b.

The Sn-Pb solder methodology (that is, Cu wire coating and joint) was not used to evaluate the 5742 barrier material by itself (condition #6 above). Due to the rapid dissolution (scavenging) of Au by molten Sn-Pb solder, those joints were made with 50In-50Pb solder. The Cu wires were electroplated with a Ni layer followed by a Au finish. The resulting data did not indicate, a postiori, that the different solder impacted the intrinsic strength behavior of these joints compared to those made with the Sn-Pb alloy.

2.3 Pull test procedure

The shepard's hook and extended length of Cu wire as shown in Fig. 2b were clipped away. The ends of the Cu wires were bent upwards at a sufficient distance away from the pad so as to not disturb that solder joint. A schematic diagram in Fig. 4a shows the geometry of the test specimen at this point. The red arrows show the direction of the pull test load. The test samples were placed into a servo-hydraulic test frame. The substrate was secured to a platen while one end of the up-turned wire was attached to the load frame. Only the A1, A3, B1, B3, C1, and C3 joints were pull tested. The center joints A2, B2, and C2 were *not* tested because prior experiments confirmed that the pull strengths of those center sites deviated from the strengths of the outer pads. The source of that deviation was the distortion of the wire after the first pull tests as well as the fact that the axis of the tension force was significantly displaced relative to the position of the center pads. Therefore, the center joints were reserved for cross section analysis.
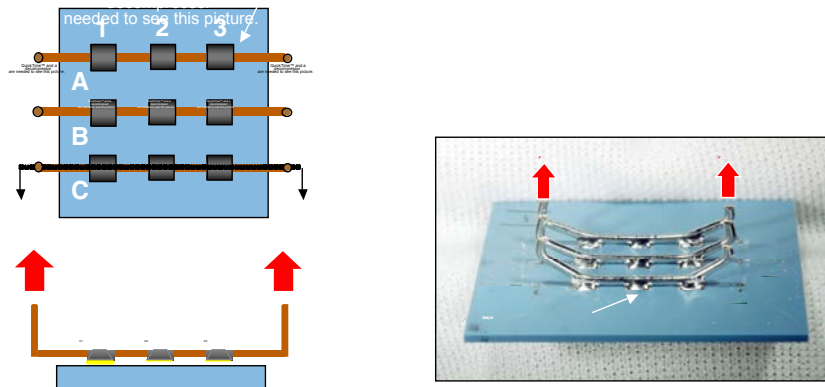
Fig. 4 (a) Schematic diagram showing the configuration of the pull test sample after the shepard's hook and excess length had been clipped away from the Cu wire, followed by bending the leads upwards for the pull test (red arrows). (b) Stereo photograph of the test specimen after the pull test had been performed. The red arrows and "F" indicate the point of application and the direction of the pull load applied by the test frame.

The pull tests were performed at a crosshead speed of 12 mm/min. The pull test was continued until a maximum load had been reached after which, the test was terminated. Therefore, in all cases, a portion of the wire remained attached to the bond pad. The specimen appeared as that shown by the stereo photograph in Fig. 4b. The maximum load was used as the strength metric for each test. Three substrates were tested per condition. The strength values of each of the eighteen (18) tests were combined and represented by a mean value and either ±one standard deviation or a 95% confidence interval. The two error analysis methodologies allowed for a comparison to be made with historical data (standard deviation) and to determine significant trends in the current results (confidence interval).

The first failure mode analysis was performed by *visual inspection*, using a stereo microscope and magnifications in the range of 10 – 20 x. The specific failure modes were established in earlier studies. However, for the present evaluation, the failure mode types were modified to improve the descriptive details, but at the same time, could still be compared with archived results. Schematic diagrams of the failure modes are shown in Fig. 5. The identification of the "front" and "rear" locations of the joint was important in the subsequent failure mode study that was based upon metallographic cross sections of the joint.

15
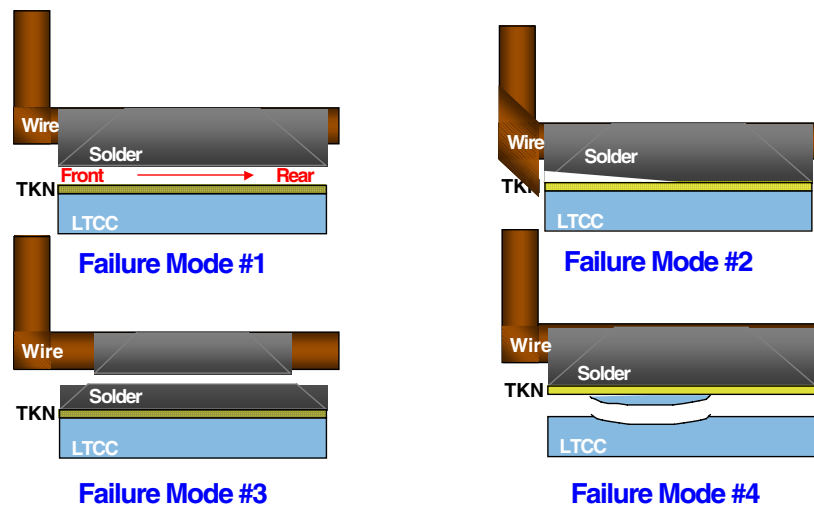
Fig. 5 Schematic diagram showing the failure modes that were determined from *visual inspection* of the pull test sites. In the failure mode analysis based on metallographic cross sections, the front and rear locations of the joints were considered.

A description of each failure modes is as follows:

Failure mode #1: The solder separates completely from the thick film and substrate. This failure mode description does not make a provision of whether that actual fracture path occurs (a) at the solder/IMC interface, (b) within the intermetallic compound (IMC) layer, or (c) the IMC layer/thick film interface. Each of these potential fracture sites are generally indistinguishable from one-another under visual inspection.

Failure mode #2: The solder pad partially pulls off of the substrate. This case differs from that of #1 because of the absence of complete separation between the solder and the bond pad. As such, it was presumed that this failure mode indicated a less brittle joint vis-à-vis case #1. Unfortunately, the extent of this failure mode may be affected by the point at which, the test is halted after maximum load has been achieved.

Failure mode #3: The wire separates from the solder fillet. Separation typically occurs within the solder material; but, it may also include failure along the solder/Cu wire interface.

Failure mode #4: The thick film pad separates from the substrate; there may also be a "divot" of LTCC material removed from the substrate. This failure mode is distinguished by separation of the thick film layer from the LTCC base material. The appearance of the blue LTCC material is an indication of this failure mode. Often, the divot of LTCC material can also be detected, but not always, particularly if it is very shallow.

The visual inspection and failure mode analysis were limited to the front of the joint, which was underneath the bend in the wire. Thus, it was expected that the observed failure mode would most likely correlate to the maximum strength. The extent of the bond line that constituted the "front" of the joint was estimated to be 60% of the distance from the front edge. This premise will be used later to discuss the failure modes as determined by metallographic cross sections.

It was often the case that more than one failure mode occurred at a pull test site. Therefore, a quantitative metric was established to include all of the failure modes that were recorded for each specimen. The metric was determined as follows: There were eighteen pull tests per thick film configuration (Fig. 3). The *absence* or *presence* of any one of the four failure modes was recorded as a "0" or "1", respectively, for each pull tested site. No attempt was made to determine the fraction of the fracture surface that was represented by each failure mode, due to the limited view offered by visual inspection. A percentage of the eighteen test sites having a particular failure mode (#1, #2, #3, or #4) was calculated from the inspection results. Because *more than one failure mode* could be present, the modes were not mutually exclusive so that the sum of the percentages did not necessarily equal to 100%.

Upon completion of the visual inspection, one of the three substrates was designated for metallographic cross section analysis. The row of solder joints designated A1 (pull tested, A2 *(untested)*, and A3 (pull tested) was cross sectioned along the centerline of the pad dimensions. The potential failure modes that could be observed in the metallographic cross sections are listed here:

1. *Solder/thick film interface*. Whenever possible, it was noted whether the failure occurred in the IMC layer, solder/IMC, or IMC/thick film interfaces. However, these details were not included, explicitly, in the metric.
2. *Thick film /LTCC interface*. Here, it was noted whether the fracture path occurred in the glassy phase.

3. *Bulk solder*. This failure mode included fracture within the solder as well as at the solder/Cu lead interface.

4. *LTCC divot*. Fracture occurred in the LTCC base material, producing a divot of LTCC material.

5. *Bulk thick film failure*. Fracture took place within the thick film layer, itself.

The quantitative analysis of the cross section failure modes was different from that used with the visual inspection. The percentage of each failure mode was recorded for the bond line in the plane of the solder joint cross section. Moreover, the failure modes were listed as the percentage of the total bond line, from the front to the rear of the joint.

The objective of the visual inspection and cross section failure mode analysis was to provide quantitative metrics, which together with the pull strength values, could be used to distinguish the performances of the candidate thick film configurations. Those distinctions were then used to, not only establish recommendations for the engineering applications of LTCC technology, but to also gain further insight into the behavior of these rather complex materials systems.

3. Results and Discussion

3.1 As-fabricated microstructures

As noted above, metallographic cross sections were made of a row of three solder joints, two which had been pull tested and a third that went untested. The untested interconnections will be examined at this time. Shown in Fig. 6 is an SEM/SE photograph of the solder joint made to the single print of the 4596 thick film. The low-magnification image in Fig. 6 (a) showed the entire solder joint. The extent of void formation was not unexpected. There were no indications of large-scale cracking in the LTCC under the solder joint. The SEM/SE photograph in Fig. 6 (b) showed the sound integrity of the solder/thick film and thick film/LTCC interfaces with no evidence of separation. As indicated in the photograph, the glassy phase from the thick film ink infiltrated the near-interface region of the LTCC base material. There was no evidence of cracking of either the thick film or LTCC materials. The single print of 4596 thick film measured approximately 8 – 10 µm thick. The solder/thick film interface was shown at higher magnification in Fig. 6 (c). Here, too, there was no evidence of cracks or other defects.

It was interesting to note in Fig. 6 (c) that, because the Sn-Pb solder polished away faster than did the thick film, it was possible to see the top surface of the thick film to which the solder had wetted. The morphology of large, interconnected pores was very similar to that observed in cross section plane of the layer.
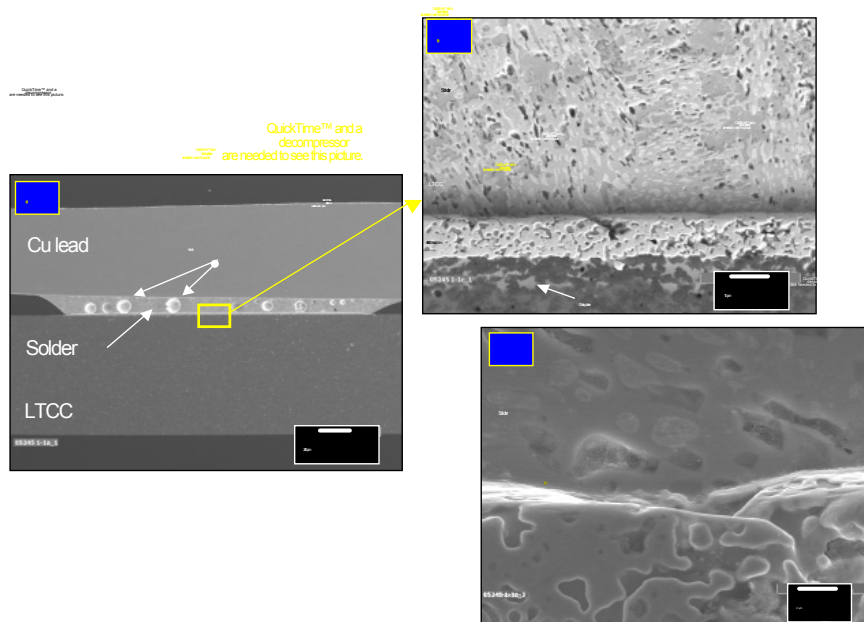
Fig. 6 SEM/SE images of the untested solder joint fabricated with the single print (1x) of 4596 thick film (no vias): (a), low magnification view of the entire interconnection; (b) medium magnification showing the solder joint gap; and (c) a high magnification image of the solder/thick film interface.

Similar observations were also compiled from the cross sections of the triple printed (3x) 4596 thick film. Of course, the 3x 4596 layer was significantly thicker at approximately 20 – 25 µm. Also, because the firing process sintered both the newly deposited thick film print *and* the previously deposited layer, the post-fired thickness was less than three-times the thickness of the single thick film layer.

Shown in Fig. 7 are SEM/SE photographs of the cross sections of the In-Pb solder joint made between the Au-Ni-coated Cu lead and the 5742 thick film layer. No via was present in these joints. The 5742 thick film was considerably denser than the 4596 thick film layer depicted in Fig. 6. This higher density resulted from two factors: (1) the pure Au composition allowed for a more complete sintering of the metal component during the firing process and (2) minimal porosity resulting from the migration of the

5742 glassy phase to the thick film/LTCC interface. A fuller density is typically not realized with the 4596 composition because the considerably higher melting temperature of the Pt component prevents complete sintering of the metal component. (It is the Pt component of the 4596 thick film that is largely responsible for its improved resistance to dissolution or "leaching" by the molten Sn-Pb solder.) Also, it has been observed that the glassy phase does not completely migrate to the thick film/LTCC interface, due either to inherently slow diffusion kinetics or simply because there is an excess quantity of the glassy phase.
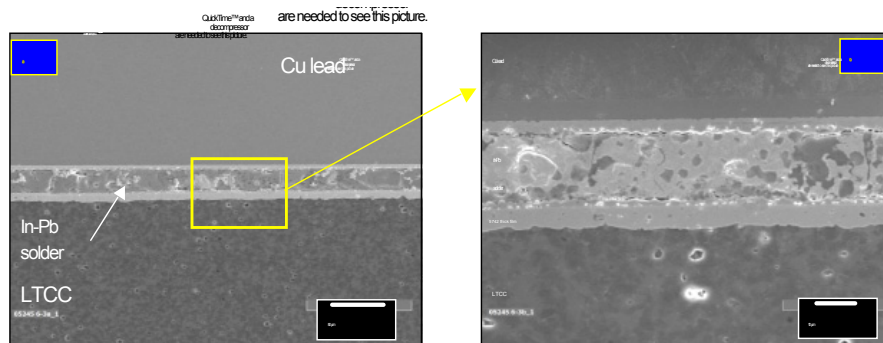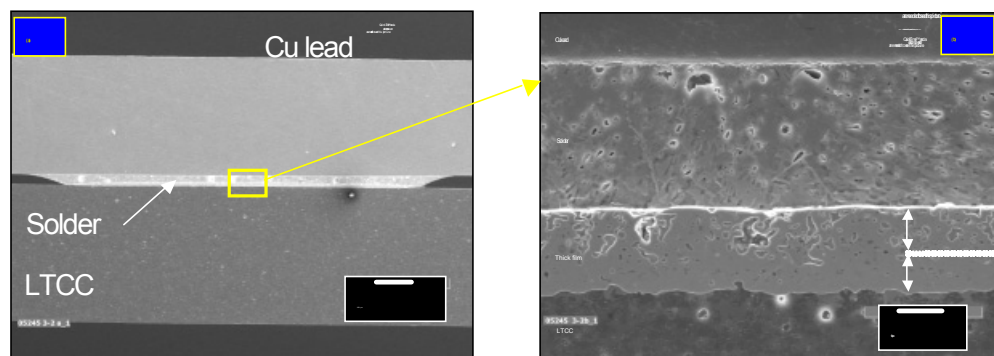

Fig. 7 SEM/SE images of the untested solder joint fabricated with a single print of the 5742 thick film. This area was away from the via: **(a)**, low magnification view of the interconnection; **(b)** a high magnification image of the solder joint gap region.

A close examination was made of the interface between the 5742 thick film and LTCC base material. There were no indications of delamination or cracking along that interface nor within the neighboring LTCC base material. Also, there was no recognizable diffusion of a glassy phase into the LTCC microstructure, which was clearly in contrast to the 1x 4596 layer shown in Fig. 6 **(b)**. The absence of such diffusion may be due to a more limit quantity of glassy phase in the thick film or its inherent lack of diffusivity into the LTCC. It should be noted that the In-Pb solder microstructure appeared to be damaged. The poor appearance was due in large part to the metallographic techniques. First of all, the soft In-Pb alloy is inherently very difficult to polish. Second, the metallographic preparation procedures were conducted to optimize the interface microstructures associated with the 5742 thick film. The trade-off was damage to the In-Pb microstructure.

Next, the metallographic cross sections were examined, which were obtained from the test specimen having single layers of both the 4596 and 5742 thick film layers on the LTCC base material. Vias were not present in these joints. The footprints of both the 5742 and 4596 thick films were equal to one-another, that is, the 4596:5742 ratio was 1.0:1.0. The SEM/SE photographs of the Sn-Pb solder joints were shown in Fig. 8. Fewer voids were observed in the solder (Fig. 8 (a)). The two thick film layers could be distinguished in Fig. 8 (b) by the different layer densities. The 5742 layer was considerably denser (as was noted above) than the 4596 layer over it. It was observed in Fig. 8 (b) that there was an absence of glassy phase in the LTCC. This observation was important because it indicated that the 5742 layer served as an effective barrier to the diffusion of the glassy phase components (and other constituents) from the 4596 layer into the LTCC. There were no indications of delamination between the two thick films or at the 5742/LTCC interface.

Fig. 8 SEM/SE images of the untested solder joint fabricated with single prints of both the 4596 and 5742 thick films. No vias were present in the LTCC: (a), low magnification view of the entire interconnection and (b) a high magnification image of the solder joint gap region and thick film layers.

The above analysis, which referred to Figs. 6 – 8, established the integrity of the solder joints made with single prints of 5742 or 4596 thick films as well as the combination of the two layers, together. Next, the role of the via was examined. Shown in Fig. 9 is the case of a single layer of the 4596 over a via.

(a)

(b)
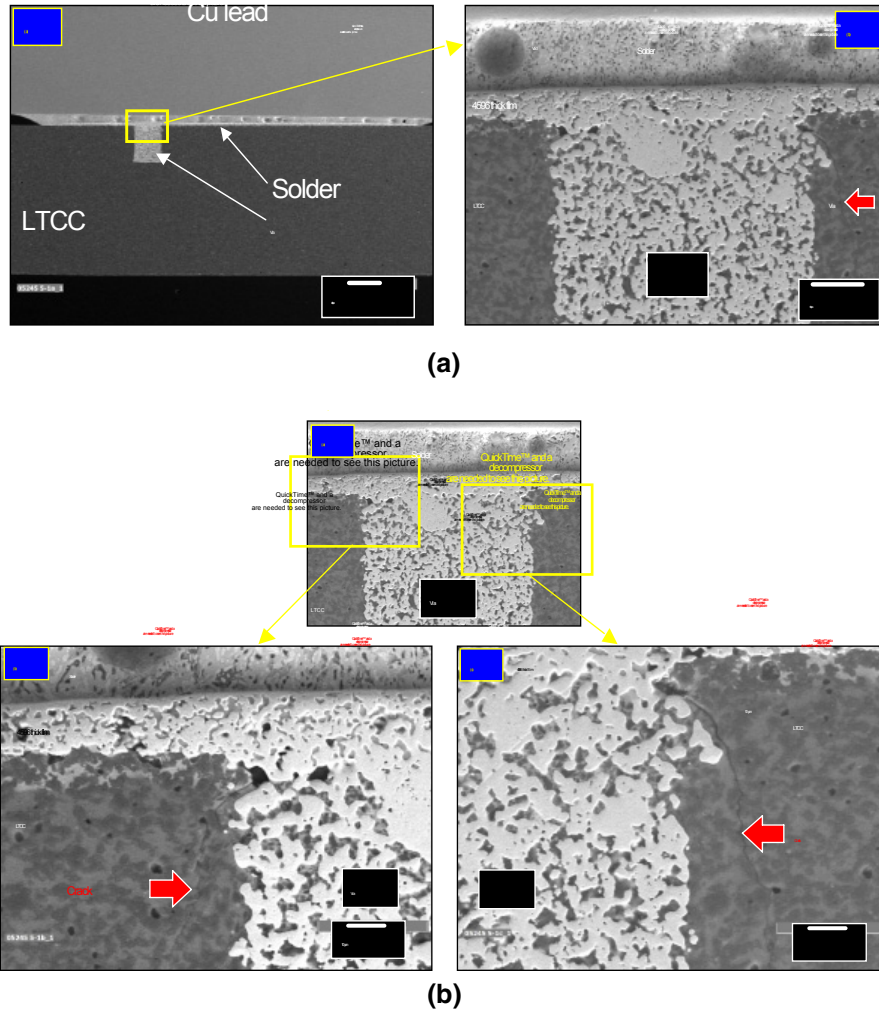
Fig. 9 SEM/SE images of the untested solder joint fabricated with a single print (1x) of the 4596 thick film over a via: (a) **(a)** Low magnification image of the solder joint. **(b)** Medium magnification photographs showing the via and the solder joint above it. The red arrow indicated the location of the side wall crack. (b) **(a)** Repeated low magnification image of the via identifying the side wall locations that were viewed at higher magnification in **(b)** and **(c)** and that show more clearly the side wall cracks.

The SEM/SE photographs in Figs. 9a confirmed the good integrity of the Sn-Pb solder joint at low magnification (Fig. 9a **(a)**). There was no evidence that the via affected the microstructure of the solder as shown in Fig. 9a **(b)**. Voids were observed in the solder (Fig. 9a **(a)**); but, they were not of a degree that was considered excessive or unexpected for this geometry.

Side wall cracking was evident in Fig. 9, beginning with the photograph in Fig. 9a (b) (red arrow). The cracks were more clearly visible in the images in Fig. 9b. The crack segments, which in fact represented a crack that extended around the entire circumference of the via, appeared to have initiated at small voids between the via-fill material and the LTCC side wall. The cracks then propagated into the LTCC, appearing to follow a path through the glassy matrix phase of the LTCC. Aside from the side wall cracks, there was no other damage observed in the joint structure.

The test specimen having the single print (1x) of the 5742 thick film was examined more closely where the layer passed over a via to confirm that it, by itself, did not create cracks in the side walls. Shown in Fig. 10 (a) is a low magnification SEM/SE photograph of the In-Pb solder/5742 thick film joint over a via. The medium magnification image in Fig. 10 (b) confirmed the absence of side wall cracks in the LTCC base material. The photograph in Fig. 10 (c) showed the excellent integrity of the 5742 thick film/LTCC interface away from the via. Again, the glassy phase of the 5742 was not apparent in the near interface microstructure of the LTCC material.

The next sample to be evaluated had the 1x 5742 and 1x 4596 thick films over vias in the LTCC base material. The corresponding SEM/SE photographs were shown in Fig. 11. These samples had the 4596:5742 ratio of 1.0:1.0. Shown in Fig. 11a (a) is a low magnification view of the solder joint. Two locations were examined, one at a distance away from the via and a second location directly over the via. The solder joint at a distance from the via is shown in Fig. 11a (b). Excellent integrity was observed at the 4596/5742 interface. There were no specific markings that distinguished the boundary between the two thick films; rather, that delineation was made, based upon the different layer densities. Likewise, the solder/4596 and 5742/LTCC interfaces exhibited no indications of crack development.
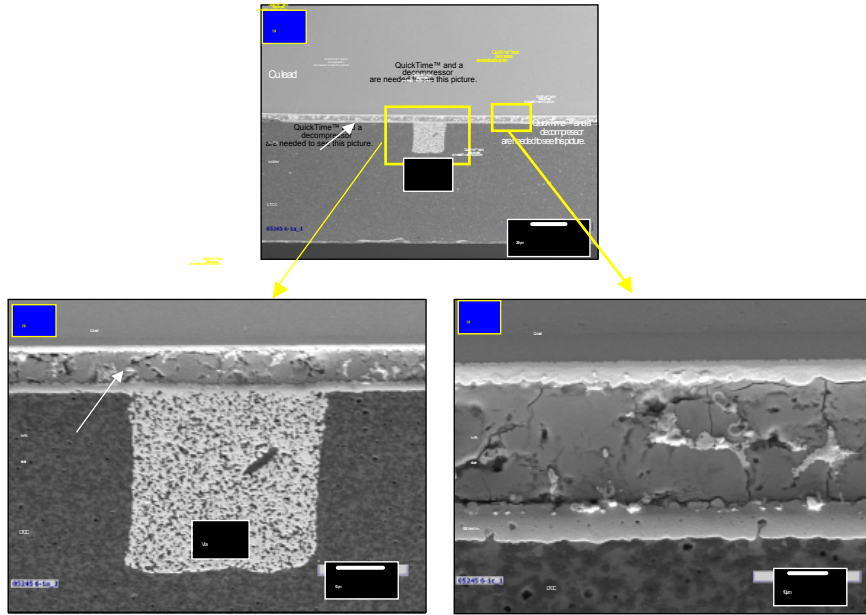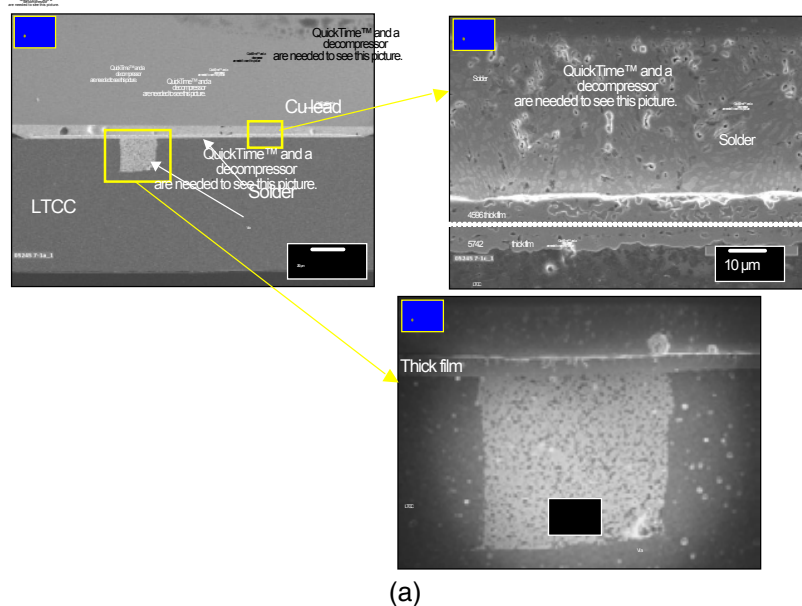
Fig. 10 SEM/SE images of the untested 50In-50Pb solder/5742 thick film joint over a via. **(a)** Low magnification photograph showing the overall solder joint; **(b)** Medium magnification of the solder joint over the via structure. Side wall cracks were absent from around the via. **(c)** High magnification photograph showing the excellent integrity of the solder/thick film and thick film/LTCC interfaces away from the via.

The region of the LTCC underneath the composite thick film layer was examined for crack damage; none was observed. The extent of glassy phase was evaluated, which would have originated from the 4596 thick film, and then breached the 5742 layer to diffuse into the LTCC base material. Only a very few, isolated locations were observed at which the 4596 glassy phase had penetrated to the LTCC. Such areas were not entirely unexpected. Although the 5742 thick film produced a denser layer vis-à-vis the 4596 thick film, it was not 100% dense. Therefore, there was a likelihood that some of the 4596 glassy phase would have reached the underlying LTCC base material.

The SEM/SE photograph in Fig. 11a **(c)** showed that side wall cracking was absent from around the via. The observation was further substantiated through the higher magnification photographs provided in Fig. 11b that examined, specifically, the side wall regions of the LTCC. The 4596 glassy phase, as well as voids that have appeared at the via-fill/LTCC wall interface and suspected to play a role in the initiation of sidewall cracks, were not observed in Fig. 11b.

(a)

Fig. 11 SEM/SE images of the untested solder joint fabricated from single prints of both 4596 and 5742 thick films over a via. The ratio of 4596/5742 was equal to 1.0:1.0: (a) **(a)** Low magnification photograph of the overall solder joint. **(b)** High magnification photograph showing the solder, thick film, LTCC, and interface structures at a location away from the via. **(c)** Low magnification photograph of the via and solder joint directly above the via. *(con't)*
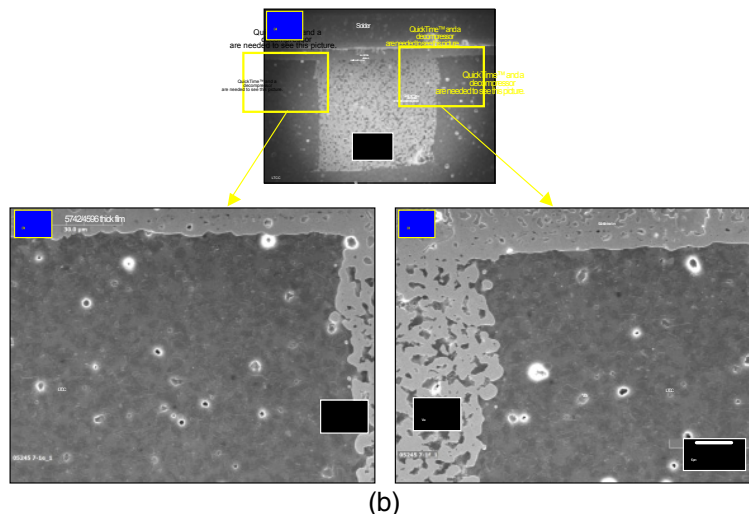
(b)

Fig. 11 SEM/SE images of the untested solder joint fabricated from single prints of both 4596 and 5742 thick films over a via. The ratio of 4596/5742 was equal to 1.0:1.0: (b) **(a)** Low magnification photograph of the via, identifying the side wall locations that were examined at higher magnification in **(b)** and **(c)**. The latter photographs confirmed the absence of side wall cracks around the via.

Lastly, a comparison was conducted of solder joints that were documented by the low magnification SEM/SE images presented in Figs. 6 – 11, that is, joints either with or without vias. There did not appear to be a correlation between the location of voids in the solder joint (gap) and the position of the via. Also, the morphology of the voids did not provide conclusive evidence that their source was the thick film layer. Therefore, it was more likely that the voids were caused by flux volatization during the soldering process. Additional evidence to this effect was that the thicker gap in Fig. 6 also had the greater propensity for void development. Void formation did not appear to be a function of the stack-up of the thick film layer.

The next sample configuration was that in which, the footprint of the 1x 5742 thick film had one-half the annular radius of the 1x 4596 layer. That is the case of the 4596/5742 ratio of 1.0:0.5 (Fig. 3f). Shown in Fig. 12a (a) is a low magnification, SEM/SE photograph of the untested solder joint. There appeared to be more voids in this solder joint than the previous cases. As in previous instances, the voids were not correlated to the position of the via. The greater propensity for voids was likely due to the wider gap coupled with flux volatization. There was no reason to believe that the ratio of 4596/5742 equal to1.0:0.5 would have explicitly caused a greater propensity for voids in the solder. The extent of void development would not have impacted the physical or mechanical functionality of the joint.
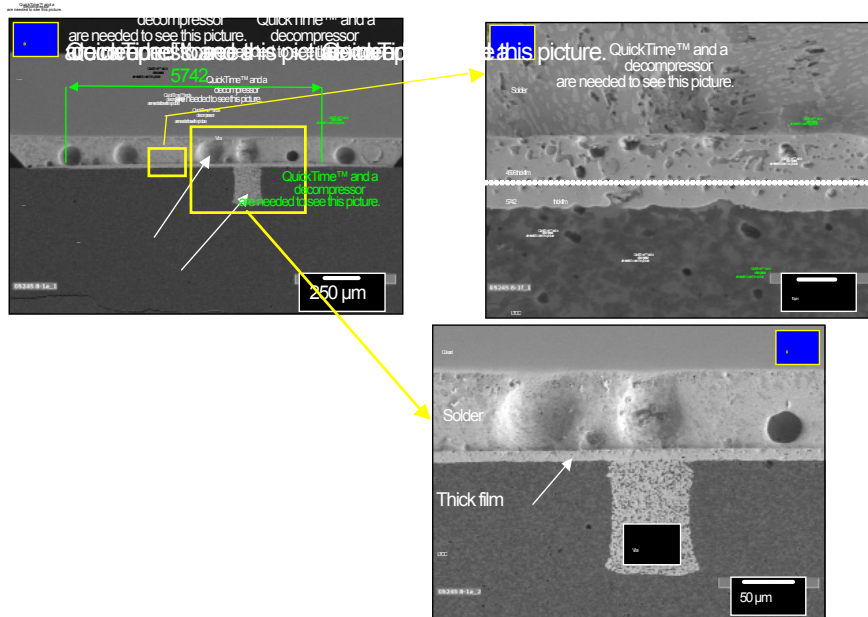
(a)

Fig. 12 SEM/SE images of the untested solder joint fabricated from single prints of both 4596 and 5742 thick films over a via and at a 4596/5742 ratio equal to1.0:0.5: (a) The image (a) is a low magnification SEM/SE photograph of the solder joint signifying the via location and a location away from the via that were subsequently evaluated. The green line shows the extent of the 5742 layer under the 4596 thick film. (b) Photograph of the solder, thick film, LTCC, and associated interface structures at the location away from the via. The dotted line shows the approximate demarcation between the 4596 and 5742 layers. (c) Low magnification view of the via and solder joint above it. *(con't)*
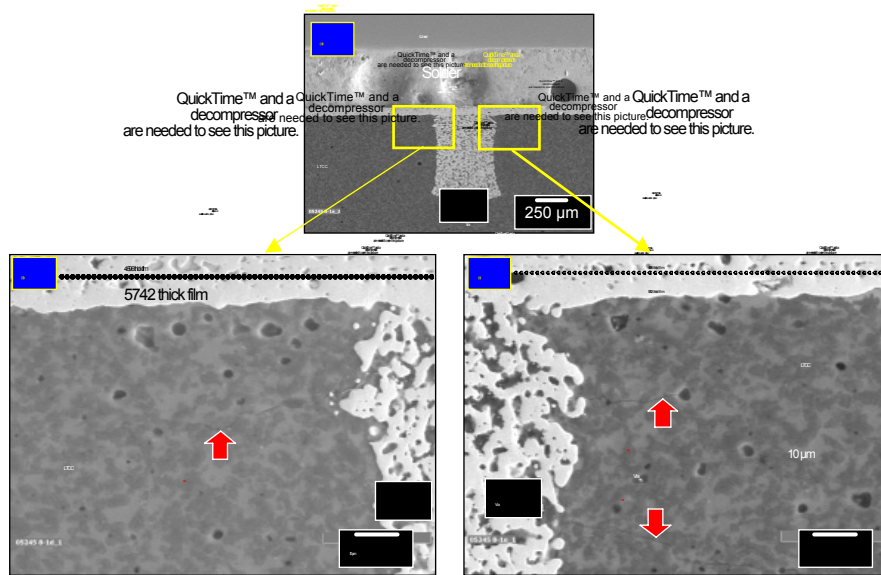
(b)

(c)

Fig. 12 SEM/SE images of the untested solder joint fabricated from single prints of both 4596 and 5742 thick films over a via and at a 4596/5742 ratio equal to1.0:0.5: (b) (a) Low magnification view of the via, identifying the side wall locations that were examined at higher magnification in (b) and (c). The red arrows indicate horizontal cracks in the LTCC. (c) The photograph in (a) was a repeat, low magnification view of the via used to identify the location examined in (b) at higher magnification that shows horizontal cracks in the LTCC material next to the via. *(con't)*
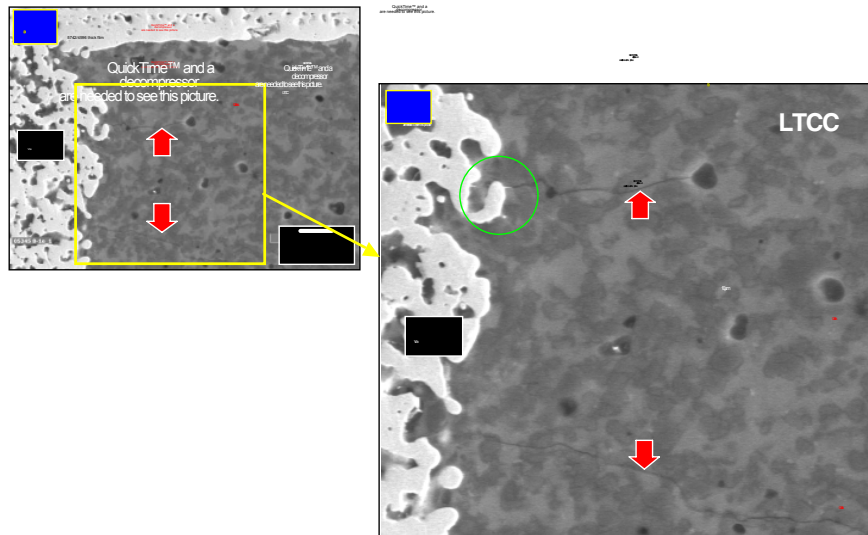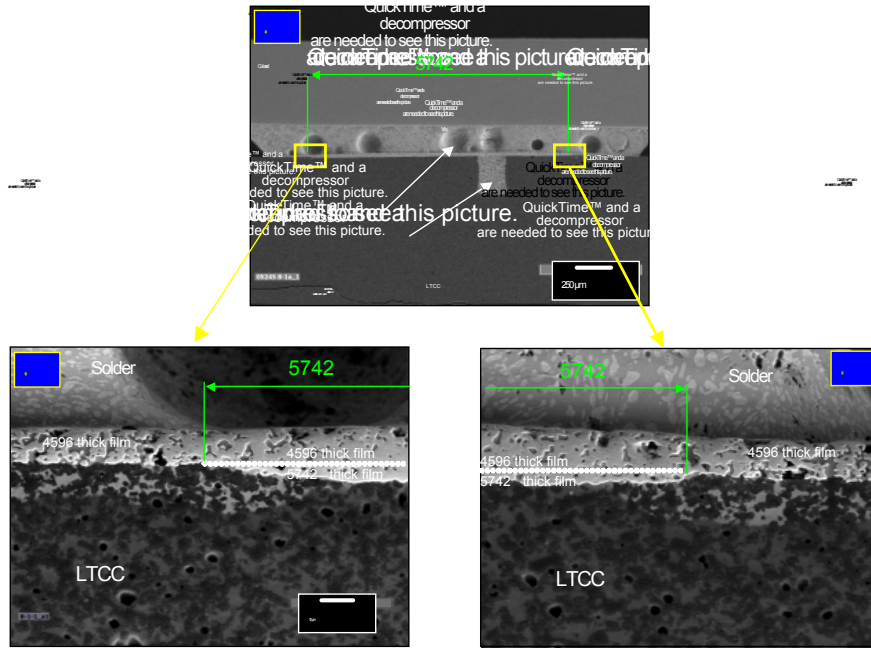
(d)

Fig. 12 SEM/SE images of the untested solder joint fabricated from single prints of both 4596 and 5742 thick films over a via and at a 4596/5742 ratio equal to1.0:0.5: (d) The image (a) shows the location of the terminations of the 5742 layer to either side of the via. (b) and (c) are high magnification images of the end boundaries of the 5742 layer.

The green lines indicated the boundaries of the 5742 layer. Two additional observations were worth noting. First, the 5742 layer was not centered precisely under the 4596 thick film. This offset was caused by the limits in alignment capability of the sample fabrication process. Secondly, the via was not centered under either pad. That via was one of three vias that formed a triangle. The center of the triangle was located in the center of the pad. Therefore, none of the three vias would be located at the center of the pad along its length dimension (or width dimension, for that matter).

The SEM/SE image in Fig. 12a (b) shows the 1x 5742, 1x 4596 solder joint structure. In this case, the two layers were delineated approximately by a row of voids or glassy phase material. Defects were not observed in the solder, thick film structure, the LTCC material below the thick films, or at any of the mutual interfaces. Also, there did not appear to be a significant infiltration of the glassy phase from the 4596 layer, into the LTCC under the 5742 layer. In Fig. 11a (c), the solder joint structure above the via was represented. There were no artifacts to suggest that the via affected the integrity of the solder joint there.

The analysis was continued with the micrographs in Fig. 12b, which examined, specifically, the via structure. It was confirmed that side wall cracking was not present. However, horizontal cracks were observed in the LTCC, which were indicated by the red arrows in the higher magnification micrographs of Figs. 12b (b) and (c). These types of cracks were not observed in the via structures of any of the other test specimens. *Clearly, these cracks do not have the same morphology as the "traditional" side wall cracks in terms of point-of-origin as well as path.* Although certainly less likely to open an internal trace, they were nonetheless a defect that was recorded.

A closer examination of these horizontal cracks was provided by the photographs in Fig. 12c. The low magnification micrograph in Fig. 12c (a) identified the location of the cracks. The origin of the upper crack, which was denoted by a green circle in Fig. 12c (b), indicated the presence of via fill material in the crack path. (The origin of the bottom crack was out of the plane of the cross section.) The same observation was made of a similar crack in a different cross section from this test specimen. The observation of via fill material in the crack suggested that, most likely, the horizontal cracks originated at the time that the via fill material was put into place. There was no obvious explanation for the horizontal cracks to have occurred only in the sample having 1.0:0.5 for the 4596/5742 ratio. It may be possible that there was an "aberration" in the green tape firing process used to make these samples,.

Lastly, the outer boundary at which, the 5742 layer ended, was also examined. Beyond this boundary, the 4596 thick film, alone, was in contact with the LTCC. The corresponding SEM/SE micrographs were provided in Fig. 12d. The low magnification view in Fig. 12d (a) showed the location of the 5742 boundaries; higher magnification views of those two locations were shown in Figs. 12d (b) and (c). The glassy phase that originated from the 4596 layer, extending laterally underneath the 5742 layer for distances of 32 μm and 27 μm in the two respective photographs. There was no degradation to the thick film, the LTCC, nor their respective interfaces, per se, that was caused by the lateral glassy phase diffusion.

The effect of reducing the 4596/5742 ratio to 1.0:0.2 was investigated for the single prints of both the 5742 and 4596 thick film layers. Shown in Fig. 13a (a) is an SEM/SE image of the cross section of the untested joint. Several large voids were noted in the solder; otherwise, the joints exhibited excellent integrity. The boundaries of the 5742 layer were indicated by the green lines. High magnification SEM/SE images were

provided in Figs. 13a (b) and (c) that show the outer boundary of the 5742 layer. The glassy phase of the 4596 layer diffused laterally 27 μm and 25 μm, respectively, under the 5742 layer. These values were very similar to the average of the two measurements made in Figs. 12d (b) and (c). However, in Fig. 13a (c), a small area of the glassy phase (red arrow) was observed approximately 60 μm distant from the 5742 boundary. Two sources of the isolated region of 4596 glassy phase were proposed. One, it could have reached the LTCC base material by diffusion through the 5742 layer. Second, the glassy phase diffused laterally under the 5742 layer, beginning at the latter's boundary where the 4596 layer contacted the LTCC base material.

(a)
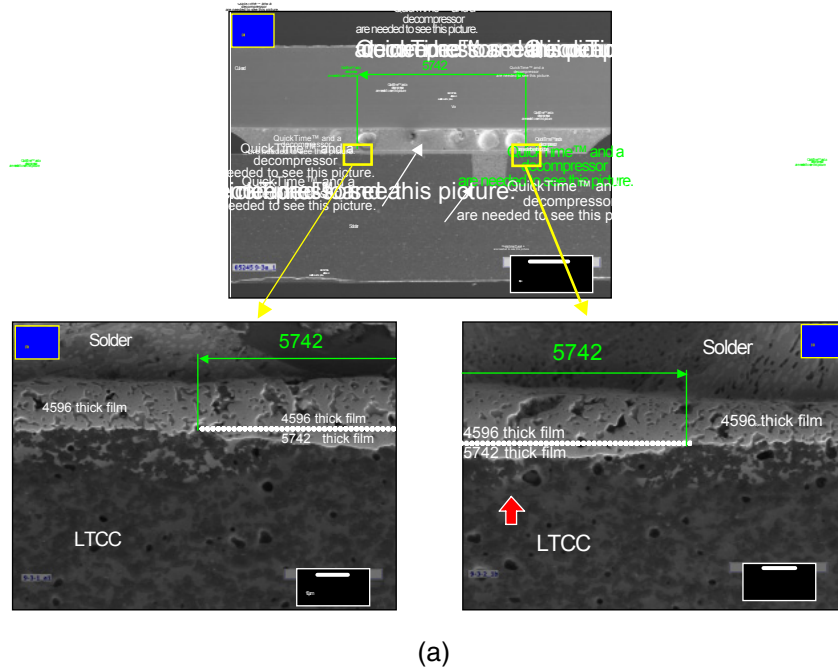
Fig. 13 (a) (a) Low magnification SEM/SE image showing the structure of the untested solder joint fabricated from 1x 5742 and 1x 4596 thick films over a via, having 4596/5742 ratio equal to1.0:0.2. The termination points of the 5742 layer were identified by the green lines. The SEM photographs (b) and (c) showed the outer boundaries where the 5742 thick film layer. The red arrow in (c) pointed to an isolated region of the 4596 glassy phase that developed further away from the boundary. *(con't)*

QuickTime™ and a
decompressor
are needed to see this picture.

Click to see the Flash this picture.

4596 thick film
5742 thick film

LTCC

QuickTime™ and a
decompressor
are needed to see this picture.

250μm
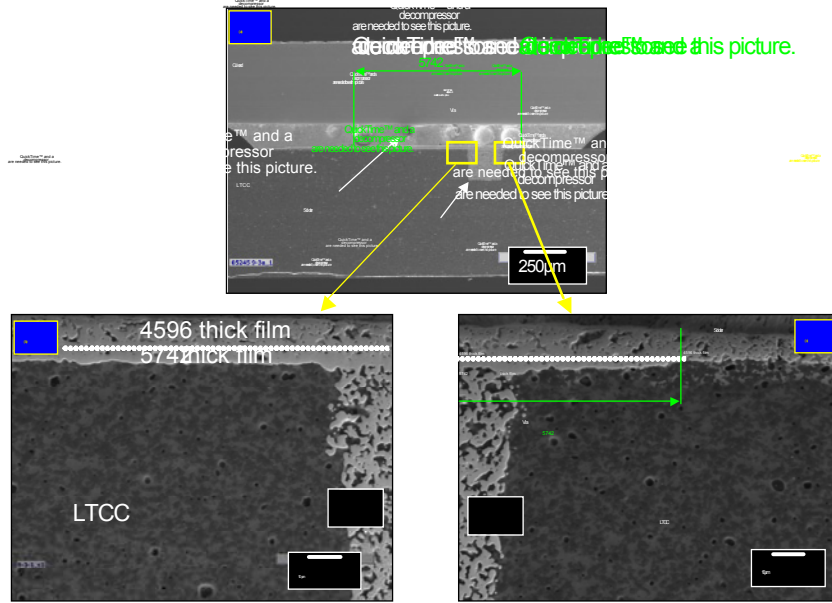
(b)

Fig. 13 (b) (a) Low magnification SEM/SE image showing the structure of the untested solder joint fabricated from 1x 5742 and 1x 4596 thick films over a via, having 4596/5742 ratio equal to1.0:0.2 that highlights the via structure. The SEM photographs (b) and (c) show the two sides of the via at high magnification, revealing an absence of side wall cracks.

An examination was also made of the via side walls. The corresponding SEM/SE photographs were shown in Fig. 13b. There were no indications of side wall cracks, in spite of the close proximity of the 4596 thick film and its glassy phase to the via. The distance between the via and the edge of the 5742 layer in Fig. 13a (c) provided an indication of the closest proximity that the 4596 thick film could have to the via and still prevent the occurrence of side wall cracking in the via.

In summary, the analysis above clearly showed that single prints of the 4596 and 5742 would result in via structures that did not experience side wall cracking. The resulting solder interconnections exhibited excellent integrity for the different configurations.

Next, the effect on the solder joint microstructure was evaluated for various 5742 thick film footprint size and the triple print (3x) 4596 thick film layer over a via. As noted earlier, the 3x 4596 thick film was required for the present application in order to

provide sufficient conductor to support multiple soldering steps. Therefore, it was necessary to determine whether the elevated temperature conditions associated with the additional firing steps would affect the integrity of the solder joints.

The analysis began with an evaluation of the test specimen having the 4596/5742 ratio of 1.0:0.5. The sample having the ratio of 1.0:1.0 showed microstructural features very similar to those described below for the 1.0:0.5 ratio specimens. Shown in Fig. 14a **(a)** is a low magnification SEM/SE photograph of the untested solder joint made with a 1x 5742 layer and 3x 4596 thick film over a via. The boundaries of the 5742 layer were marked by the green lines
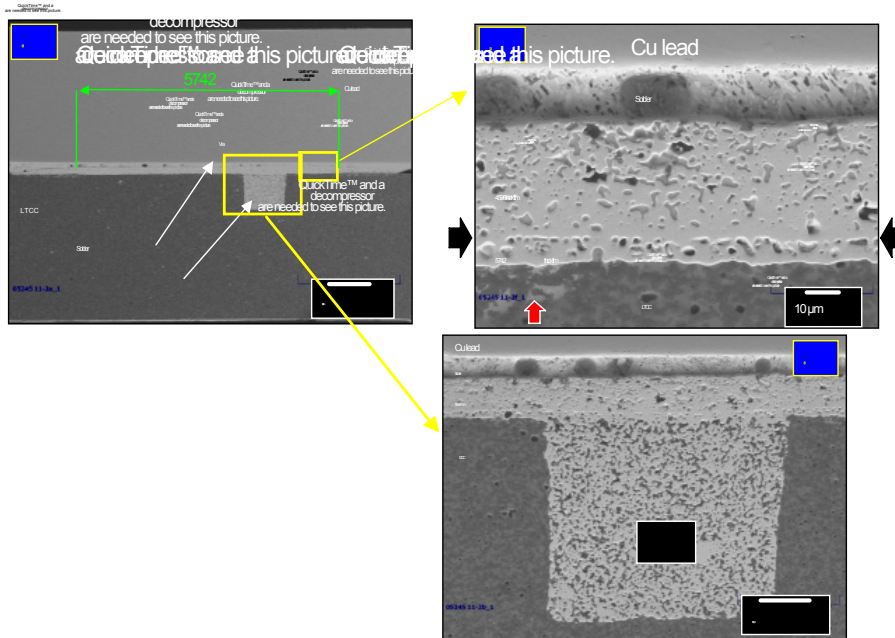
(a)

Fig. 14 (a) **(a)** Low magnification SEM/SE image showing the untested solder joint fabricated 1x 5742 thick film and 3x 4596 layers. The ratio of 4596/5742 was equal to1.0:0.5. The boundaries of the 5742 layer were identified by the green lines. SEM photograph in **(b)** shows the solder joint structure. The black arrows indicate the likely boundary between the 5742 and 4596 layers. The red arrow indicates where the 4596 glassy phase penetrated into the LTCC material. The image in **(c)** showed the solder joint structure above the via as well as the side walls adjoining the via. *(con't)*

33
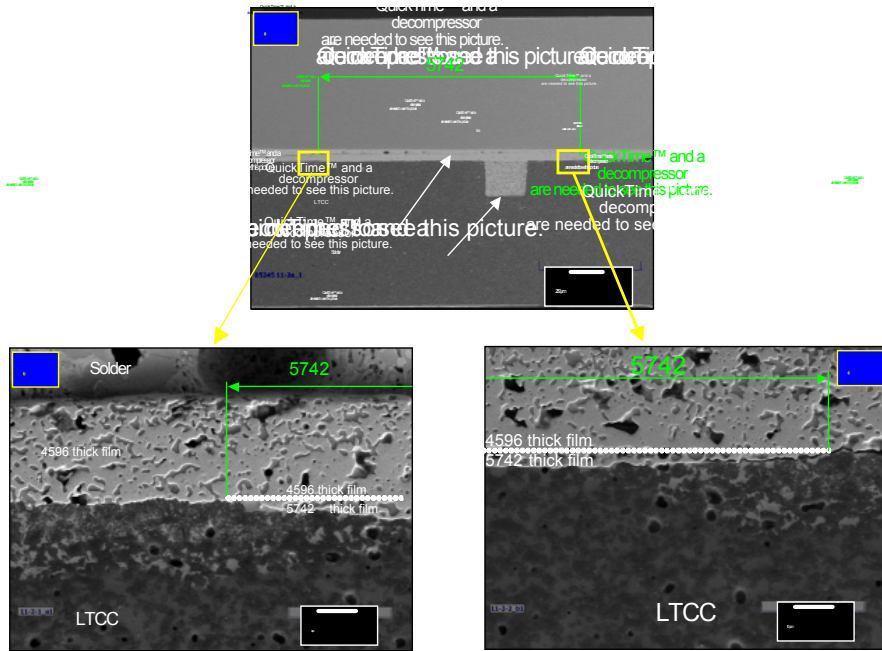
(b)

Fig. 14 (b) (a) Low magnification SEM/SE image highlighting the boundaries at which, the 5742 layer ended in the untested solder joint fabricated 1x 5742 thick film and 3x 4596 layers. The ratio of 4596/5742 was equal to1.0:0.5. The photographs in (b) and (c) are high magnification images of the ends of the 5742 thick film that clearly show the extent of diffusion by the 4596 glassy phase. *(con't)*
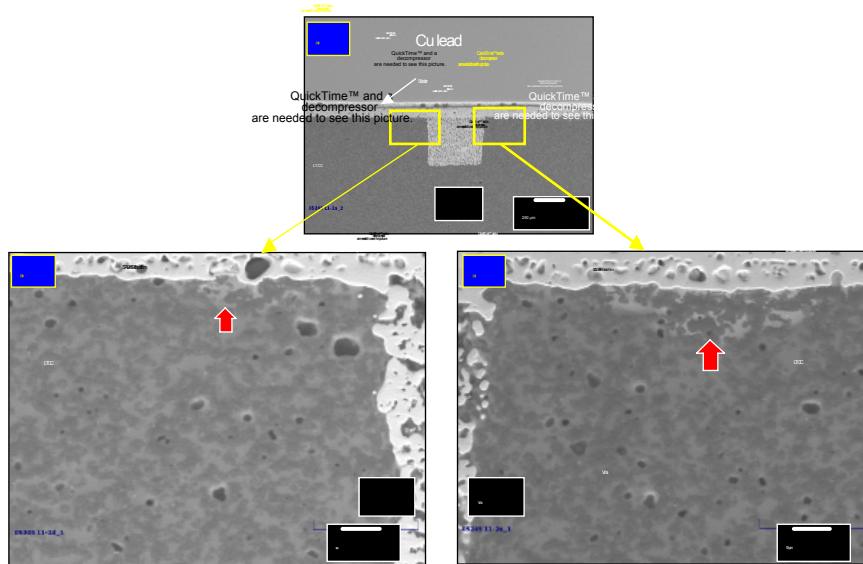
(c)

Fig. 14 (c) A low magnification image in (a) highlights the via structure of the untested solder joint fabricated 1x 5742 thick film and 3x 4596 layers. The ratio of 4596/5742 was equal to1.0:0.5.. The photographs in (b) and (c) are high magnification images showing the side wall regions of the via.

There was also a significant amount of glassy phase remaining in the 4596 layer, which was accompanied by significantly less void development when compared to a 3x 4596 layer placed directly over the LTCC or, more so, when fired on to the traditional alumina substrate. A red arrow in Fig. 14a (b) showed a region where the 4596 glassy phase had breached the 5742 barrier and diffused into the LTCC layer. There were no indications of degradation to the LTCC base material or to the thick film/LTCC interface. The SEM photograph in Fig. 14a (c) shows the solder joint above the via. The interconnection was excellent with no defects detected in any of the structures. The SEM photographs in Fig. 14a provided ample evidence that the 1x 5742 layer and 3x 4596 layer, when placed over a via in LTCC base material, would support the formation of a sound Sn-Pb solder interconnection.

Next, a careful examination was made of the end boundaries of the 5742 layer. These locations were shown in Fig. 14b. The extent to which the glassy phase extended underneath the 5742 layer from the latter's boundary was 46 μm and 51 μm in Figs. 14b (b) and (c), respectively. These distances were nearly twice those measured for the single 4596 layer interconnections (Figs. 12d and 13a). The increased diffusion of

35

the glassy phase was expected, given the two additional firing steps required to create the 3x 4596 layer versus a single layer. Nevertheless, there was no degradation observed to any of the structures, except for an interface crack to the very right-hand side of Fig. 14b **(c)**. That crack will be discussed in detail later on.

It was observed in both **(b)** and **(c)** images of Fig. 14b as well as that of Fig. 13a that the morphologies of the 4596 glassy phase *within* the LTCC base material differed between the single and triple layers of 4596 thick film. First, the extent of diffusion of the glassy phase into the LTCC base material was greater for the 3x 4596 layer. This observation was expected, given the increased quantity of glassy phase provided by three 4596 layers as well as the additional firing steps that enhanced the diffusion process. Secondly, the single layer morphology, which was observed in Fig. 13a, exhibited a relatively coarse particle size. On the other hand, when a triple layer of 4596 was present, the coarse particles were combined with a region of finer scale particles between the coarse-particle region and the interface. This two-stage morphology was documented in Fig. 14b. It was construed that the two morphologies were caused by a gradient in glassy phase concentration away from the interface; that is, the lower the concentration of the phase, the coarser were the phase particles.

The side wall regions of the via were shown in Fig. 14c. There were no indications of side wall cracking in the LTCC material, despite the nearby regions of 4596 glassy phase as indicated by the red arrows in Fig. 14c **(b)** and **(c)**.

A direct comparison was made of the microstructures of the single and triple thick film layers of 4596 over 5742, using the two SEM/SE photographs in Fig. 15. The 1x 4596 layer system was shown in **(a)** and the 3x 4596 layer was shown in Fig. 15 **(b)**. The green line established the position of the 5742 thick film/LTCC interface. The black arrows indicate approximately the boundary between the 5742 layer and the 4596 layer. The white arrows mark the interface between the 4596 layer and the Sn-Pb solder. Several observations were made from Fig. 15. First of all, the multiple firings that accompanied the three 4596 layers resulted in a further densification of the 5742 layer because the latter was thinner in Fig. 15 **(b)**. Second, there was a greater extent of voids and glassy phase particles along the apparent boundary between the 5742 and 4596 layers after the three print-dry-fire cycles versus the single 4596 thick film layer. This phenomenon was caused by the accumulation of glassy phase from the 3 x layers of 4596 thick film above the 5742 layer and that, in fact, the 5742 layer blocked the movement of the 4596 glassy phase into the LTCC substrate material.
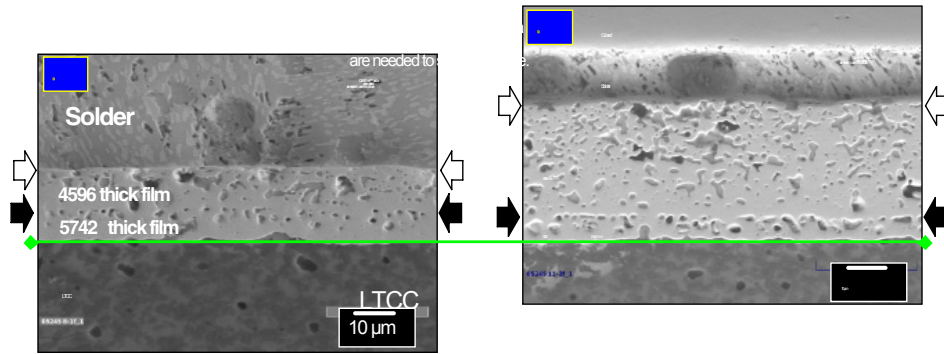
Fig. 15 (a) SEM/SE image showing the microstructure of the untested solder joint fabricated from a single print of 5742 thick film and a single layer of 4596. (No via was present in this sample.) (b) SEM/SE image showing the microstructure of the untested solder joint fabricated from a single print of 5742 thick film and three layers of 4596 thick film. (This sample had a via and a 4596:5742 ratio of 1.0:0.5.) The green line marked the interface between the 5742 layer and the LTCC base material. The black arrows indicated the approximate position of the interface between the 5742 layer and the 4596 layer. The white arrows showed the position of the interface between the 4596 layer and the Sn-Pb solder.

The third observation was the development of a gradient in the density of the 3x 4596 layer in Fig. 15 (b). That gradient developed because of further densification in the lower, previously deposited layers, that resulted from the subsequent firing steps. In fact, a direct comparison of the 4596 layers between the two SEM images in Fig. 15 showed that the layer microstructure in Fig. 15 (a) was very similar to that of the very top region of the same layer in Fig. 15 (b) because the former region was created by the third and final 4596 layer, which experienced only a single firing step.

It was noted above that a crack was observed in Fig. 14b (c). The source of the crack was likely the pull test that was performed on the neighboring pad; the test was not halted in time to prevent some damage to the "untested" pad. More importantly, however, this crack provided valuable insight into the strength properties of the thick film/LTCC interface. The morphology of that crack was further investigated by the SEM/SE photographs, which were shown in Fig. 16. The low magnification SEM/SE image in Fig. 16 (a) indicated that the crack initiated at the edge of the pad and propagated a substantial distance into the interconnection. The photograph in Fig. 16

(b) showed the starting point of the crack at the edge of the pad. Recall that at this location, the thick film was entirely 4596. It was clear that the crack initiated at the interface between the 4596 layer and the glassy phase adhesion layer that had formed at the LTCC surface. This was a commonly observed failure mode in Au- and Ag-based thick film interconnections [4, 5]. The diffusion of Sn to the thick film (metal)/glassy phase interface causes the bond to weaken between the metal and the glassy phase. No secondary or "branch" cracks were observed to have propagated into either the thick film layer or into the LTCC base material.

The SEM/SE image in Fig. 16 **(c)** showed the termination point of the crack. The 5742 layer was present at this location; however, as was noted above, the glassy phase extended under the 5742 thick film for some distance (towards the via).
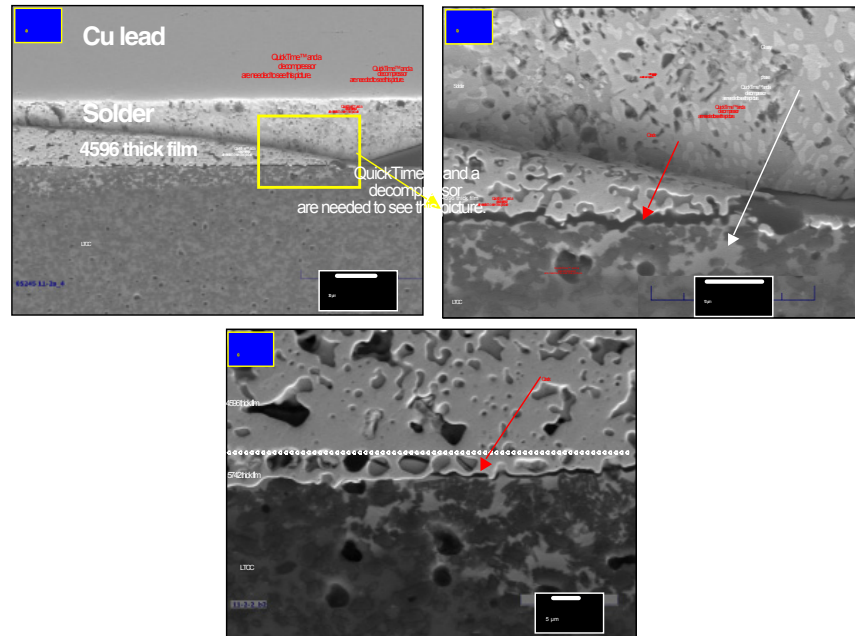
Fig. 16 (a) SEM/SE image showing the crack observed in the untested solder joint fabricated with the 1x 5742 and 3x 4596 thick film layer. (This sample a 4596:5742 ratio of 1.0:0.5 and vias.) **(b)** SEM/SE image showed the crack initiation point and fracture microstructure. **(c)** SEM/SE showing the termination point of the crack.

The crack continued to propagate along the interface between the 5742 thick film and the laterally-diffused, 4596 glassy phase until the later was no longer present. Then, the crack turned into the thick film layer where it ended. Even within the thick film, fracture occurred preferentially in the glassy phase contained in pores in the 5742 layer.

In summary, the photographs in Fig. 16, which captured crack growth under the 5742 layer on the 1x 5742, 3x 4596 thick film, demonstrated the weakness of the interface between the thick film metal and, specifically, the 4596 glassy phase, along the interface with the LTCC base material. Once the presence of that glassy phase had been exhausted, the crack turned into the thick film, which in this case, was the 5742 composition. Because the crack did not continue to propagate along the 5742/LTCC interface, that interface, which had the glassy adhesion layer of the 5742 ink, was considerably more robust than the glassy phase layer generated by the 4596 thick film.

The specimen was examined, which was constructed with a thick film conductor having a single 5742 layer and three 4596 layers, but at a ratio of 1.0:0.2. The edge of the 5742 layer , which was closer to the via, exhibited the same microstructure as was observed for the 1.0:0.5 ratio sample (Fig. 14b). Two SEM/SE photographs were provided in Fig. 17 that showed the side wall regions of the via. In Fig. 17 (b), the edge of the 5742 layer and, so too, the 4596 glassy phase, were close to the via. Lateral diffusion of the 4596 glassy phase under the 5742 thick film layer was 50 µm. Yet, in neither photograph were cracks observed in the via side walls.
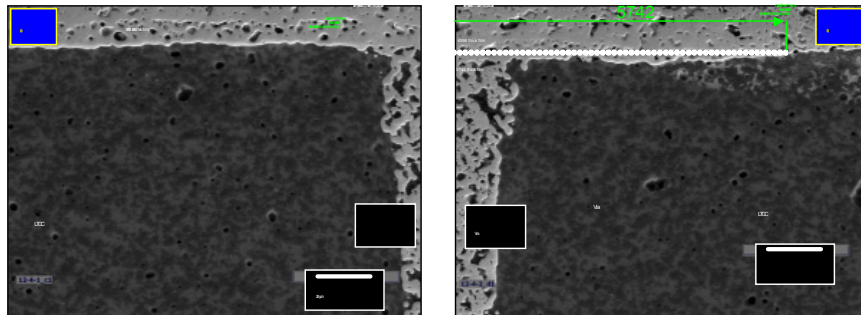
Fig. 17 (a) and (b): SEM/SE images showing the sidewalls of the vias attached to the untested solder joint fabricated from a single print of 5742 thick film and three layers of 4596 thick film. The sample had a 4596:5742 ratio of 1.0:0.2 and vias underneath the pads.

Lastly, it was noted earlier that the diffusion of Bi from the glassy phase of the 4596 thick film was believed to be responsible for side wall cracking in the vias of the LTCC substrate material. An attempt was made to determine whether energy dispersive x-ray analysis (EDXA) could detect an elevated Bi concentration in the LTCC substrate a distance away from the 4596 glassy phase. Shown in Fig. 18 (a) is a high

magnification, SEM/SE photograph showing the boundary between the 4596 glassy phase and the LTCC base material, which had its own glassy phase matrix. When EDXA was performed on the 4596 glassy phase (Fig. 18 (b)), a small Bi signal was observed, as indicated by the inset image. On the other hand, there was a significant Au signal, the Au having originated from metal component of the film. In fact, the contrast that identified the 4596 glassy phase within the LTCC base material was caused largely by the Au content and, to a lesser degree, the Pb, and Bi contents. When the same analysis was performed on the glassy phase of the LTCC, the Bi signal decreased to a level that was difficult to discern above background. Therefore, this technique was not sufficiently sensitive to detect the diffusion of Bi into the glassy phase of the LTCC base material if, in fact, such diffusion had occurred.
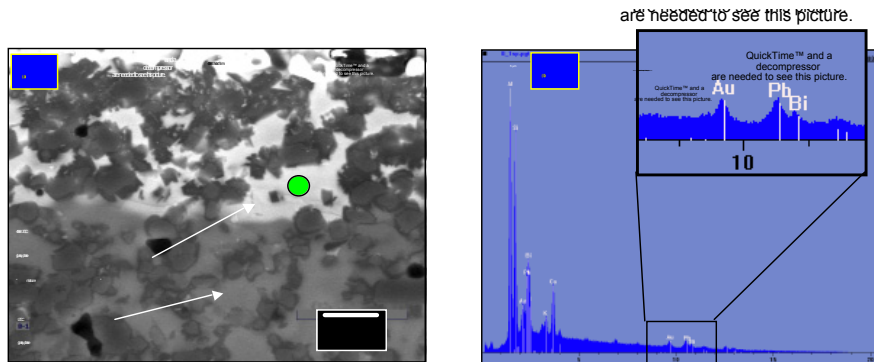
Fig. 18 (a) High magnification SEM/SE photograph that shows the boundary between 4596 glassy phase and the LTCC. **(b)** Energy dispersive x-ray analysis (EDXA) of the 4596 glassy phase showing the Au, Pb, and Bi peaks. This particular sample was made of single prints of both 4596 and 5742 thick films over a via at a ratio of 4596/5742 equal to1.0:0.5.

A summary is made below, which consists of a compilation of the observations made with reference to the microstructures of the untested solder joints.

1. The solder interconnections representing the different combinations of the 5742 and 4596 thick film layer structures – single (1x) or triple (3x) layers of 4596 and different footprint ratios – exhibited excellent integrity. There were no indications of deformation or damage in any of the individual layers (solder, thick film layers, or the LTCC base material) or unaccounted failures at any of the mutual interfaces. The presence of the via did not appear to affect the interconnection microstructure.

40

2.   The solder gaps exhibited the anticipated levels of void formation. However, void development did not appear to be correlated to the particular thick film layer stack, dimensions (ratio), or the presence of a via under the pad.

3.   The single print of 5742 thick film provided an effective barrier against the diffusion of glassy phase from the 4596 layer into the LTCC base material. A few, isolated regions were noted where the 4596 glassy phase appeared to have breeched the 5742 layer. There was no quantitative data to confirm that the number of such breeches was directly sensitive to the number of 4596 layers (1x or 3x) or, indirectly, to the number of firing steps required to establish those layers.

4.   The presence of the 5742 thick film prevented the occurrence of side wall cracks in the vias. The specimens used in the present study resulted the 4596 thick film being as close as 122 μm to the via, resulting in the diffusion zone of the 4596 glassy phase was within 73 μm of the via (3x 4596 thick film). Yet, side wall cracks were not observed.

Lastly, a survey of the side wall regions of the vias did not reveal the presence of the horizontal cracks that were observed in Fig. 12c. Therefore, it was surmised that those cracks represented a one-time occurrence, which was not further repeated.

3.2 Pull strength analysis

The pull strength data are shown in Fig. 19. The graph in Fig. 19a is that of the mean pull strength values and error bars that were determined from ±one standard deviation. (The case of the 5742 (1x) thick film sample with vias was placed at the far right of the plot.) The error format presented in Fig. 19a allowed for a direct comparison with historical test data obtained primarily at Honeywell/Kansas City Plant (KCP).

The mean and standard deviation values in Fig. 19a were compared to historical results for Sn-Pb solder joints made to the 4596 pads on *alumina* substrates [3]. Those results for the alumina substrates showed a mean strength of 4.3 lbs and a standard deviation of 0.87. The mean strength values obtained in the current study on the LTCC substrate were slightly lower for both single or triple print-dry-fired 4596 thick film pads. The lower pull strengths were likely a consequence of the LTCC base material, per se, and its higher glass content. However, the standard deviation was reduced by nearly one-half in the current study, being in the range of 0.3 – 0.5 lbs. It was not expected that the slightly lower strengths would impact the electrical or mechanical functionality of the interconnections in an actual application.
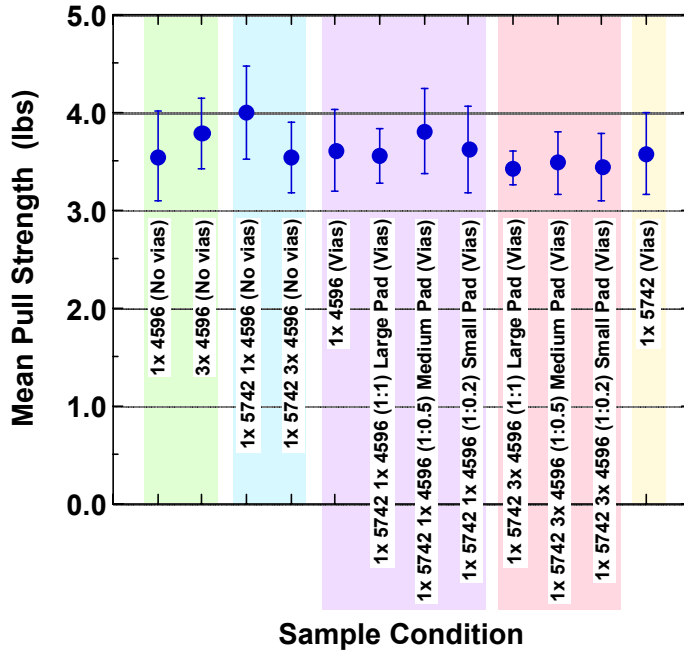
(a)

Fig. 19 Pull strength as a function of thick film configuration: (a) error bars established from ±one standard deviation and (b) error bars based upon a 95% confidence interval for the mean. *(con't)*
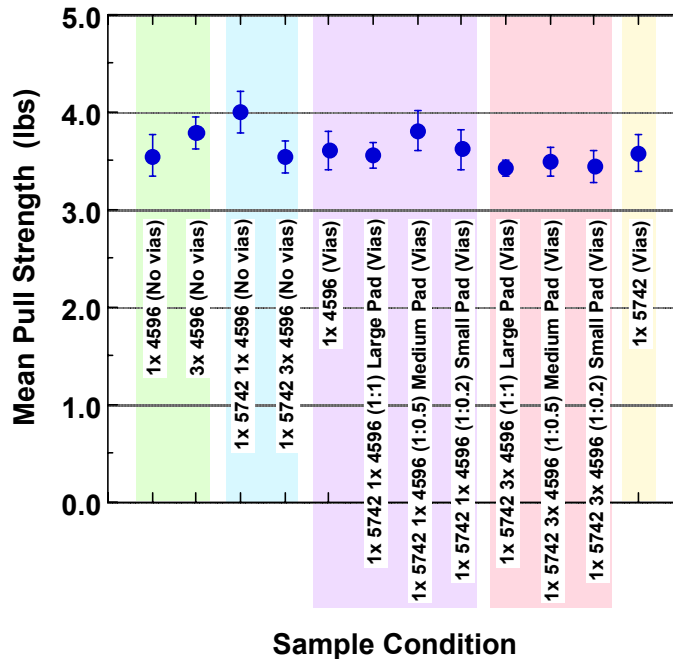
(b)

Fig. 19 Pull strength as a function of thick film configuration: (b) error bars based upon a 95% confidence interval for the mean.

Shown in Fig. 19b is the same plot of mean pull strength versus thick film configuration, but with the error bars established via a 95% confidence interval about the mean. The following trends were obtained from Fig. 19b:

1. In the absence of vias, the 3x 4596 layer exhibited a slightly higher mean pull strength that the 1x 4596 layer. However, this difference lacked statistical significance because of overlapping 95% confidence intervals.
2. The addition of the 5742 barrier layer caused a significant increase in the solder joint strength of the 1x 4596 thick film – again, no vias were present. However, when the 5742 layer was added to 3x 4596 layer, there was a decrease in the pull strength.
3. The pull strength did not change significantly when a via was added under the 1x 4596 thick film. (The case of the 3x 4596 layer by itself was not tested.) A similar result was observed for the 1x 5742, 3x 4596 thick film system. However, the addition of the via decreased the pull strength of the 1x 5742, 1x 4596 layer stack, causing the maximum load values to be comparable to those of the other aforementioned test specimens.
4. The 5742 barrier layer over a via had the same strength as did the single print 4596 layer over a via. Therefore, there would be no *direct* loss of joint strength by replacing the 4569 thick film/LTCC interface with a 5742 thick film/LTCC interface. Moreover, there was no degradation in pull strength when the 1x 5742 and 1x 4596 layers were combined over a via (that is, the 1.0:1.0 ratio case) when compared to the cases of only the individual 4596 layer or 5742 layer over the via.
5. Several trends were observed with respect to the 4596:5742 ratio. Although these trends lacked statistical significance according to the 95% confidence interval criterion, they provide valuable insight into the performance of these material systems. First, for all three pad designs, the 1x 5743, 1x 4596 thick film had consistently higher mean strengths than did the 1x 5742, 3x 4596 thick film. Secondly, within each of the two groups distinguished by 1x versus 3x 4596 layer, the highest mean strength was recorded for the 1:0.5 ratio pad design.

Several of the trends summarized above were based upon the mean pull strength value. When considering the 95% confidence band, they lacked statistical significance. This point implies that the strength of the Sn-Pb solder joints will not be highly sensitive to these variations of the thick film structure for LTCC interconnections.

The next section examined the failure modes as determined by visual inspection. The quantitative assessment included all of the pull tested solder joints. The pull strength data were also referenced during the analysis.

3.3 Failure mode analysis by visual inspection

The failure mode analysis was performed on the pull test samples, using the visual inspection criteria. Shown in Fig. 20 is a graph of the failure modes as a function of the thick film and via specimen parameters. Recall that the percentage values pertain to *the percentage of the eighteen (18) pull test sites having that particular failure mode and not the degree to which, that failure mode was present in all of the joints*. Therefore, as noted above, the percentages will not add to 100%.
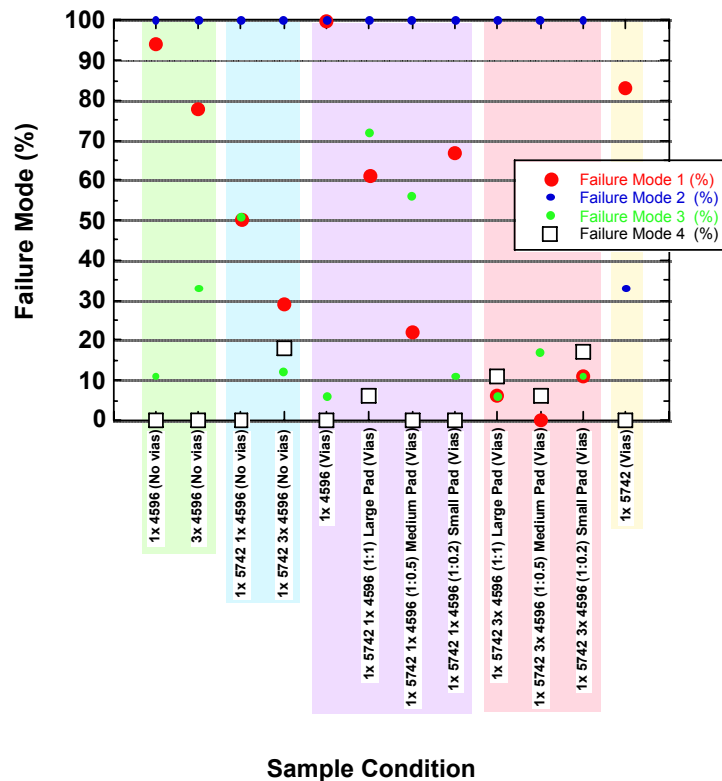
Fig. 20 Failure mode analysis of the pull test samples. The percentage values reflect the percentage of the eighteen (18) solder joints that had that particular failure mode.

All of the pull test sites, with the exception of the single print 5742 tests, exhibited failure mode #2, which was *partial* separation at the solder/TKN interface. Therefore, the discussion will address, specifically, the other failure modes, which varied between the different test specimens. Also, it was not possible in the visual inspection to discern failures along the 5742 thick film/4596 thick film interface. A postiori, metallographic

cross sections showed that this failure mode was not very prevalent. Therefore, this discrepancy in the visual inspection method was not particularly significant in the failure mode analysis. The following observations were compiled from Fig. 20:

1. *1x 4596 v. 3x 4596 (no vias):* The strength of the solder/thick film interface was greater for the 3x 4596 layer, as indicated by the decrease of mode #1 failures and the preference for fracture in the solder fillet (mode #3).
2. *1x 4596 v. 1x 4596, 1x 5742 (no vias)*: The significant strength increase was accompanied by a decrease in the mode #1 solder/thick film failures and increase in the mode #3 solder failures, implying a strengthening of the solder/thick film interface. There was no degradation to the thick film/LTCC interface.
3. *3x 4596 v. 3x 4596, 1x 5742 (no vias)*: A decrease of pull strengths was observed. Because both modes #1 and #3 decreased, the strength drop was attributed primarily to the increase of mode #4, which was failure at the thick film/LTCC interface and/or LTCC divots.
4. *1x 5742, 1x 4596 v. 1x 5742, 3x 4596 (no vias):* Similar to case 3, the strength drop associated with having 3x 4596 layers was attributed to a reduced strength of the thick film/LTCC interface and/or LTCC base material.
5. *Effect of via. There were three (3) cases:*
    a. *1x 4596 without vias v. 1x 4596 with vias:* There was very little difference in the failure modes observed between these two cases. Also, there was no significant difference in the strengths between the two sets of solder joints. The failure mode and strength data also indicated that the side wall cracks did not significantly affect the mechanical performance of the interconnections.

    b. *1x 5742, 1x 4596 without vias v. 1x 5742, 1x 4596 (1.0:1.0) with vias:* There were increases in each of the #1, #3, and #4 failure mode percentages with the addition of the via. However, it was likely that the increase in the #4 failure mode, which implied that there was a weakening of the thick film/LTCC interface and/or LTCC base material, was responsible for the significant loss of strength observed in Fig. 19b. Recall that Figs. 12b and 12c showed horizontal cracks associated with the via structure of the latter test samples. It cannot be determined with certainty that the horizontal cracks associated with the introduction of vias reduced the strength of the 1x 5742, 1x 4596 system because the prevalence for such cracks was not determined. Also, a similar trend was not observed in case (a) nor in case (c) discussed below.

c. *1x 5742, 3x 4596 without vias v. 1x 5742, 3x 4596 (1.0:1.0) with vias:* The addition of the vias caused decreases in the #1, #3, and #4 failure modes. These trends indicated that there was less degradation to the solder/thick film interface, the thick film/LTCC interface, and/or LTCC bulk material. Nevertheless, there remained a significant presence of the #4 failure mode, which kept the pull strengths largely unchanged between the two cases (Fig. 19b). Also, horizontal cracks were not observed around the vias in the latter set of samples.

In summary, the following scenario was developed from the comparisons outlined in (1 – 4) above for samples without vias. In the first two cases (1) and (2):

(1)   1x 4596 → 3x 4596

(2)   1x 4596 → 1x 5742, 1x 4596

the strength increases were due to improvements to the strength of the solder/thick film interface. However, in cases (3) and (4):

(3)   3x 4596 → 1x 5742, 3x 4596

(4)   1x 5742, 1x 4596 → 1x 5742, 3x 4596

strength decreases were a result of an apparent weakening of the thick film/LTCC interface and/or underlying LTCC material. These data suggested that the mechanical performance of the interconnections may be correlated to the *number* of thick film layers on the LTCC substrate, not only the specific chemistries of the two thick film materials.

Lastly, the comparisons in 5 (a – c) indicated that the effect of the addition of vias to the LTCC depended on the thick film structure. In two of three cases, there were largely insignificant changes to joint strength, albeit, the failure modes were sometimes different. Side wall via cracks did not affect joint mechanical properties. In the exception case, 1x 5742, 1x 4595 thick film, there was a substantial decrease in the joint strength. Now, in one of the two cross sectioned joints, there were observed the horizontal cracks. Unfortunately, the significance of those cracks vis-à-vis the strength drop could not substantiated.

Finally, the single print 5742 specimen (In-Pb solder) experienced similar strengths and failure modes in the presence of a via as did the single 4596 layer, with or without a via. This comparison provided ancillary evidence that the 5742 thick film layer did not degrade the joint mechanical properties.

6. *The effect of the ratio of the 4596 thick film pad size to the 5742 pad size was examined for the two cases that were distinguished by the single layer of 4596 (a) versus triple layers of 4596 (b):*

   a. *Single layer (1x) of 4596 conductor:* Progressing from the 1.0:1.0 geometry to the1.0:0.2 geometry, there was a minimum in the mode #1 failures (solder/thick film separation) and the elimination of the mode #4 failures (thick film/LTCC and/or LTCC divots) at the 1.0:0.5 configuration. There was a consistent decrease in the solder fillet failures (mode #3) for the sequence.

   Referring to Fig. 19b, there was a maximum in the strength at the ratio of 1.0:0.5. The lower strength observed with the 1.0:1.0 geometry was most likely caused by a greater presence of the mode #4 failure type, that is, weakening of the thick film/LTCC interface. The lower strength at the 1.0:0.2 ratio was accompanied by an increase of the mode #1 failures, implying a weakening of the solder/thick film interface. Both #1 and #4 failure modes were minimized at the 1.0:0.5 ratio.

   b. *Triple layer (3x) of 4596 conductor:* Nearly the same trends was observed for the Modes #1 and #4 as were described in (a) above. That is, the strength maximum at 1.0:0.5 (Fig. 19b) coincided with minimums of both failure modes #1 and #4 (Fig. 20). However, the persistence of the #4 failure mode was likely responsible for generally lower strengths when compared to values generated a 1x 4596 thick film layer.

In summary, the failure mode and pull strength data indicate that the optimum pad geometry was 1.0:0.5. The failure modes #1 and #4 were strongly associated with the strength behavior. The failure mode #4 was most prominent when the 4596/5742 ratio was 1.0:1.0 and, overall, when there were 3x 4596 thick film layers.

The pull strength data (Fig. 19b) and the failure mode results (Fig. 20) indicated that the presence of single print (1x) 5742 barrier layer, in-and-of-itself, did not degrade the mechanical strength of the interconnection. Rather, the more significant factor appeared to be the number of 4596 layers placed on top of the 5742 layer. This behavior was further interpreted to suggest that it may have been the *number* of print-dry-fire cycles required to construct the total thick film layer that affected the solder joint strength.

In order to investigate this hypothesis, two analyses were performed. In the first evaluation, the pull strength data were plotted as a function of the number of firing cycles. This graph appeared in Fig. 21. The error bars represent the 95% confidence interval on the pull strength values. A curve fit routine was performed to determine a trend in the mean strength values. A second-order polynomial curve fit was performed on the data. The R^2 value was relatively low at 0.57, not all that surprising, given the different solder joint structures in the individual specimens. Nevertheless, the plot in Fig. 21 indicated that, at least to a first-order estimation, a maximum in the strength was realized between two and three (2.3) firing steps.
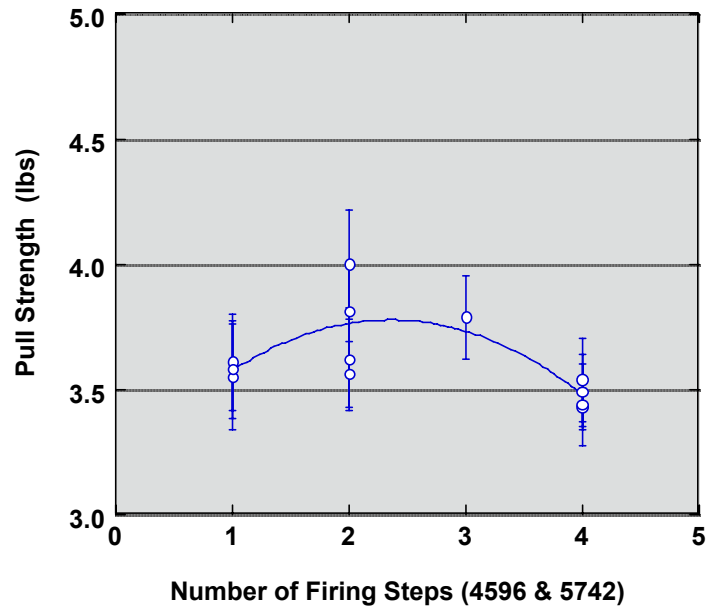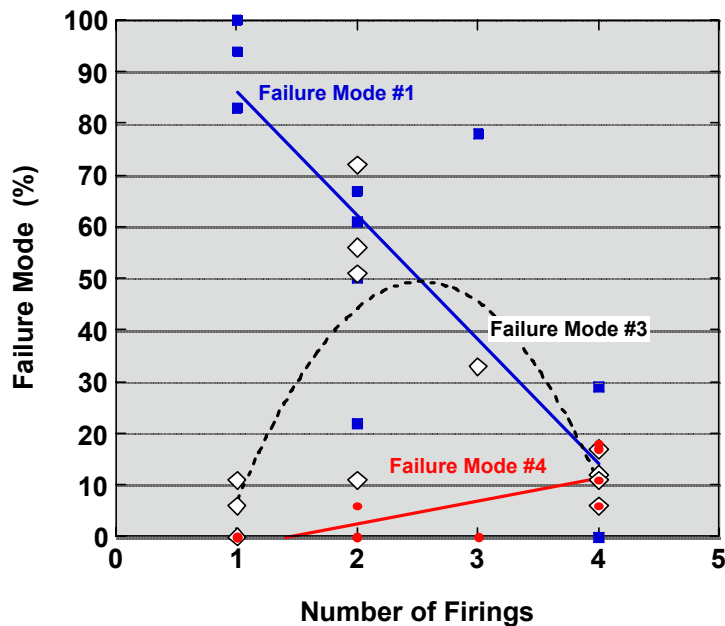

Fig. 21 Pull strength as a function of the number of firing steps used to deposit the 5742 layer, if present, and the 4596 layer(s), combining all of the data taken in this study.

Next, the failure mode data were evaluated as a function of firing steps. Shown in Fig. 22 is a graph of the percentage of occurrence of failure modes #1, #3, and #4 as a function of the number of firing steps. The mode #2 data were omitted from the plot since it prevailed across all of the specimen conditions. Both the mode #1 and mode #4 points were fit to a least-squares line; the R^2 values were 0.70 and 0.63, respectively. The mode #3 data were observed to be best represented by a second-order curve fit; the R^2 value was 0.61.

The following observations were compiled from Fig. 22: As the number of firing steps increased, there was a drop in the presence of the mode #1 failures. This trend indicated that the strength of the solder/thick film interface improved with the number of firing steps. In particular, this improvement from one to approximately two firing steps forced the failure into the solder fillet (failure mode #3). However, as the number of firing steps increased further, so did the frequency of failure mode #4, implying an increased degradation to the thick film/LTCC interface and/or underlying LTCC material. Between three and four firing steps, the failure mode #4 dominated the fracture behavior and loss of joint strength, resulting in a decreased contribution by the failures modes #1 and #3.

Fig. 22 Failure mode as a function of the number of firing steps used to deposit the 5742 and 4596 layers, combining all of the data taken in this study. The failure mode #2 was omitted from the analysis.

3.4 Failure mode analysis – metallographic cross sections

Metallographic cross sections were made of the solder joints after pull testing. Two joints were evaluated per sample. Initially, a qualitative analysis was made of the fracture morphology associated with the pull-tested samples, using SEM/SE images. Then, those observations were compiled into a quantitative assessment of the different failure modes.

Shown in the (a) SEM/SE photograph of Fig. 23a is a cross section of the pull tested solder joint made with the single layer of 4596 thick film in the absence of a via. The crack associated with the pull test progressed from left to right in the photograph. The image showed that 75% of the fracture surface (bond line) was at the interface between the solder and the thick film. The remaining 25% was fracture at the interface between the thick film layer and the LTCC base material. (It was these fracture surface percentages that were used to make the quantitative assessments as discussed later on.) The higher magnification SEM/SE image in (b) was taken at the transition between the two failure modes. It is possible that the void may have instigated the change of failure mode although there is no evidence to suggest that voids, in general, acted in this manner, in either the current test samples or other related studies.

The image in Fig. 23a (c) showed the solder joint structure where failure had occurred at the solder/thick film interface. The extent of IMC layer growth was very minimal. Therefore, it was not possible to determine, precisely, the location of the separation (i.e., either the solder/IMC layer interface; within the IMC layer; or at the IMC layer/thick film interface).

The second pull-tested solder joint, which was provided in the cross section, was depicted by the SEM/SE photographs appearing in Fig. 23b. In this case, the failure propagated from the right to the left. The low magnification image in Fig. 23b (a) showed the three failure modes present in the joint: (a) solder/thick film separation; (b) thick film/LTCC separation; and (c) an LTCC divot. A significant number of voids were observed in the joint. Although, generally speaking, the voids did not appear to have affected the fracture morphology at the interface, it was noted that below each void, the thick film layer had formed a vertical separation. The vertical cracks were probably caused by bending of the joint during testing and the absence of solder causing a lack of mechanical reinforcement for the thick film.
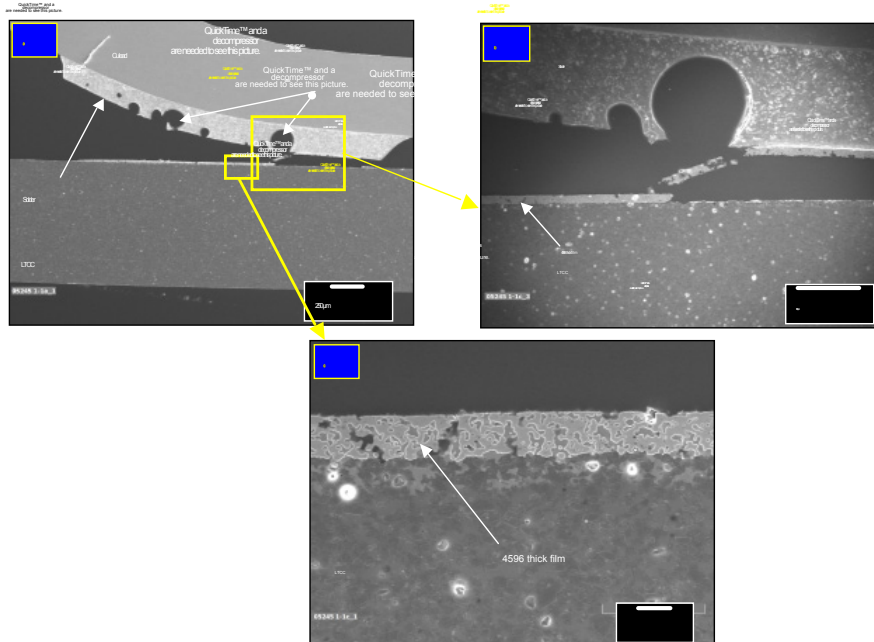
(a)

Fig. 23 (a) **(a)** Low magnification SEM/SE image of the cross section of the pull tested solder joint from the test sample having a single 4596 layer and no via. The fracture progressed from left-to-right. **(b)** High magnification SEM/SE photograph showing the transition point between the solder/thick film interface failure to the thick film/LTCC interface failure. **(c)** High magnification SEM/SE photograph of the solder/thick film failure interface. *(con't)*
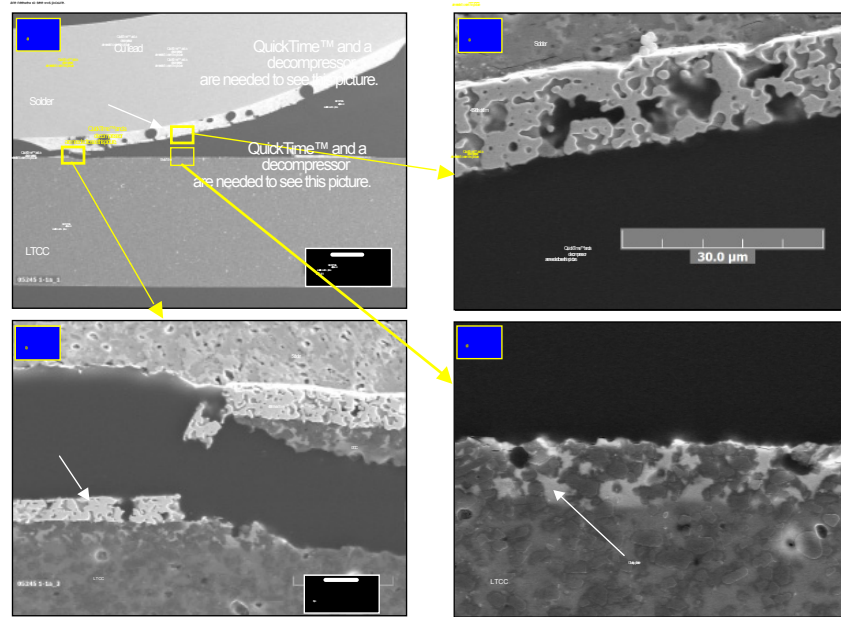
(b)

Fig. 23 (b) **(a)** Low magnification SEM/SE image of the cross section of the second pull tested solder joint from the test sample having a single 4596 layer and no via. The fracture progressed from right-to-left. **(b)** High magnification SEM/SE photograph showing the transition point between the solder/thick film interface failure and the formation of a divot in the LTCC base material. **(c)** and **(d)** Paired high magnification SEM/SE photographs showing the mating sides created at the thick film/LTCC failure site.

The SEM/SE photograph in Fig. 23b **(b)** shows the transition between the solder/thick film failure and the LTCC divot. There was no defect or other artifact in the interconnection structure that would have been explicitly responsible for the change in failure mode. The crack propagated in the LTCC primarily along the pseudo-interface formed by the 4596 glassy phase diffusion zone and the remaining LTCC material under it. Secondary cracks and crack branches were not observed in the LTCC material.

The most prevalent failure mode was fracture at the thick film/LTCC interface. High magnification SEM/SE photographs were provided in Figs. 23b **(c)** and **(d)** that showed the thick film and LTCC sides, respectively, at the same location. There was evidence that the fracture path occurred specifically at the interface between the glassy phase and the 4596 thick film. Now, this failure mode has been reported in other studies that

examined the adhesion properties of Ag-based and Cu-based thick films [5, 6]. It was determined in those cited works that Sn had migrated from the solder to the thick film (metal)/glassy phase interface by solid-state diffusion. The Sn atoms degraded the glassy phase at that interface, resulting in the loss of adhesion strength. However, direct evidence of this phenomenon was not observed in the present study.

In the photographs that comprised Figs. 23a and 23b, there were no other defects observed in the solder joint, the thick film, or the LTCC material.

The same analysis was performed on the specimens that had the triple layers of 4596 thick film without the via. The failure modes were nearly identical to those observed with the single 4596 layer, except that they occurred to different extents, respectively, which will be discussed later on in the quantitative analysis.

Next, the metallographic cross sections were examined, which came from the specimen that was constructed with single layers of the 5742 and 4596 thick films. A via was not present under the solder joint. (The ratio of the two layers was 1.0:1.0.) Recall from Fig. 19b that these solder joints exhibited the highest strength of the test program. The SEM/SE photographs appear in Fig. 24. The low magnification photograph in (a) showed the entire fracture surface. The crack propagated from right-to-left. There was nearly an equal presence of the fracture at the solder/thick film interface as there was failure within the solder, which was commensurate with the visual inspection data (Fig. 20). The solder/thick film interface failure morphology was very similar to those cases described earlier. Therefore, further discussion will examine the solder failure mode. Higher magnification images of this failure mode, which were provided in Figs. 24 (b) and (c), showed the fracture to have occurred near the solder/Cu lead interface rather than in the bulk solder. Although not readily apparent in the SEM/SE images, there was a significant thickness of solder remaining on the Cu lead (red box marked "A" in Fig. 24 (b)). Therefore, the fracture occurred *in close proximity to* the solder/Cu lead interface, yet, remained within the solder, itself.
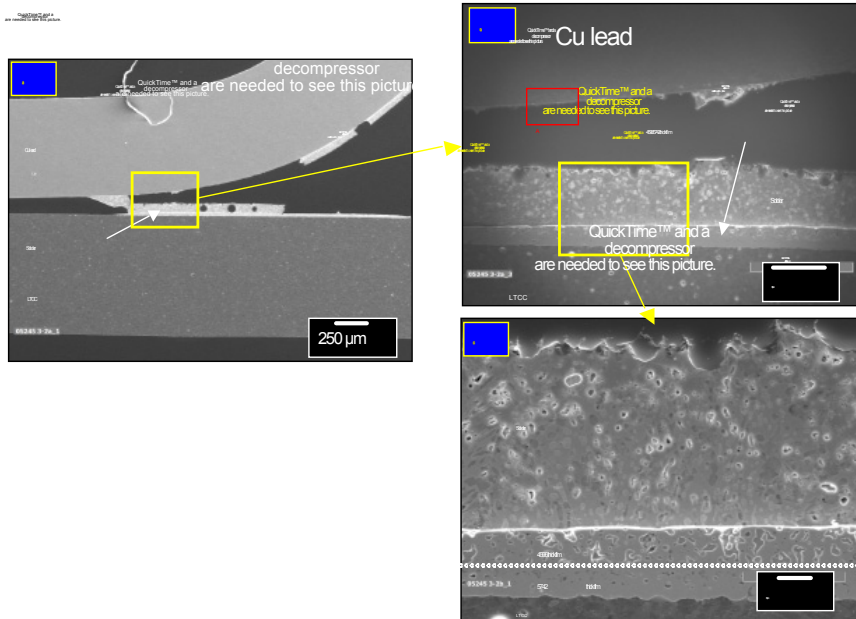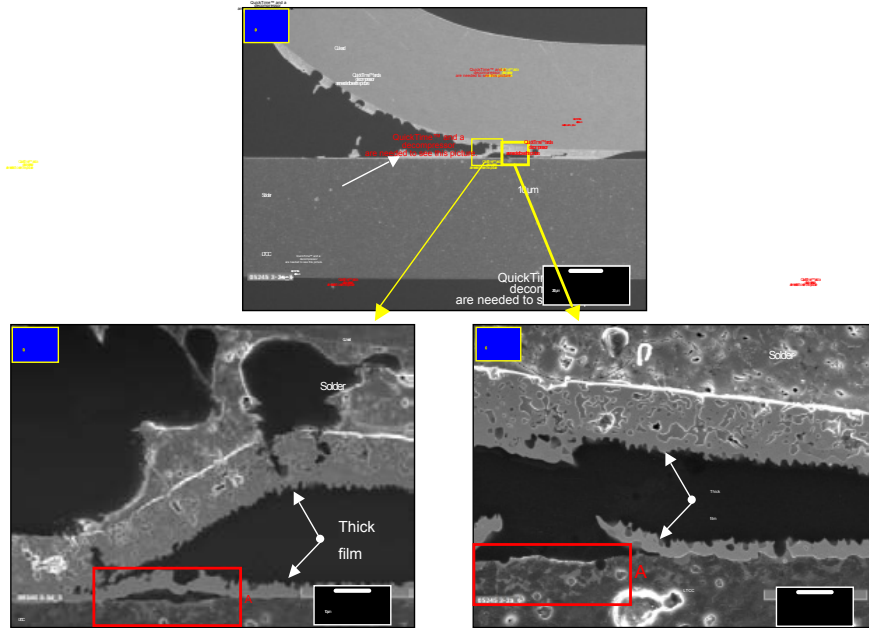
Fig. 24 (a) Low magnification SEM/SE image showing the cross section of one of the pull tested solder joints made with single layers of 5742 and 4594 thick films; there was no via. **(b)** Medium magnification view of the failure site at the interface between the solder and the Cu lead. The red box indicated the solder/Cu lead interface where a significant layer of solder remained attached to the Cu lead. **(c)** High magnification SEM/SE photograph of the solder and thick film structures in the tested joint.

The SEM/SE photograph in Fig. 24 **(c)** illustrated two additional observations. First of all, at the top of the image, the fracture surface of the solder exhibited a considerable degree of ductile void formation. *These voids were generated by the deformation of the solder; they were not present prior to the pull test.* Secondly, there was no damage at the solder/thick film interface; the 4596/5742 interface; or at the 5742/LTCC interface.

The more interesting behavior was observed on the second solder joint, the SEM/SE photos of which, appear in Fig. 25. A low magnification view of the solder joint appeared in Fig. 25a **(a)**. The crack propagation direction was from left-to-right. The front of the solder joint showed the solder and solder/thick film failure modes that were noted in the visual inspection, failure mode analysis. It is important to note that the density of "void-like" artifacts in the solder joint and, in particular, where failure took

54

place in the solder (30% of the bond line) was greater than the number of voids that were present at the time of fabrication. That is, several voids were generated by the void coalescence process that characterized ductile deformation in the solder.

(a)

Fig. 25 (a) **(a)** Low magnification SEM/SE image showing the cross section of the second pull tested solder joint made with single layers of 5742 and 4596 thick films; there was no via. The fracture progressed from left-to-right. **(b)** and **(c)** High magnification SEM/SE photographs showing the failure mode between the 5742 and 4596 thick film layers. The red box labeled "A" indicated a region of failure at the thick film (5742)/LTCC interface and the observation of glassy phase that had originated from the 4596 layer. *(con't)*
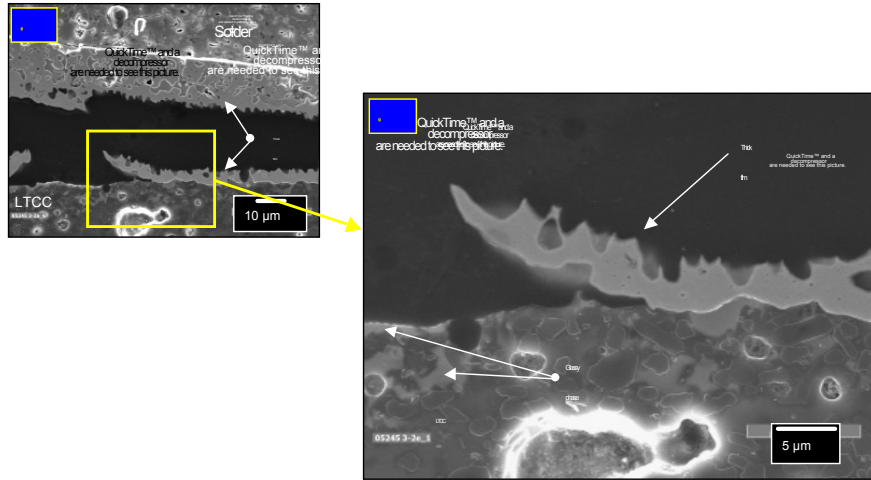
(b)
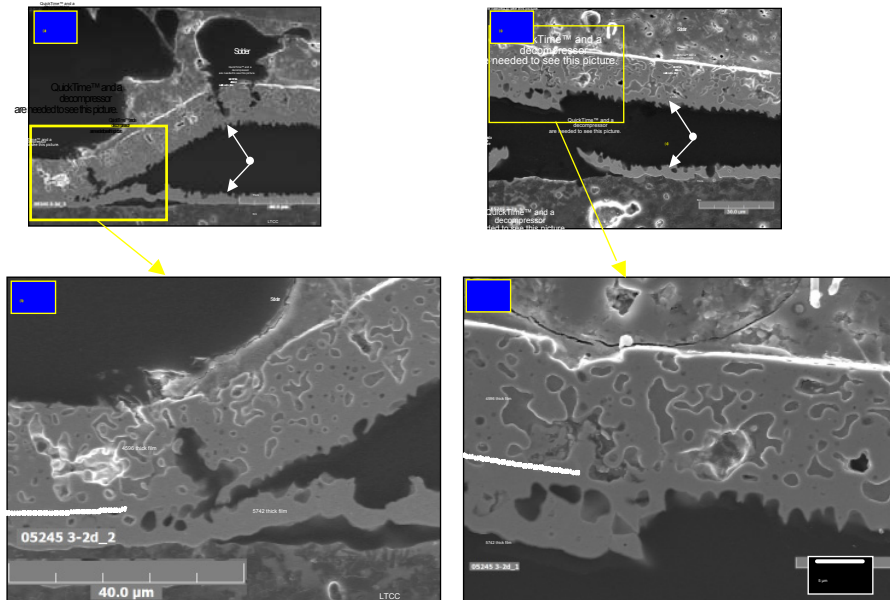
(c)

Fig. 25 (b) Single layers of 5742 and 4596 thick films; there was no via. The fracture progressed from left-to-right. (a) and (b) Medium and high magnification SEM/SE images identifying the transition region between the thick film/LTCC failure and failure between the 5742 and 4596 layers. (c) Low magnification SEM/SE images (a) and (c) and high magnification photographs (b) and (d) that illustrated the morphology of the fracture surface when failure occurred between the 5742 and 4596 layers. *(con't)*
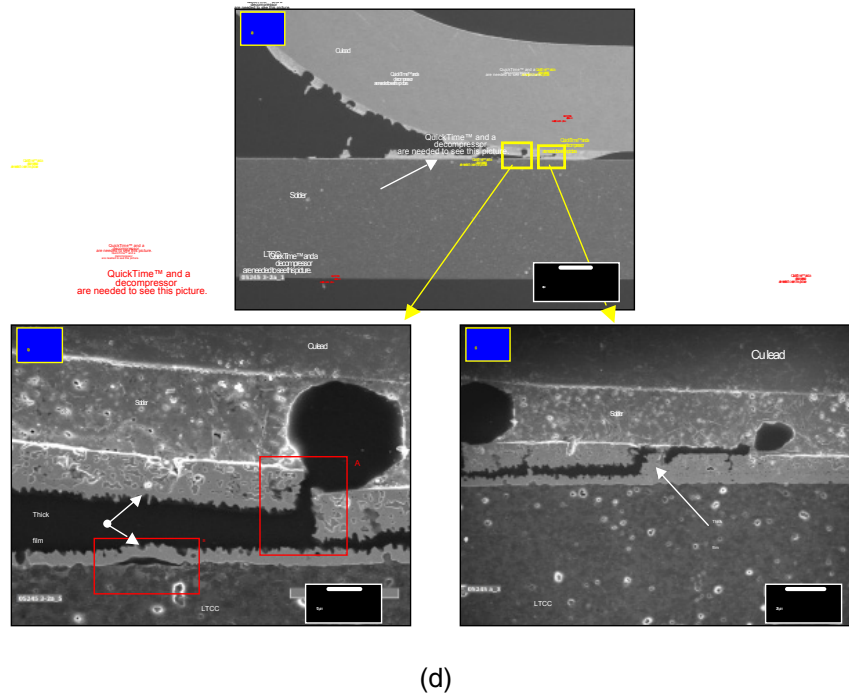
(d)
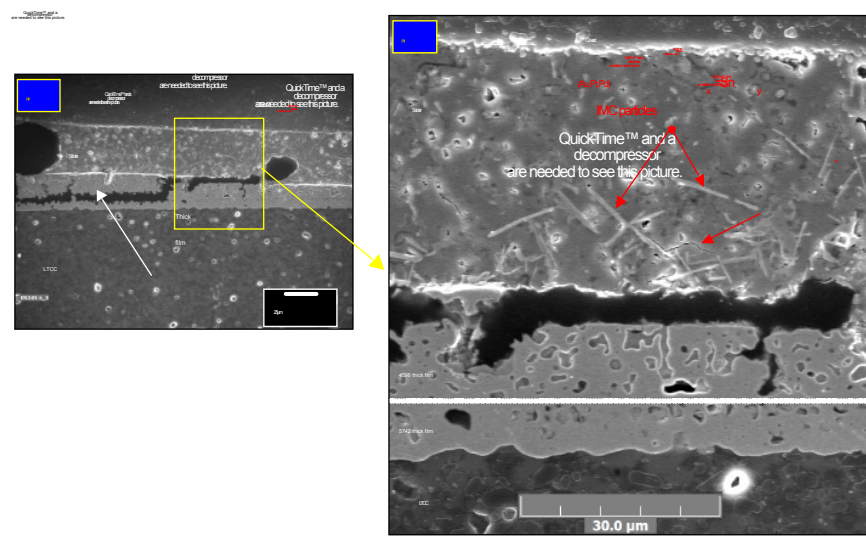
(e)

Fig. 25 (d) Single layers of 5742 and 4596 thick films; there was no via. The fracture progressed from left-to-right and the view is near the back end of the solder joint: the low magnification view in (a) identified the two shown at higher magnification in (b) and (c). (e) SEM/SE photographs of the solder/thick film separation: (a) low magnification image showing the location of the high magnification view in (b). The red arrows pointed to IMC needles as well as cracks in the solder.

High magnification photographs appeared in Fig. 25a (b) and (c) that showed failure between the 5742 and the 4596 layers. The red box labeled "A" indicated a region where fracture occurred at the 5742 thick film/LTCC interface. There was a larger concentration of the 4596 glassy phase under the 5742 thick film/LTCC separation. This observation was further exemplified by the high magnification images in Fig. 25b. The image in Fig. 25b (b) showed an extensive presence of 4596 glassy phase at the 5742 thick film/LTCC interface of the fracture, which suggested that the presence of the glassy phase lowered the strength of the interface, thereby allowing fracture to take place there rather than between the 5742 and 4596 layers. In fact, it appeared that failure occurred precisely between the 5742 thick film and the glassy phase that formed at the interface.

The images in Fig. 25c were used to examine, specifically, the fracture between the 5742 and 4596 layers. The low magnification images in (a) and (c) located the areas-of-interest that were then viewed at high magnification in (b) and (d), respectively. The particular observation made from Figs. 25c (b) and (d) (including Fig. 25b (b) which was the opposite side of a portion of the fracture surface in Fig. 25c (d)) was the "saw tooth" morphology to the fracture surface. The saw tooth morphology was generated by micro-void coalescence that often precedes the fracture of a very ductile material, in this case, the combined Au-based thick films. Those voids were not pre-existing in the thick film layer. This stipulation was confirmed In Fig. 25c (b), which indicated that the extent of voids in the thick film ahead of the crack (dotted white line) did not correspond to the "void-like' characteristics of the fracture surface behind the crack front. A similar conclusion was drawn in Fig. 25c (d), in which the uncracked region to the left of the separation (dotted white line) did not exhibit voids or even glassy phase particles that would correspond to the periodic saw tooth morphology of the fracture surface to the right side of either figure.

A second observation that was drawn from the saw tooth fracture morphology was that there was not a well-defined interface between the 4596 and 5742 thick film layers. Of course, this lack of "step-wise" change in material properties was not unexpected. The firing process step associated with the 4596 thick film caused inter-diffusion between the two layers that effectively washed-out any discrete interface.

A qualitative analysis was made to determine more precisely the location of the fracture path within the thick film layer, using Figs. 25c (b) and (d). Within both of those SEM/SE photographs, a dotted line was created that identified, approximately, the

boundary between the 4596 and 5742 layers. Per that dotted line, it appeared that the fracture occurred *within the 5742 layer, near its interface with the 4596 layer.* This trend would be expected, given the fact that a nearly pure Au 5742 layer would have a lower yield and ultimate tensile strengths than would the Au-Pt-Pd 4596 thick film alloy. The Pt and Pd additions would have contributed to solid-solution strengthening of the Au-based element.

The SEM/SE images in Fig. 25d were taken at the back portion of the pull tested solder joint. The location was identified by the low magnification SEM/SE image in Fig. 25d (a). The region of the interconnection shown in Fig. 25d (b) has the predominant failure mode, which was fracture within the thick film layer. Highlighted by the red box labeled "A" is the vertical fracture of the thick film layer caused by the combination of the void and bending of the Cu lead. Closer scrutiny of the region in the red box indicated that the separation within the thick film had occurred *prior to* the vertical fracture of the thick film, implying that the latter and, more importantly, the void above, did not directly affect the primary failure mode of separation in the thick film. The red box labeled "B" indicated a very localized region where the thick film had separated from the LTCC. There was evidence of the 4596 glassy phase under the 5742 thick film/LTCC separation. The SEM/SE image in Fig. 25d (c) shows the transition from the fracture path within the thick film to fracture at the solder/thick film interface.

A higher magnification view of the solder/thick film separation was illustrated via the two SEM/SE photographs in Fig. 25e. Besides showing details of the aforementioned failure mode, it was also apparent that there was a considerable quantity of $(Au, Pt, Pd)_x Sn_y$ IMC needles present in the solder. These IMC particles arose from dissolution of the thick film by the molten Sn-Pb solder during fabrication of the test sample and was not unexpected. The presence of these IMC needles suggested that the solder was likely strengthened by them through precipitation strengthening. Similarly, Au, Pt, or Pd, which were dissolved in the Sn-Pb solder, would have also contributed solid-solution strengthening of the joint. Although precipitated IMC needles were not observed in previously discussed specimens, it is likely that the solid-solution strengthening effect was active all of the test specimens to various degrees.

The pull tested solder joints were also examined on the sample formed with one 5742 layer and three layers of the 4596 thick film (no vias). The SEM/SE photographs were not shown in this report. The predominant failure mode – 75% and 100% for the two pull tested solder joints – was separation along the solder/thick film interface. One pull

test site had 25% of the bond line with a divot in the LTCC material. These failure modes concurred with observations compiled in Fig. 20, even the occurrence of failure within the LTCC. Separation within the 5742/4596 combined thick film layer was not observed in either of the two cross-sectioned solder joints.

The pull test failure modes were examined for those samples having a single printing of 4596 thick film over a via. The SEM/SE image in Fig. 26a (a) shows one of the two pull tested joints. A number of voids were observed in the solder of both joints; however, their propensity did not affect the fracture of the interconnection, except for the small vertical cracks in the thick film layer that were described earlier. At the test site shown in Fig. 26a (a), approximately 70% of the fracture occurred along the thick film/LTCC interface. The remaining 30% of the failure mode was separation at the solder/thick film interface. The fracture morphology of the other sample was 50% for both the thick film/LTCC and solder/thick film modes.
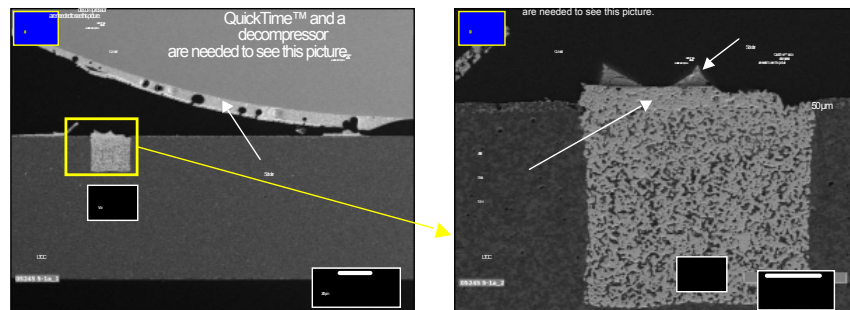
(a)

Fig. 26 (a) (a) Low magnification SEM/SE image showing the cross section of one of the pull tested solder joint made with a single layer of 4596 thick film over a via. The fracture progressed from left-to-right. (b) High magnification SEM/SE photographs showing the failure modes associated with via structure under the solder joint. *(con't)*
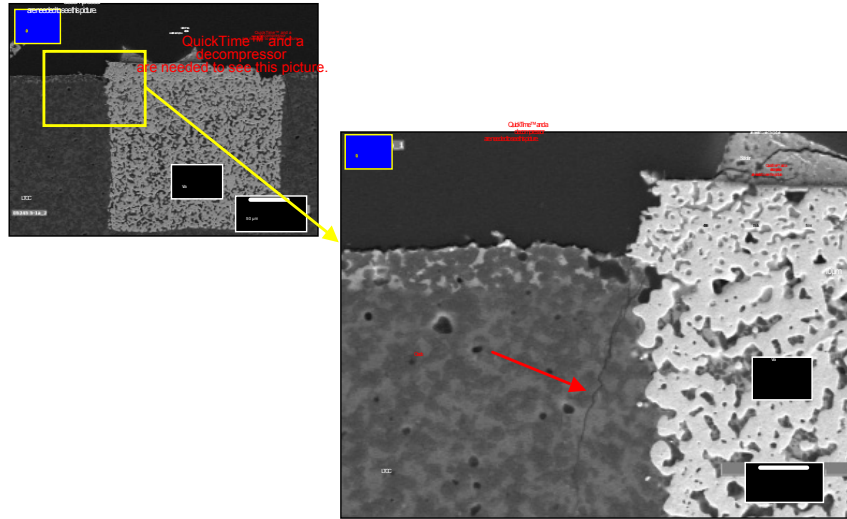
(b)
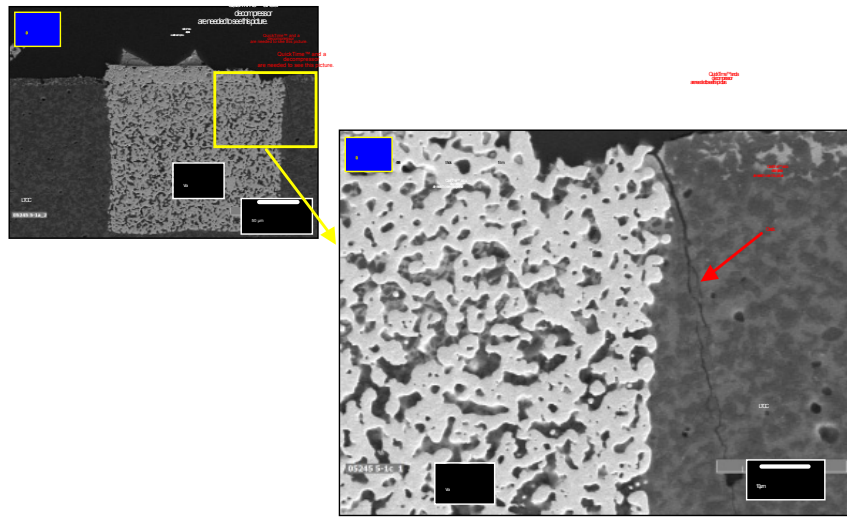
(c)

Fig. 26 (b) and (c) **(a)** Low magnification SEM/SE image showing the cross section of one of the pull tested solder joint made with a single layer of 4596 thick film over a via. The fracture progressed from left-to-right **(b)** High magnification SEM/SE photographs showing the side wall cracks of the via.

Because the solder/thick film failure mode dominated the front part of the joint, it was recorded in the visual inspection whereby the thick film/LTCC separation was not noted because of the difficulty of seeing further back into the fracture. The thick film/LTCC failure occurred at the 4596 glassy phase present along the interface.

It was observed in Fig. 26a (b), which is a higher magnification of the via structure of the interconnection, that the via fill and adjoining LTCC material were not damaged during the pull test. However, it was interesting to note that, over the via, fracture occurred by a combination of the following modes; ductile fracture of the solder; fracture at the solder/thick film interface; and even some fracture within the 4596 thick film. Therefore, the elimination of the glassy phase structure that characterized the 4596 thick film/LTCC interface, but which was not continuously present over the via, allowed for the multi-mode fracture morphology noted in Fig. 26a.

The SEM/SE images in Figs. 26b and 26c confirmed the presence of the side wall cracks in the vias (in the absence of the 5742 layer). As observed in prior studies, the cracks propagated through the glassy phase of the LTCC base material, having originated typically in a void at the via fill/LTCC interface. No other damage was recorded in either the via-fill or neighboring LTCC materials, thereby further substantiating the fact that side wall cracks did not affect, explicitly, the mechanical integrity of the interconnection.

The pull tested specimens were examined, which had the 5742 layer placed between the LTCC base material and a single layer of the 4596 thick film, and having a via in place. This specimen had the footprint ratio, 4596/5742, of 1.0:1.0. Low magnification SEM/SE micrographs were provided in Fig. 27, which show the overall failure modes of the two cross sectioned sites. In (a), the front of the solder joint exhibited a mixture of thick film/LTCC and solder/thick film failure modes; the remainder of the fracture progressed in the solder, at the solder/Cu lead interface. The second test site shown in (b) exhibited entirely a solder/thick film separation and the addition of an LTCC divot at the rear location of the joint. These observations were commensurate with the visual observations assessed in Fig. 20. The joints exhibited a nominal number of voids but, as in the previous cases, the voids did not appear to affect the fracture behavior of the joint.
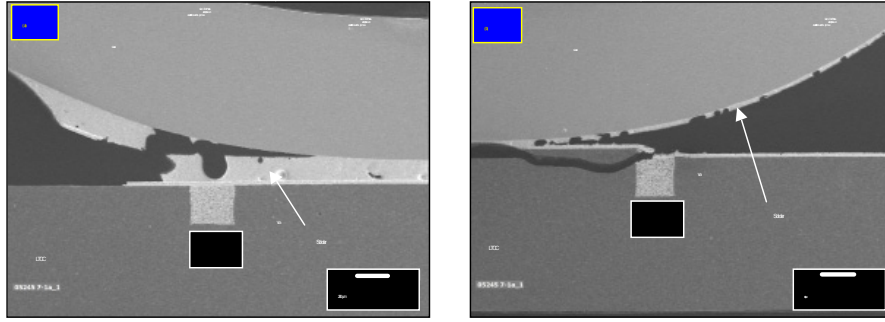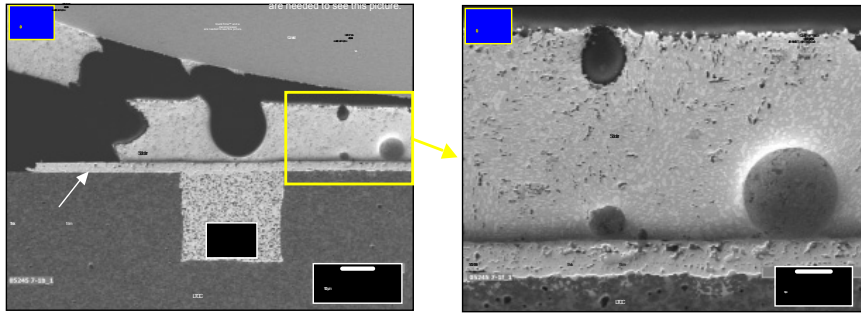
Fig. 27 **(a)** and **(b)** Low magnification SEM/SE photographs showing failure of the two solder joints constructed with single layers of 5742 and 4596 over LTCC that contained a via under the interconnections. This specimen had the footprint ratio, 4596/5742, of 1.0:1.0.

High magnification SEM/SE photographs were used to examine specific locations in the two interconnections shown in Fig. 27. Shown in Fig. 28a **(b)** is an image of the solder failure mode, the location of which was identified in **(a)**, as initially presented in Fig. 27 **(a)**. The fracture occurred near the solder/Cu lead interface. There were no indications of damage in the solder, thick film, or LTCC materials. Also, the respective interfaces between these material structures did not exhibit delamination.

A closer examination of the side wall regions neighboring the via was made via the SEM/SE images in Fig. 28b. No cracking was observed in the LTCC material. The red boxes labeled "A" exemplified regions in which the glassy phase from the 4596 layer had apparently bypassed the 5742 layer and diffused into the LTCC material. The occurrence of this artifact was more frequent in this particular specimen, relative to all of the other interconnections evaluated in this study. There was no degradation to the via structure.

The second solder joint, which was shown in Fig. 27 **(b)**, exhibited failure that was entirely along the solder/thick film interface. A low magnification SEM/SE photograph of the joint was provided in Fig. 29 **(a)**; a high magnification view of the fracture surface was shown in Fig. 29 **(b)**. The approximate demarcation between the 5742 and 4596 layers was noted in the photograph.

(a)
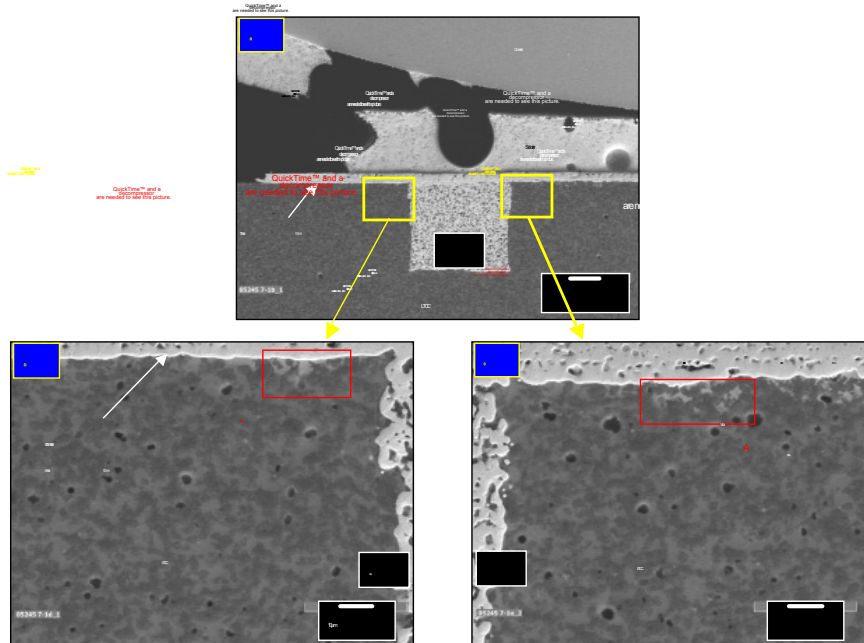
(b)

Fig. 28 (a) **(a)** Low magnification SEM/SE photograph of a region examined at higher magnification in **(b)** showing the solder failure mode. The solder joint had single layers of 5742 and 4596 over a via. This specimen had the footprint ratio, 4596/5742, of 1.0:1.0. (b) **(a)** Low magnification SEM/SE photograph locating the side wall regions of the via. High magnification photographs **(b)** and **(c)** showed the via side wall areas. The red boxes labeled "A" indicated regions in which the glassy phase of the 4596 layer appeared to have diffused past the 5742 layer, and into the LTCC base material.

Small, intermittent sections of solder remained attached to the thick film. There was no damage observed within thick film layers, the mutual interface between the individual 4596 and 5742 layers, or at the interface between the 5742 layer and the LTCC base material. Although not shown here, an examination of the side wall region of the via did not reveal crack damage.
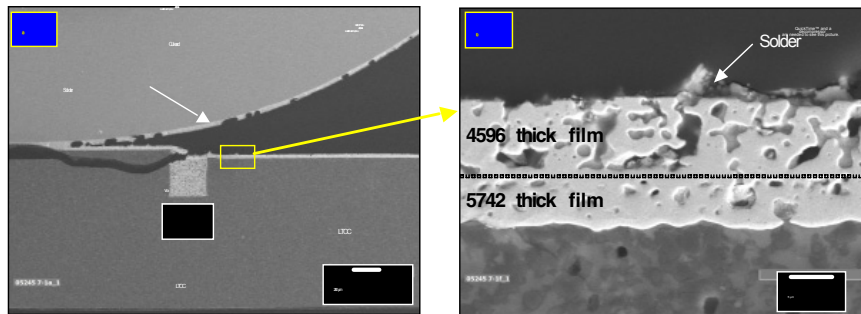
Fig. 29 (a) Low magnification SEM/SE photograph of the failure of the joint having single layers of 5742 and 4596 over a via. The footprint ratio was 4596/5742, of 1.0:1.0.   (b).   High magnification SEM/SE image of the solder/thick film fracture morphology.

The discussion of the LTCC divot failure mode that was observed in the second solder joint (Fig. 27 (b) and Fig. 29) will be postponed until later in the analysis.

The pull tested samples were examined, which had a ratio of 1.0:0.5 for the annular regions of the 4596 and 5742 thick film footprints. Shown in Fig. 30a (a) is a low magnification SEM/SE image of one of the two solder joints. The extent of the 5742 layer was noted by the green lines. The fracture path progressed from the left to the right of the image. In this particular sample, approximately 60% of the bond line exhibited the solder/thick film failure mode; 30% was failure in the solder at its interface with the Cu lead; and the final 10% (red arrow) was failure at the thick film/LTCC interface. In the last case, the 4596 thick film was located on the LTCC as that layer extended beyond the 5742 footprint.

4596 thick film

5742 thick film

Solder

4596 thick   film

5742 thick   film
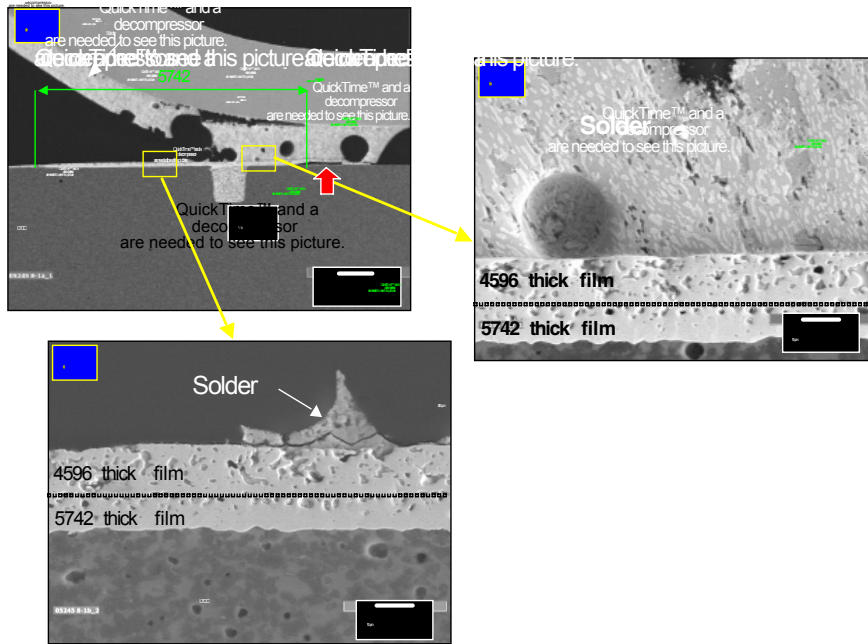
(a)

Fig. 30 (a) (a) Low magnification SEM/SE photograph of the pull tested sample having single layers of 5742 and 4596, and footprint ratio of 4596:5742 equal to 1.0:0.5. (b) High magnification image showing the solder joint structure to the right of the via. (c) High magnification photograph showing the solder/thick film fracture surface. Pieces of solder remained attached to the thick film surface. *(con't)*
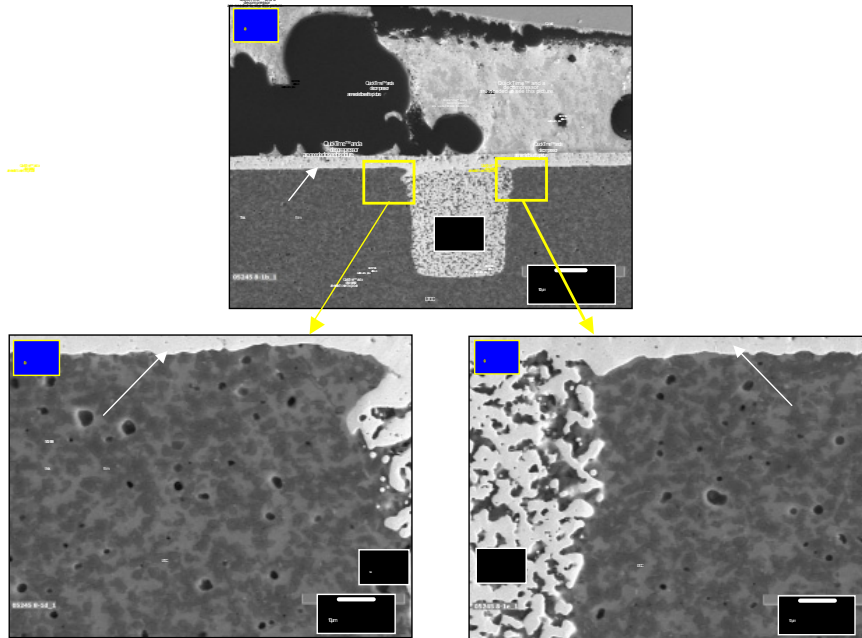
(b)

Fig. 30 (b) (a) Medium magnification image of the solder joint structure over the via and the via structure. (b) and (c) High magnification images showing the side wall regions of the via and the absence of cracking there.

It should be noted that the void in the center of the photograph was not that large prior to the pull test. Rather, the void was extended as a result of deformation to the solder. These failure mode extents were in-keeping with the visual inspection results shown in Fig. 20.

The photograph in Fig. 30a (b) shows the solder joint structure near the thick film layers. A line marked the approximate boundary between individual 5742 and 4596 layers. The solder, thick film layers, and LTCC did not exhibit cracking; their mutual interfaces also did not show evidence of delamination.

The high magnification SEM/SE photograph in Fig. 30a (c) was taken at the solder/thick film failure site as denoted in (a). In spite of the relatively severe condition placed on the structure due to the pull test, the 4596 and 5742 layers did not separate from one another nor did the 5742 separate from the LTCC base material. Along the fracture surface, pieces of solder remained attached to the 4596 thick film surface. Although these isolated regions of remaining solder showed an overall morphology of ductile tearing, brittle cracks were also noted in the photograph. The cracks resulted

67

from regions of solder that had become embrittled due to the dissolution of the Au, Pt, and Pd components from the nearby 4596 thick film layer. Finally, as was also the case in Fig 30a (b), there were very few areas in which the glassy phase belonging to the 4596 material had diffused past the 5742 layer and into the LTCC base material.

Two other observations were made from Fig. 30a that were worth noting. First, near the location of the red arrow in (a), the failure mode transitioned from fracture along the solder/thick film interface to a thick film/LTCC failure path. This transition occurred where the 5742 layer had already ended, causing the fracture path to occur at the 4596 thick film/LTCC interface. As in those previous cases, the latter separation occurred specifically between the metal and glassy phase layers.

The second observation was that, under the void, the separation at the 4596 thick film/LTCC interface ceased. The solder material around the void had deformed, thereby preventing the entire magnitude of applied stress from being imposed onto the thick film layer located under the void. This was a very localized phenomenon and occurred well to the rear of the joint. Otherwise, as in previous cases, voids in the solder did not have an appreciable effect on the fracture behavior of the samples.

The SEM/SE photograph in Fig. 30b (a) was a medium magnification image of the solder joint in Fig. 30a (a), showing the solder joint structure above the via and the via structure, itself. It was observed that the crack path was located near the solder/Cu lead interface, but still remained in the solder. In fact, ductile tearing of the solder was quite evident along the fracture path. There was no indication of damage to the via or the thick film layer over it that would have resulted from the pull test, confirming that this "junction of different materials" was very robust.

The high magnification images in Figs. 30b (b) and (c) showed the side wall regions of the via. Side wall cracking was not observed in either image.

The sample, which was fabricated having the single layers of both 5742 and 4596 thick films over a via and 4596/5742 ratio of 1.0:0.2, was examined next. The two pull tested interconnections were shown in Fig. 31. The location of the 5742 layer footprint boundary was designated by the green lines. Slightly more-numerous voids were observed in the solder. However, the sizes of the voids in Fig. 31 were not representative of voids at the time of joint fabrication because the voids in Fig. 31 were distorted during deformation of the solder. Instead, reference should be made to the

microstructure shown in Fig. 13, which was more representative of the extent of voids in Fig. 31 prior to testing. The test samples represented in Figs. 31 and 13 had similar gap thicknesses.
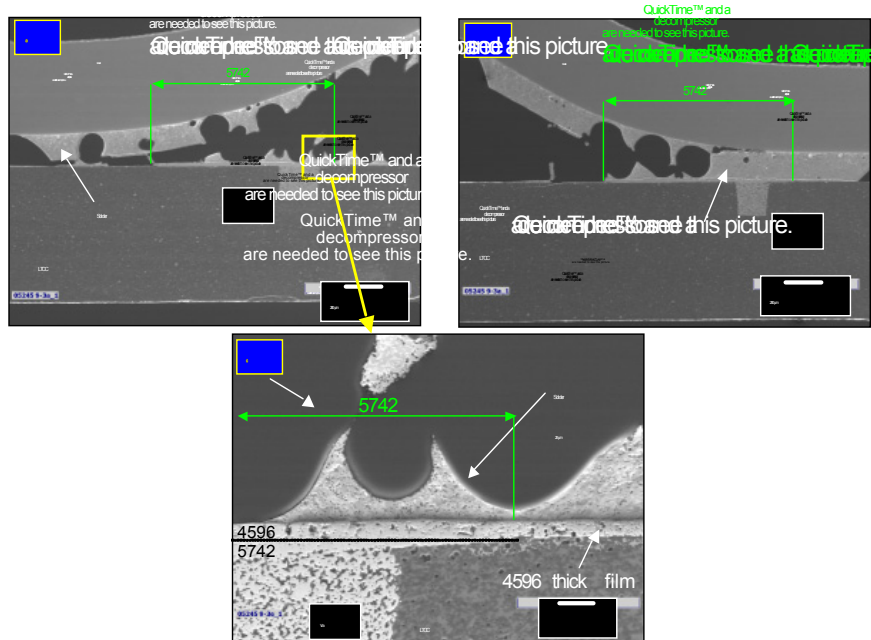
Fig. 31 (a) and (b) Low magnification SEM/SE photographs of two pull tested solder joints on a sample having single layers of 5742 and 4596, but with a footprint ratio of 4596:5742 equal to 1.0:0.2. (c) High magnification photograph showing the solder joint structure at the via.

Fracture within the solder or at the solder/Cu lead interface contributed significantly to the overall failure of both interconnections. The predominant failure mode noted in Fig. 20 was that of solder/thick film separation. The discrepancy was understandable because the failure occurred near thick film rather than near the solder/Cu lead interface. Also, it was observed that, where the 5742 layer was present, the thick film/LTCC failure mode was absent. Interestingly enough, beyond the 5742 layer where the 4596 layer was bonded to the LTCC, the thick film/LTCC failure mode did *not* predominate. Instead, solder failure and solder/thick film separation modes were observed at those locations – see Figs. 31 (a) and (b).

The high magnification SEM/SE image in Fig.31 (c) was taken at the via location. The lateral diffusion of 4596 thick film glassy phase under the 5742 layer was evident at the latter's boundary that was demarked by the green lines. However, there were no indications of side wall cracking in the via. Also, the entire via structure was very

robust because the loads imposed by the pull test did not cause damage to any of the materials nor their respective interfaces. Lastly, it was observed that the fracture of the solder away from the thick film was ductile, having no signs of brittle cracking. Therefore, the brittle cracks that were observed in the Sn-Pb solder remnant observed previously – e.g., Fig. 30a (c) – were localized near the solder/thick film interface, at least for the thicker joint gaps.

The next sample pedigree was that of a single layer of 5742 followed by three layers of the 4596 thick film, all over a via in the LTCC material. The predominant failure mode was separation at the solder/thick film interface, which accounted for 50% and 75% of the fracture in the two respective samples. The first sample was illustrated in Fig. 32a. The low magnification SEM/SE image in Fig. 32a (a) shows the fracture morphology. The failure mode transitioned from solder/thick film separation to a combination of solder failure and cracking in the LTCC material. The joint failure propagated from right-to-left except for the divot crack in the LTCC material. The latter cracking was further investigated with the assistance of images (b) and (c) in Fig. 32a. The crack originated at the location shown in Fig. 32a (b), where the glassy phase from the overlapping 4596 thick film had locally infiltrated the LTCC material. The crack terminated in the thick film in Fig. 32a (c), resulting in a separation between the 4596 and 5742 layers.

The SEM/SE images in Fig. 32b targeted the via structure under the solder/thick film fracture path. The image in (b) shows the via. There was no damage to the via nor surrounding LTCC material, including an absence of side wall cracks. A high magnification photograph was provided in Fig. 32b (b) that showed the thick film layers above the via. Fracture was not observed within the 4596 or 5742 layers or in the via-fill material as well as at their respective interfaces. The solder remnants that remained attached to the 4596 layer, showed ductile fracture on the macro-scale. However, on the micro-scale, there were brittle cracks near the solder/thick film interface. The brittle cracks likely originated from a localized region of embrittled solder caused by the dissolution of Au, Pt, and Pd that originated from the 4596 thick film layer.

The companion pull tested solder joint to that in Fig. 32 exhibited a 75% solder/thick film failure mode. The remaining 25% of the fracture surface was culmination of fracture in the LTCC; ductile separation between the 5742 and 4596 layers where the LTCC crack terminated as was observed in Fig. 32a (c); and solder/thick film failure. That fracture morphology is shown in Fig. 33. The pull test crack progressed from left to right.
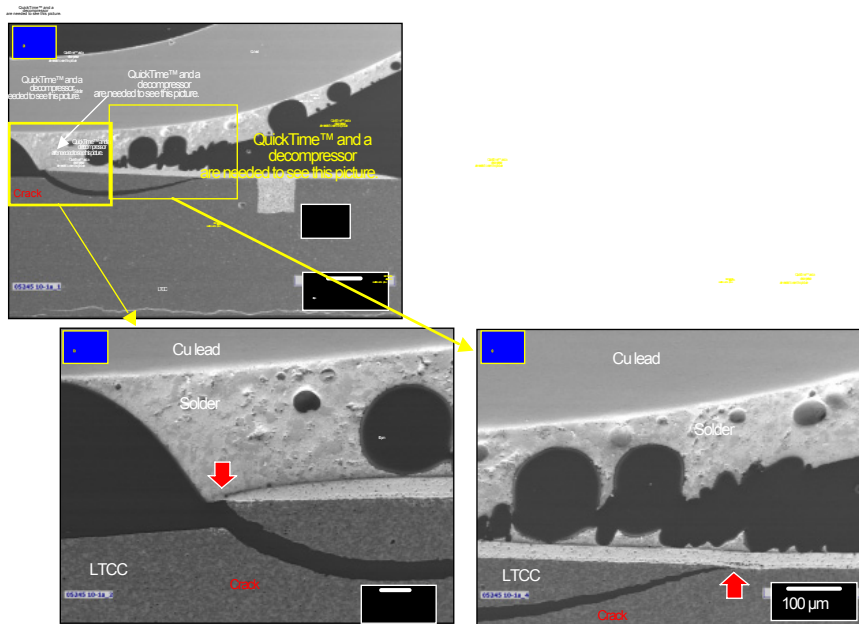
(a)

Fig. 32 (a) (a) Low magnification SEM/SE photographs of the pull tested solder joint on a sample having a single layer of 5742 and three layers of 4596 thick film over the via. The footprint ratio of 4596:5742 was equal to 1.0:1.0. (b) and (c) High magnification photographs showing the initiation and termination points, respectively, of the LTCC crack as indicated by the red arrows. *(con't)*

4596 thick film

5742 thick film

30.0 µm
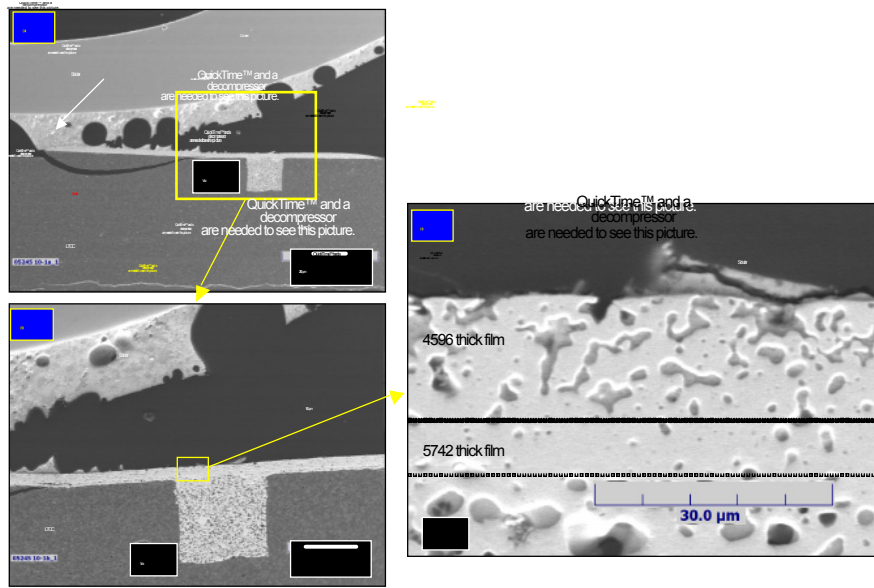
(b)

Fig. 32 (b) **(a)** Low magnification SEM/SE image locating the area of interest, which was the via structure. **(b)** Medium magnification image showing the via structure. **(c)** High magnification image of the thick film layers over the via. Remnants of the solder were observed that remained attached to the 4596 layer. (The sample had a single layer of 5742 and three layers of 4596 thick film over the via. The footprint ratio of 4596:5742 was equal to 1.0:1.0.)

A close examination of the fracture path in Fig. 33 indicated that at no point was there separation between the 5742 layer and the LTCC. The 5742/4596 separation transitioned into the start of the divot crack in the LTCC material at the location labeled with red box "A". At that point, the gray contrast indicated the diffusion of the 4596 glassy phase into the base material. Thus, it was concluded that, like the crack initiation behavior discussed with respect to Fig. 32a **(b)**, the presence of the 4596 glassy phase weakened the LTCC material.
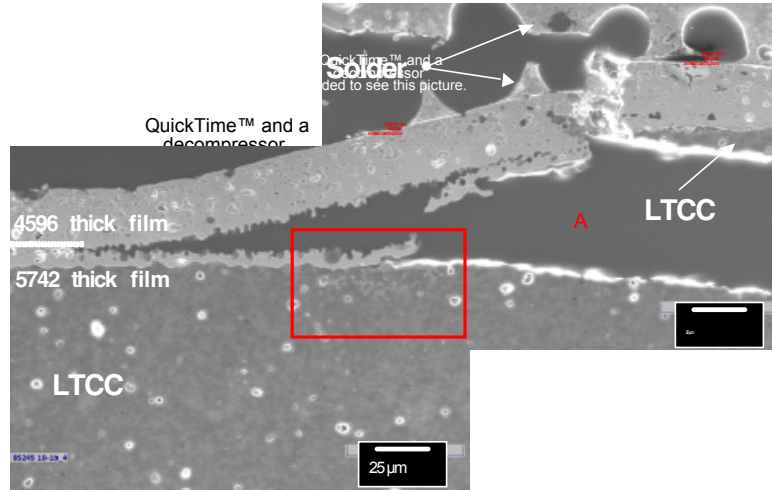
Fig. 33 SEM/SE photograph of the second pull tested solder joint on a sample having a single layer of 5742 and three layers of 4596 thick film over the via. The fracture path of the *overall* interconnection progressed from left-to-right. The area showed the combination of the following failure modes: solder/thick film interface separation; fracture between the 5742 and 4596 thick film layers; and a divot crack in the LTCC base material. The red box labeled "A" indicated a region of 4596 glassy phase diffusion into the LTCC, which coincided with the initiation of the LTCC divot crack.

The pull tested samples were also examined for which, there were three 4596 layers over the reduced annular extents of the single 5742 layer. The first case was the 4596:5742 ratio of 1.0:0.5. A low magnification, SEM/SE photograph was provided in Fig. 34a (a) that showed the overall fracture morphology. Sixty-six percent of the fracture occurred along the solder/thick film interface. The remaining 33% exhibited a combination of LTCC divot and continued solder/thick film separation. Because creation of the divot would have required that the solder joint above it remain intact, the divot was likely created prior to separation at the solder/thick film interface. Therefore, the failure mode was recorded as 66% solder/thick film separation and 33% LTCC divot crack. The second pull tested joint, which was not exhibited here, exhibited 80% failure in the solder due to a heavier than normal occurrence of voids; the remaining 20% of the fracture occurred at the solder/thick film interface.

73

(a)

(b)

Fig. 34 (a) **(a)** Low magnification SEM/SE photograph of the pull tested solder joint on a sample having a single layer of 5742 and three layers of 4596 thick film over th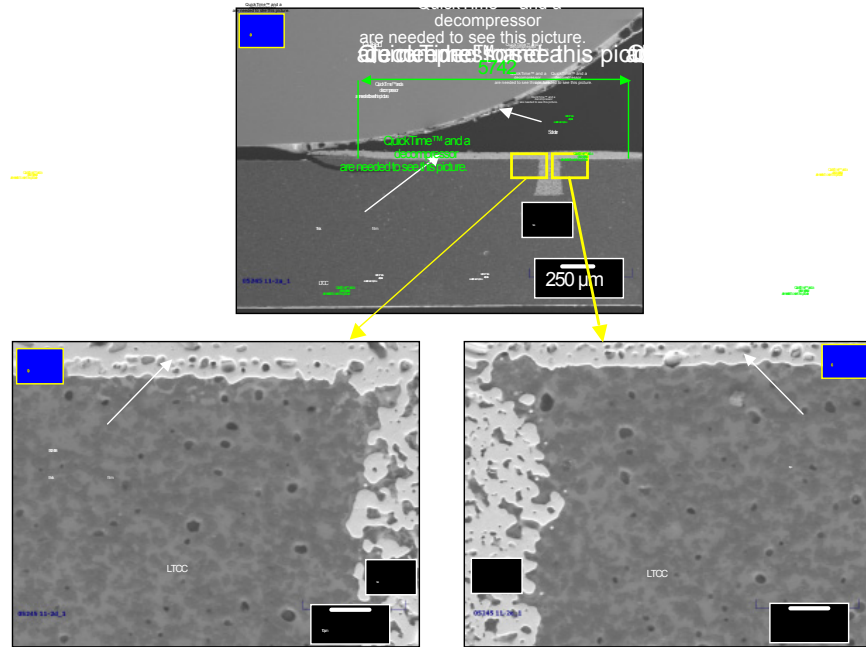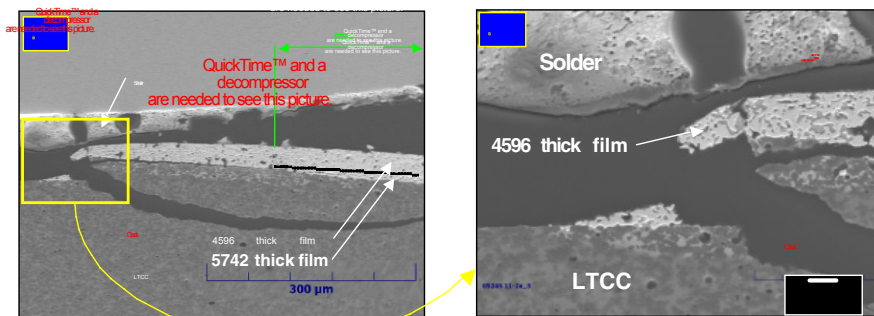e via. The footprint ratio of 4596:5742 was equal to 1.0:0.5. The green lines indicate the location of the 5742 thick film footprint. **(b)** and **(c)** High magnification photographs show the side wall regions of the via. (b) **(a)** Low magnification SEM/SE image showing the LTCC divot crack. **(b)** High magnification image showing the initiation point of the LTCC crack. Limited crack propagation was also observed at the thick film (4596)/LTCC interface.

The side wall regions of the via were shown in Fig. 34a (b) and (c) photographs. There were no signs of crack development. Isolated regions were observed along the 5742/LTCC interface at which, the glassy phase of the 4596 thick film had diffused in the LTCC base material.

The micrographs in Fig. 34b displayed the characteristics of the LTCC divot crack. The low magnification photograph in (a) showed that the edge of 5742 layer was located some distance away from the crack initiation site. The pull test resulted in an overall crack direction that was right-to-left; however, the LTCC divot crack propagated from left-to-right. The concurrent solder/thick film failure mode could also be observed. The high magnification image in Fig. 34b (b) provided additional information on the cracking process by targeting the crack initiation point. The crack began at the 4596 thick film/LTCC interface. Then, the crack progressed a short distance into the LTCC where it separated into two paths. The primary path continued into the LTCC, creating the divot. The second path had a crack return to the thick film/LTCC and progress a short distance there.

More specifically, it appeared that the initiation of the LTCC divot crack was in the 4596 glassy phase at the 4596 thick film/LTCC interface. The "ease" of crack propagation along that interface was evidenced by the secondary crack, which was observed to continue to propagate along the thick film/LTCC after cracking in the LTCC had commenced.

Another observation that was drawn from Fig. 34b and, which was equally applicable to Fig. 32b, was that the LTCC divot cracks originated at the "back end" of the solder joint. Reviewing Fig. 4, it would be expected that the maximum tensile load, which would maximize the Mode I cracking stresses, would occur at the front of the solder joint. Once failure of the joint begins and the separation propagates towards the back end, a shear or Mode II component will develop to the moving crack front as the latter becomes non-aligned with the pulling force vector. That Mode II component would be maximized at the back end location, which is where the divot cracks have been observed to initiate in the test samples. This observation implied that the Mode II (shear) stress component, when combined with the residual Mode I stress component, likely had a role in the initiation of the LTCC divot crack, particularly with the presence of the 4596 glassy phase and the 4596 thick film/LTCC interface.

It would be expected that the Mode II stresses, like the Mode I stresses, would be enhanced as the gap became thinner because of the increasing plain strain load condition placed on the solder. The plain strain condition increases the apparent strength of the solder alloy, thereby reducing the latter's ability to deform under the load. The result is that more of the applied load would be transferred to the thick film/LTCC interface and LTCC material. It was not possible to confirm this hypothesis through the limited number of samples available in this study.

The pull tested samples were examined, which were fabricated with a single 5742 layer and three prints of the 4596 thick film. In this case, however, the 4596/5742 ratio of annular dimensions was shortened to 1.0:0.2. The SEM/SE micrograph in Fig. 35a (a) showed the multiple failure modes that were observed in these solder joints. The failure propagated from left-to-right. Approximately the front 50% of the fracture path was characterized by fracture in the solder and solder/Cu lead interface. Again, the voids were larger than they were at the time that the joint was assembled due to their distortion resulted from deformation of the solder during the pull test. The solder/Cu lead fracture morphology was shown in Fig. 35a (b). The separation actually occurred in the solder near to its interface with the IMC layer. This morphology corresponded to the predominance of the failure mode #2 in Fig. 20.

(a)
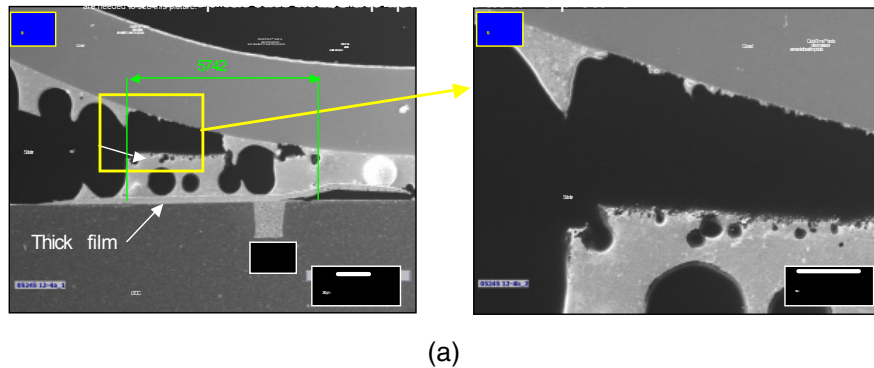
Fig. 35 (a) (a) Low magnification SEM/SE photograph of the pull tested solder joint on a sample having a single layer of 5742 and three layers of 4596 thick film over the via. The footprint ratio of 4596:5742 was equal to 1.0:0.2. The green lines indicate the location of the 5742 thick film footprint. (b) High magnification image of the solder/Cu lead failure mode. *(con't)*
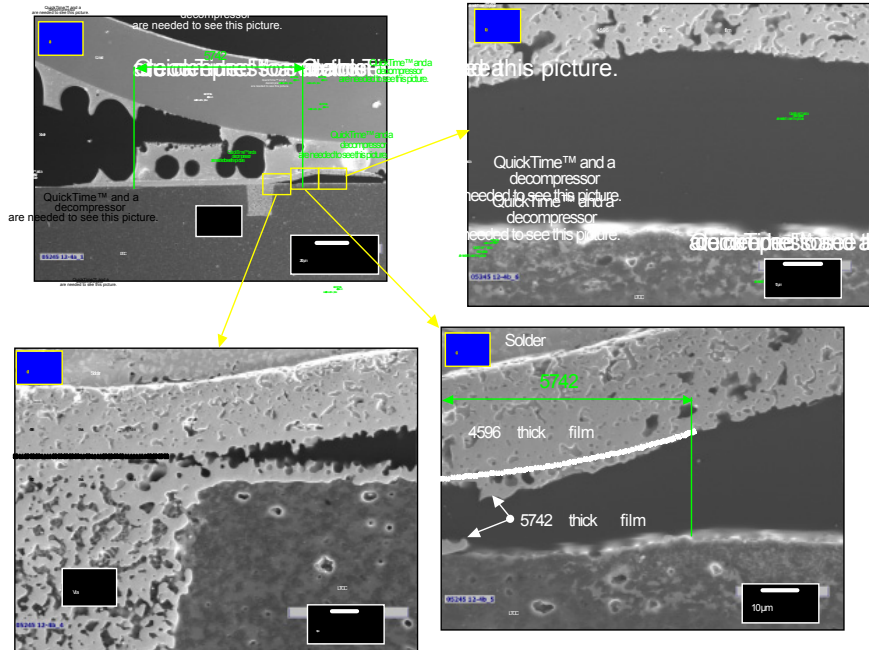
(b)
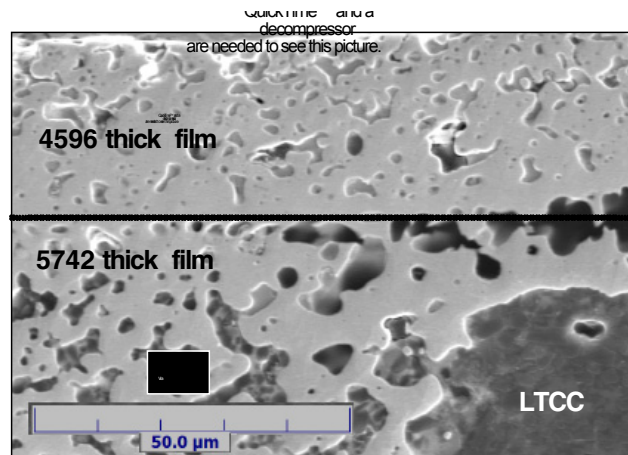
(c)

Fig. 35 (b) **(a)** Low magnification photograph identifying areas of interest at the rear location of the fracture path. **(b)**, **(c)**, and **(d)** High magnification SEM/SE images showing crack propagation towards the via. (c) High magnification SEM/SE image showing initiation of the separation between the 5742 and 4596 layers. (The sample had a single layer of 5742 and three layers of 4596 thick film over the via. The footprint ratio of 4596:5742 was equal to 1.0:0.2. The green lines indicate the location of the 5742 thick film footprint.

The sequence of SEM/SE photographs in Fig. 35b describe the fracture morphology at the rear location of the solder joint. In fact, the morphology indicated that fracture propagated in the *reverse* direction, that is, from the rear boundary back to the via in the sequence of photographs: (b), (c), and (d). Fracture began with separation between the 4596 thick film and the LTCC base material where the 5742 thick film pad did not extend ((b)). The extent of glass phase, which included the two different particle morphologies, was clearly evident under the 4596 thick film layer. At the boundary of the 5742 layer ((c)), the fracture path transitioned to separation between the 5742 layer and the 4596 layer which progressed to the via ((d)). This transition confirmed the higher strength of the 5742 thick film/LTCC interface vis-à-vis the 4596 thick film/LTCC interface. The latter micrograph also confirmed the absence of side wall cracks, or any other damage for that matter, around the vias.

A high magnification SEM/SE photograph of the crack front between the 5742 and 4596 thick film layers was provided in Fig. 35c. The photograph showed microvoid coalescence that characterized the ductile fracture within the 4596/5742 thick film structure.

Several points were worth noting with respect to Fig. 35b. First of all, it was clear that, like the case in Fig. 34, the stress state generated by the pull on the Cu wire initiated failure at the rear location of the solder joint as well as at the front location. Instead of culminating into an LTCC divot crack, the 1.0:0.2 ratio provided an ample bond line of the weaker 4596 thick film/LTCC interface for crack propagation. Fracture then propagated towards the via, where the interface separation was arrested by the "presence" of the 5742 layer and the superior strength of its interface with the LTCC material. The fracture then transitioned into failure between the two thick film layers.

Second, the photographs in Fig. 35b (b) and (c) showed the extensive penetration of the 4596 glassy phase into the LTCC in the absence of the 5742 layer. Both large and small glassy phase particle morphologies were observed, the former being created at the "front" of the glassy phase region and the latter having developed closer to the thick film/LTCC interface. At first, it appeared from the image in Fig. 35b (c) that a divot of LTCC had been removed from the base material at the boundary marking the start of the 5742 thick film. However, the LTCC divot could not be identified as it would have remained attached to the underside of the separated 5742 layer. A review was made of other boundaries at the end of the 5742 layer, namely, Figs. 12d, 13a, 13b, and 31. The thick film/LTCC interface did not line up between the 5742 layer and the 4596 layer

beyond the latter. This non-alignment suggested that the LTCC base material had *expanded* under the 4596 thick film. The likely source of this expansion or swelling was the diffusion of the 4596 glassy phase into the LTCC material. There was no evidence of the reverse process, that is, that firing of the 4596 layer resulted in a diffusion of LTCC base material (glassy phase) into the 4596 thick film. Under the circumstances of 4596 glassy phase diffusion and LTCC expansion, it could be hypothesized that residual stresses would be generated along the 4596 thick film/LTCC interface as well as within the nearby LTCC material. Such stress would be potential sources of the 4596 thick film/LTCC interface failure mode and divot cracks in the underlying LTCC base material, respectively.

Third, failure between the 5742 and 4596 thick film layers was ductile in nature (Fig. 35b (d)). Microvoid coalescence created the free surface that culminated into the crack between the two thick film layers. There was no separation between the 5742 layer and the via-fill material. These latter observations were more readily apparent in the high magnification SEM/SE photograph in Fig. 35c.

The mechanical properties of the 5742 thick film by itself were investigated with use of the 50In-50Pb solder in place of the Sn-Pb alloy. The In-Pb solder exhibits a greater resistance to dissolution of the 5742 material. The Cu leads were Ni-Au plated prior to assembly; the Au layer was not removed by hot solder dipping prior to the attachment of the wire to the pad. Three failure modes were predominant: solder/Cu lead failure; solder/thick film failure; and thick film/LTCC separation. The two low magnification SEM/SE images in Fig. 36 illustrated each of these failure modes. The extent of voiding in the In-Pb solder joints was comparable to that observed in the Sn-Pb interconnections. With respect to the first two failure modes, the fracture path was located specifically at the solder/Au-In IMC layer that formed between the solder and either the Au plated layer on the Cu lead or between the 5742 thick film.
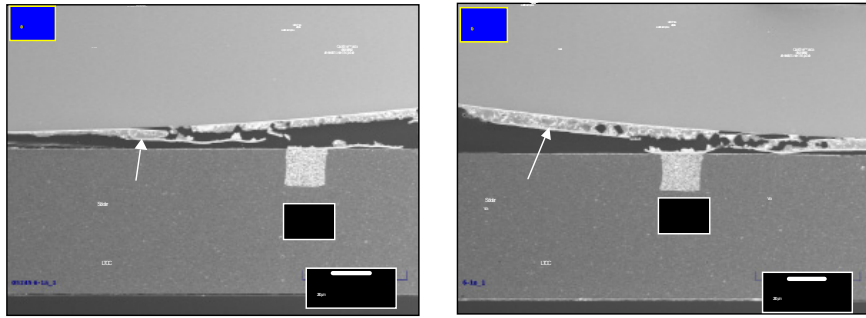
Fig. 36 (a) and **(b)** Low magnification SEM/SE photographs showing the pull tested solder joints on samples having a single 5742 thick film layer over a via. The solder was the 50In-50Pb (wt.%) composition.

The sequence of SEM/SE photographs in Fig. 37a show the details of the joint in Fig. 36 (a), specifically, the failure surface above the via. The overall fracture of the joint due to the pulling of the Cu lead was from right-to-left. The image in Fig. 37a (c) showed that the 5742 layer remained attached to the via-fill material, and that separation at the solder/5742 interface occurred at the solder/Au-In IMC interface[1]. It was clear in Fig. 37b (b) that the 5742 layer had a better adhesion to the via-fill surface than to the LTCC surface.

The photographs in Fig. 37b targeted the upper reaches of the side wall regions next to the vias as can be referenced by the low magnification view in (a). In the image in Fig. 37b (b), the separation of the 5742 layer occurred cleanly at the interface with the LTCC base material. A red arrow identified a crack that was observed in the LTCC material. This crack originated from the 5742 thick film/LTCC interface and not from the via. A similar crack was observed to the other side of the via as shown in Fig. 37b (c). In both cases, the cracks did not have the morphology of side wall cracks associated with vias. Also, the failure mode in Fig. 37b (c) was a combination of thick film/LTCC fracture and separation between the In-Pb solder and the 5742 thick film. Therefore, these two interfaces had comparable strengths.

---

[1] It was also interesting to note that small particles developed at the cusps of the IMC scallops that had formed between the 5742 layer and the In-Pb solder. The particles did not appear to have had an effect on the mechanical performance of the solder joint. Their composition was not determined, although it was speculated that they were either rejected Pb from the solder or a non-reacting component of the 5742 thick film layer.

80

The solder joint in Fig. 36 (b) was similarly evaluated, using the SEM/SE photographs in Figs. 38a and 38b. The failure modes were very similar.

The micrograph (b) in Fig. 38b showed a crack next to the via, which had the same morphology of the side wall cracks typically associated with the 4596 thick film. A similar crack was not observed on the diametrically opposing position as shown in Fig. 38b (b). Therefore, if that crack was, in fact, a manifestation of the traditional side wall crack, then it was of a lesser magnitude since it did not propagate around the entire circumference of the via. Otherwise, no other degradation was recorded in the interconnections shown in Figs. 37 and 38.
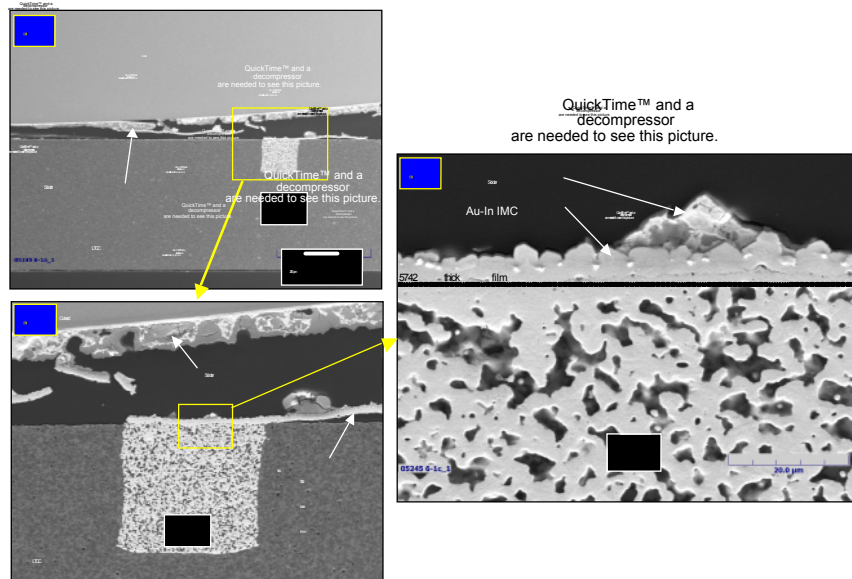
(a)

Fig. 37 (a) (a) Low magnification SEM/SE photograph of the pull tested solder joint on a sample having a single layer of 5742 and made with the 50In-50Pb solder (over a via). (b) and (c) High magnification images showing the fracture path above the via. *(con't)*
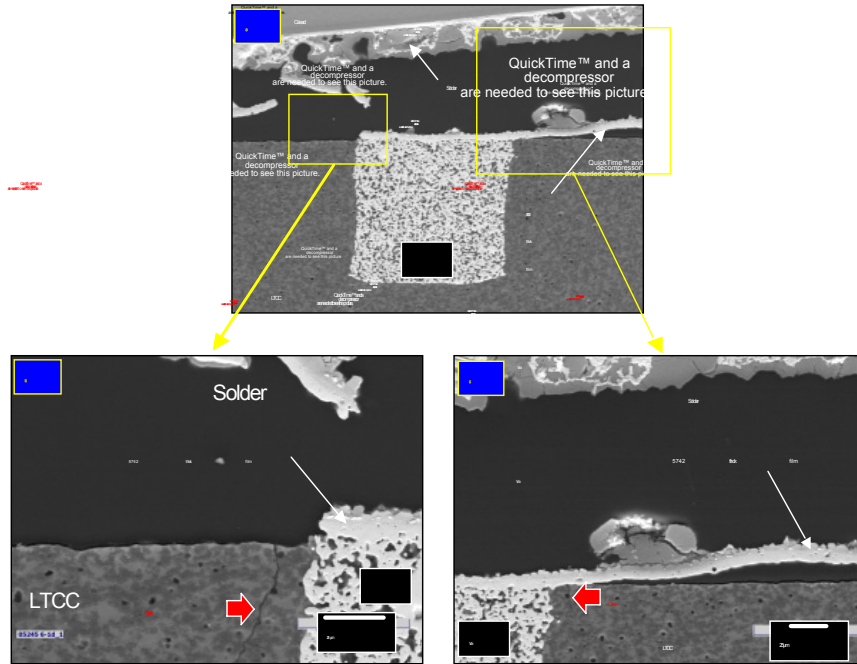
(b)

Fig. 37 (b) (a) Low magnification photograph identifying the fracture path to either side of the via. (b) and (c), High magnification SEM/SE images showing the top side regions of the via side wall. Cracks were identified by red arrows. (The sample had a single layer of 5742 and made with the 50In-50Pb solder (over a via).
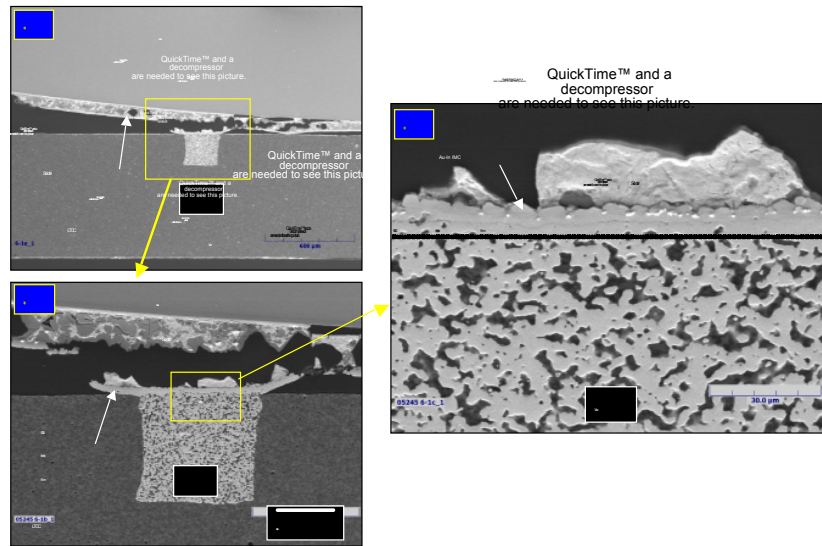
(a)
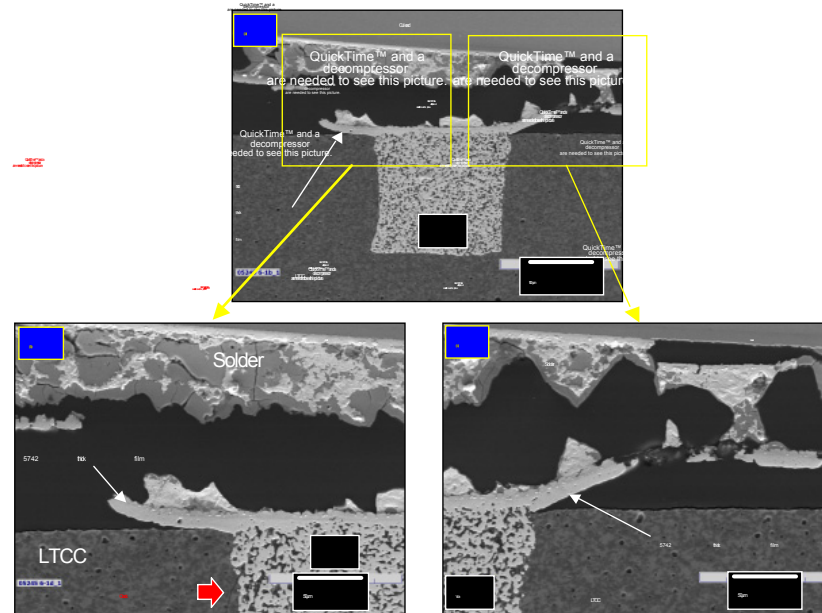
(b)

Fig. 38 (a) **(a)** Low magnification SEM/SE photograph of a second pull tested sample having a single layer of 5742 and 50In-50Pb solder (over a via). **(b)** and **(c)** High magnification images or the fracture path above the via. (b) **(a)** Low magnification photograph of the fracture path to either side of the via. **(b)** and **(c)**, High magnification SEM/SE images showing the top side regions of the via side wall. A crack was identified by the red arrow in **(b)**.

Lastly, it was observed in Figs. 37 and 38 that there was a prevalence for separation at the 5742 thick film/LTCC interface. This failure mode was nonexistent when 1x or 3x 4596 thick film layers were above the 5742 layer. The very isolated exceptions occurred when the 4596 glassy phase had accumulated under the 5742 thick film/LTCC interface. Therefore, it would appear that the high strength of the 5742 thick film/LTCC interface that was observed in the combined 4596/5742 layers was a result of the 4596 thick film component, due either to the subsequent firing cycle(s) or a result of the chemistry (e.g., glassy phase) contributed by the added 4596 layer.

In summary, the following general observations were compiled from the cross section analyses of the pull tested solder joints.

1. The predominant failure modes of the solder joint having the 4596 thick film (one or three layers) placed directly on the LTCC base material was facture along the solder/thick film and 4596/LTCC interfaces. In the latter case, the specific crack path was at the interface between the 4596 glassy phase layer and the Au-Pt-Pd metal layer.

2. In the case of 4596 thick film directly on LTCC, the more 4596 layers, that is, the more numerous the print-dry-fire cycles, the further the 4596 glassy phase penetrated the LTCC. A triple print resulted two zones of different glassy phase particle morphologies.

3. The glassy phase of the 5742 thick film formed a very thin layer at the 5742/LTCC interface; there was no evidence of its diffusion into the LTCC material according to the SEM imagery.

4. In the presence of the 5742 thick film, an increase in the number of 4596 thick film layers (firing steps) increased slightly the frequency of occurrences of the 4596 glassy phase having breached the 5742 layer and diffused into the LTCC. At such locations, there were the instances, albeit only a few, in which there was separation along the 5742 thick film/LTCC interface.

5. With the 5742 thick film between the 4596 layer and the LTCC, the preferred failure mode was solder/4596 thick film separation. The other two failure modes, which were observed to occur with lesser frequency, were ductile fracture between the 5742 and 4596 layers and fracture in the Sn-Pb solder.

6. At the rear location of the solder joint where, presumably, there were both shear as well as tensile components to the applied stress, the failure modes were listed below that were observed in the regions *beyond* of the 5742 thick

film footprint where there was a 4596 thick film/LTCC interface. In the case of the 1.0:1.0 ratio, the 4596 layer extended a small distance beyond the 5742 thick film. (Also, vias were present in each of these samples.)

1x 5742, 1x 4596:   1.0:1.0: LTCC divot
                     1.0:0.5: 4596/LTCC separation
                     1.0:0.2: 4596/LTCC separation

1x 5742, 3x 4596:   1.0:1.0: LTCC divot
                     1.0:0.5: LTCC divot and 4596/LTCC separation
                     1.0:0.2: 4596/LTCC separation

7.   The via structures were not affected by the pull tests. Both the 5742 and 4596 thick films exhibited excellent adhesion to the via-fill material.
8.   The presence of sidewall cracks in the vias did not affect the pull test fracture morphologies.
9.   The diffusion of the glassy phase of the 4596 thick film appeared to cause the LTCC material underneath it to expand.
10. A comparison of the 1x 5742 (50In-50Pb solder) and 1x 4596 cross sections (with vias) revealed similar failure modes, including significant contributions of thick film/LTCC separation, which accompanied very similar strength values between the two cases.
11. Solder failures were usually characterized by separation near the solder/Cu lead interface. Short cracks and IMC needles were observed in the solder near the solder/4596 thick film interface, indicating a nominal level of localized precipitation hardening and likely, solution strengthening effects.
12. Voids in the solder did not have a "global" effect on the fracture morphology. If breaching the solder joint gap, the void altered the "local" fracture mode underneath it, the most obvious phenomena being, vertical cracks in the thick film layer.

The trends identified in point (6) warrant further analysis. The most severe damage, as represented by the LTCC divot, occurred with the maximum extent of 5742 thick film underlying the 4596 layer. The divot cracks appeared to have originated in the small area of overlap between the 4596 thick film and the LTCC at the very edge of the pad. Specifically, the cracks originated in the glassy phase at that 4596 thick film/LTCC interface. As the 5742 thick film layer diminished

through the ratios of 1.0:0.5 and 1.0:0.2, the failure mode at the overlap between the 4596 thick film and LTCC base material appeared to transition to the 4596 thick film/LTCC interface (glassy phase) separation.

Two competing "processes" were present. On the one hand, as the 5742 pad diminished in size, there was an increased extent of the weaker, 4596 thick film/LTCC interface. On the other hand, when the 5742 thick film extended fully under the 4596 layer (1.0:1.0), there was a build up of shear and tensile stresses that could not be released at the stronger 5742 thick film/LTCC interface. The result was a divot crack in the LTCC.

A slight variation to this scenario distinguished the 1x and 3x 4596 cases, specifically at the 1.0:0.5 ratio, for point (6) above. The greater rigidity of the thicker film structure, or secondarily, the more extensive diffusion of glassy phase into the LTCC, contributed to more LTCC divots being observed for the 3x 4596 layer case.

Another observation having applicability to point (6) above, was that both the 1x and 3x 4596 thick film layers, *in the absence of both the 1x 5742 layer and via,* resulted in only very small LTCC divot cracks at the rear location of the solder joints. This trend would appear to be commensurate with the absence of LTCC divot cracks in the 1x 5742, 1x 4596 and 1x 5742, 3x 4596 combinations having the smallest ratio of 1.0:0.2, which produced the largest contact area between the 4596 thick film and LTCC base material. The fact that LTCC divots were not completely absent when only the 4596 thick film was used, suggested that the 5742 layer and via, affected the fracture behavior at the rear location.

Lastly, point (10) was an interesting observation regarding the appearance of the 5742 thick film/LTCC failure mode in the 1x 5742 (50In-50Pb) test samples. The 5742 thick film/LTCC interface failure was not prevalent when 1x 4596 or 3x 4595 layers were present. Therefore, it was concluded that, when the 1x 5742 thick film was combined with either the 1x or 3x layers of 4596 thick film, the 5742 thick film/LTCC interface was stronger than when the 5742 layer was alone. Because the glassy phase of the 4596 thick film appeared to degrade the 5742 thick film/LTCC interface (Figs. 25b (b) and 25d (b), red box "B"), it was surmised that it was the firing steps required to place the 4596 layer(s) rather than the latter's chemistry that enhanced the adhesion at the 5742 thick film/LTCC interface.

3.5 Discussion: Pull strength data and cross section failure mode analysis

An analysis was performed, which investigated possible correlations between the failure modes documented by the metallographic cross sections, and the pull strengths of the two individual joints that were cross sectioned per sample type. Shown in Fig. 39 is a plot of pull strength as a function of solder joint structure.
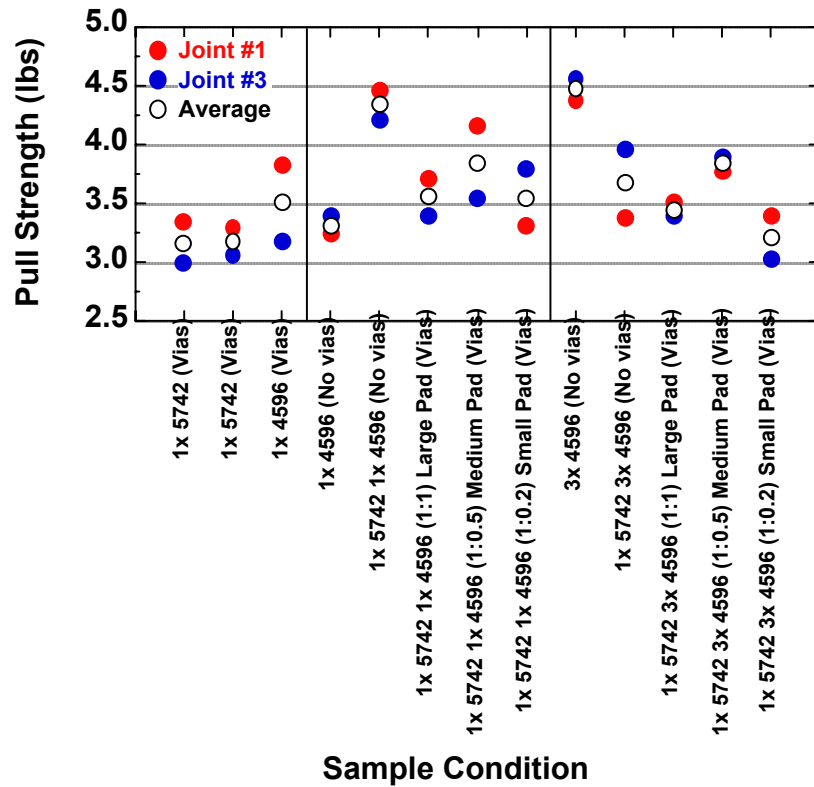
Fig. 39 Plot of the individual and average pull strengths of the cross-sectioned test sites as a function of the solder joint structure. The two pull tested joints in the two cross sections were designated Joint #1 and Joint #3.

The pull strength values – Joint #1 and Joint #3, as well as the average between them – refer to the two solder joints in the metallographic cross sections. The following trends were observed from the data in Fig. 39:

1. The two separate tests of the 1x 5742 (which had vias and used the In-Pb solder to make the joint) exhibited nearly identical strengths. Those strength values were slightly less than the strength of the 1x 4596 layer (made using the Sn-Pb solder) with or without the via.

2. The 3x 4596 thick film layer exhibited a higher strength than the 1x
    4596 layer when there were no vias.

3. Adding the 1x 5742 layer to the 1x 4596 layer (no via) significantly
    raised the solder joint strength. However, adding the 1x 5742 layer to
    the 3x 4596 layer (no via) caused a decrease in the joint strength.

4. The effect of vias was described for the following cases: (a) The 1x
    4596 thick film strength increased slightly when the via was present in
    the LTCC. (b) The strength decreased when going from the 1x 5742,
    1x 4596 (no via) to the case with a via, as represented by the 1x 5742,
    1x 4596 (1.0:1.0) (c) The strength decreased slightly when going from
    the 1x 5742, 3x 4596 (no via) to the case with a via, as represented by
    the 1x 5742, 3x 4596 (1.0:1.0) Therefore, the addition of a via
    appeared to slightly reduce the strength of the solder joint when the
    5742 thick film was in place.

5. The three 4596:5742 ratios of 1.0:1.0, 1.0:0.5, and 1.0:0.2 showed the
    same trend for either the 1x or 3x 4596 samples, which was that the
    highest strength was realized with the 1.0:0.5 ratio. Generally, the
    strengths were slightly lower for the 3x 4596 case. On the other hand,
    the maximum was more distinct in the latter case.

The strength data in Fig. 39 were compared to those in Fig. 19b. Recall that the data
presented in Fig. 19b were compiled from *all* of the pull strength measurements. The
order of the solder joint structures (x axis) was changed slightly in Fig. 39. Overall,
similar trends were observed between the two graphs so that the results in Fig. 39
were, indeed, representative of the entire data set. The only noticeable deviation was
that the data in Fig. 39 indicated a slightly stronger effect by the via on the joint
strength. This behavior could have resulted from the statistically smaller sample size.

The pull strength data in Fig. 39 also portrayed the role of the number of firings on the
joint strength. This effect is illustrated in Fig. 40, which is a graph of the individual pull
strength datum and average strengths from joints #1 and #3 versus the number of firing
steps used to deposit the 5742 and 4596 thick film layers. This result can be compared
to Fig. 21. In fact, the maximum strength, as determined by the second-order

polynomial curve fit, occurred at nearly the same abscissa values; those values were 2.3 and 2.7 for Figs. 21 and 40, respectively. The sensitivity of pull strength to the number of firing steps would explain the trends in points (2) and (3) above. For example, the 3x 4596 layer (no vias) had a higher strength than the 1x 4596 layer (no vias) because the three firing steps were closer to the optimum 2.7 value observed in Fig. 40. In the case of point (3) above, the addition of the 1x 5742 to the 1x 4596 layer would improve the strength, again, because the number of firing steps became closer to the optimum value of 2.7. On the other hand, adding the 1x 5742 layer to the 3x 4596 layer resulted in a total of four firing steps, which is well above 2.7, resulting in a loss of joint pull strength.
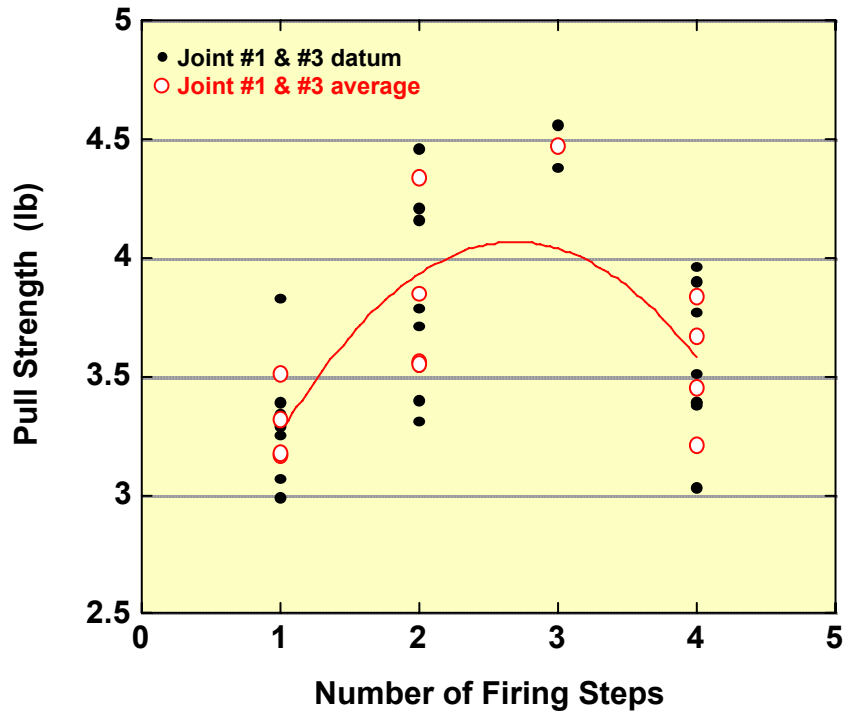
Fig. 40 Plot of the individual and average pull strengths of the pull tested joints designated Joint #1 and Joint #3 as a function of the total number of firings used to create the 5742 and 4596 thick film layers.

The *cross section* failure mode data were compiled as a function of solder joint structure. Shown in Fig. 41 is a graph of the percentage to which, each of the five failure modes occurred as a function of the solder joint structure. The failure modes represented the entire bond line length of each solder joint – from the front end directly under the pulling force to the back end. The failure mode percentages were the averages between the two joints #1 and #3 as determined through the metallographic

cross sections. The absolute error on the failure mode percentage measurements was approximately ±5%. The graph in Fig. 41 differs from that in Fig. 20, not only because the order of the solder joint structures was changed slightly, but also because Fig. 41 was based upon metallographic cross sections rather than visual inspection criteria.
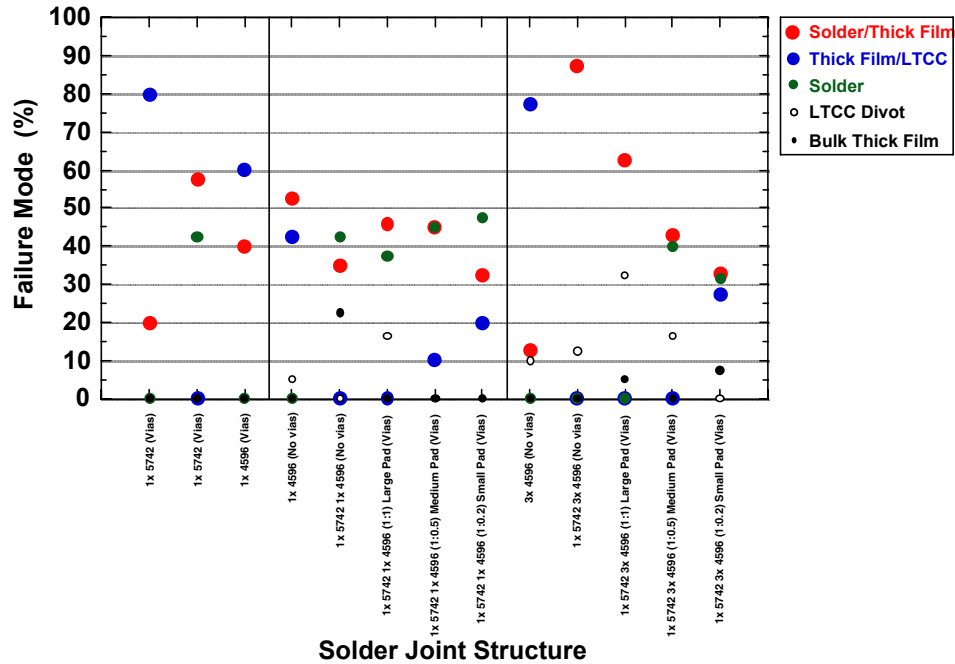
Fig. 41 Plot of the percentages of the failure modes as a function of solder joint structure as determined from the metallographic cross sections. The failure mode percentages were averaged together, which came from cross section Joints #1 and #3.

At this point, the discussion will turn to the data in Fig. 41, but will also address the strength data provided in Fig. 39. The 1x 5742 failure modes (In-Pb solder) included all three failure modes to different degrees: thick film/LTCC failure, solder/thick film separation, and separation within the solder. Very similar pull strengths were observed for the two test series in Fig. 39. Therefore, it was concluded that each of these modes had nearly equal intrinsic strengths so that the dominance of one or the other was circumstantial.

The single print of 4596 thick film exhibited a slight strength decrease when vias were added to the joint. The corresponding failure mode data in Fig. 41 showed only small differences in the solder/thick film and thick film/LTCC failure mode percentages between the two cases. The small presence of the LTCC divot failure mode, when vias were not present, may have been a factor in the slightly lower strengths of these joints.

The addition of the 1x 5742 layer to the 1x 4596 layer (no vias) caused a large increase in the pull strength. The most apparent change to the failure mode was the loss of failure at the thick film/LTCC interface and the appearance of failure within the thick film layer, which was shown earlier to be the ductile fracture between the 4596 and 5742 thick film layers. At first glance, the superior strength of the 5752 thick film/LTCC interface, in the absence of the 4596 glassy phase, was the likely source of the higher pull strength. However, the fact that there remained a similar percentage of the solder/thick film failure mode would also imply that the addition of the 5742 layer improved the strength of the solder/thick film interface. (An indirect result of this situation was a significant increase in the bulk solder failure mode percentage.

The apparent improvement in the solder/4596 thick film interface strength suggested that the microstructure of the 4596 thick film was altered by the addition of the 5742 thick film. In fact, a comparison of Figs. 6 and 11a, which showed, respectively, the 1x 4596 (no via) and the 1x 5742, 1x 4596 (no via) systems, indicated that the 4596 layer appeared denser when the 5742 thick film was present. The additional density resulted from the absence of diffusion of the 4596 glassy phase into the LTCC. It was speculated that, although the glassy phase was not wettable, its presence as small particles eliminated the larger pores that are typically created when the glassy phase diffused to the thick film/LTCC interface and into the LTCC material. The result was added bonding area, particularly when the Au-Pt-Pd metal was smeared over the near-surface glassy particles during the burnishing process, which improved the strength of the solder/4596 thick film interface.

The effect of the via on the 1x 5742 1x4596 system was ascertained by comparing the case of the 1x 5742, 1x 4596 without vias to the case of the 1x 5742, 1x 4596 sample having the 4596/5742 ratio of 1.0:1.0 that contained vias. The data in Fig. 39 showed a strength decreased from the former to the latter case. The failure mode data in Fig. 41 indicated very little difference in the propensity for the solder/thick film or solder failure modes. Also, in both cases, the thick film/LTCC interface failure mode was not observed to a significant degree. The addition of the via caused a loss of the bulk thick film failure mode that was associated with high strength. On the other hand, the failure mode that did appear with significance with the via added, was the LTCC divots located at the rear location of the solder joint.

A correlation was sought between the failure modes changes with the drop in pull strength arising from the addition of the via to the 1x, 5742, 1x 4596 structure. It did not appear likely that the presence of the via would have affected the intrinsic strength of either the bulk solder or the solder/thick film interface because these failure modes were present to a significant degree with or without the via. Also, a comparison of Figs. 24 and 25 (no via) with Figs. 27 and 28 (via, 1.0:1.0 ratio) did not reveal a significant difference between the two joint microstructures. Therefore, the strength loss was attributed to the LTCC divot cracks. It was further surmised that the via had *indirectly* altered the fracture process, perhaps by changing the local stress distribution or an undetected material effect, resulting in fracture in the LTCC (divot).

It was observed in Fig. 39 that, for the 1x 5742, 1x 4596 thick film system (made with the via), a maximum strength was recorded at a 4596/5742 footprint ratio of 1.0:0.5. With respect to the accompanying failure modes, the generalized trend was for the solder/thick film failure mode to decrease and for the thick film/LTCC failure mode to increase with decreasing thick film ratio. In other words, the increase in the thick film/LTCC failures correlated to the growing extent of 4596 thick film/LTCC interface. The increased bond line of this weaker interface (specifically resulting from the 4596 glassy phase there) was responsible for the increase in this failure mode, and certainly, for the drop in strength from the 1.0:0.5 ratio to the 1.0:0.2 ratio.

When going from the 1.0:1.0 ratio to the 1.0:0.5 ratio, the same general trends of solder/thick film failure mode and thick film/LTCC failure mode occurred. However, the pull strength *increased*. Therefore, the analysis in the previous paragraph would not provide a consistent reason. It was important to note that the LTCC divot percentage dropped from 17% to 0% between the two ratios. Therefore, it was concluded that the increased propensity of LTCC divots with the 1.0:1.0 ratio was the primary source of the lower strength of those samples (Fig. 41). The divot behavior had a greater influence on pull strength than did the increase in the 4596 thick film interface with the LTCC.

A cause of the LTCC divots at 1x 5742, 1x 4596 (1.0:1.0) was proposed, based upon the cross section microstructures. The crack initiation occurred in the weak 4596 glassy phase, which developed at the 4596 thick film/LTCC interface where the two materials overlapped just beyond the edge of the 5742 layer. However, the driving force for the crack was a high residual stress state that was created there. The

residual stress resulted from the combined effects of (1) the large diameter and (2) the thicker section (5742 + 4596) of layer, which together, resulted in a stress concentration in the LTCC material, resulting in the LTCC divot crack.

The next grouping of test data was derived from the use of 3x 4596 layers. In Fig. 41, it was observed that the primary failure mode of the 3x 4596 (no vias) test specimens was at the thick film/LTCC interface. The secondary failure modes were the solder/thick film separation and formation of the LTCC divots. By comparison, the 1x 4596 (no vias) solder joints showed a lesser presence of the thick film/LTCC and LTCC divot failure modes. Instead, both the solder/thick film and thick film/LTCC shared equally in the fracture path. Also, in Fig. 39, the 3x 4596 (no vias) solder joints had considerably higher pull strengths than did the 1x 4596 (no vias) interconnections. The strength data (Fig. 39) and failure mode results together suggested that the strengths of both the solder/thick film and thick film/LTCC interface were greater for the 3x 4596 layer (no vias) versus the 1x 4596 layer (no vias).

The improvement in the strength of the thick film/LTCC interface could be traced to the strength dependence on the number of firing steps. The 3x layer was very close to the 2.7 firing steps observed to optimize the joint strength (Fig. 40). The increased strength of the solder/thick film interface followed a similar scenario presented earlier. That is, the glassy phase of the second layer and especially, the third layer, could not completely separate from the Au-Pt-Pd metal component by diffusing to the interface with the LTCC material. Therefore, those layers remained denser than the 1x 4596 layer, thereby eliminated some of the surface porosity, which in turn, improved solderability and the adhesion of the solder to the thick film.

Two other points were worth noting. First of all, the comparison of the pull strength and failure mode data between the 3x 4596 (no vias) and 1x 4596 (no vias) indicated that the slightly more frequent appearance of the LTCC divots in the former case did not significantly reduce the pull strengths. This point allows for some bounds to be placed on the sensitivity of the pull strength to LTCC divots.

Secondly, the failure mode analysis by visual inspection (Fig. 20) showed a preponderance for the solder/thick film separation rather than the thick film/LTCC fracture as shown indicated by cross sections (Fig. 41). The same trend of decreasing solder/thick film separation from the 1x 4596 to the 3x 4596 layer structure was reproduced between the two data sets. This comparison highlighted the potential discrepancies that can arise from the difficulty to discern failure modes by visual inspection, particularly when establishing physics-of-failure information.

The addition of the 1x 5742 layer (no vias) affected the 3x 4596 thick film differently from the 1x 4596 layer. There was a strength decrease for 3x 4596 thick film, which was opposite to the trend observed with the 1x 4596 layer. In both cases, the addition of the 1x 5742 thick film eliminated the thick film/LTCC interface failure mode because of the generally superior strength of the 5742 thick film/LTCC interface. However, the 1x 5742 layer also caused a significant increase in the solder/thick film failure mode of the 3x 4596 films, which was not observed with the 1x 4596 thick film and, which coincided with the loss of pull strength. (The extent of LTCC divot failure mode was largely unchanged.)

An explanation for the concurrent strength loss and transition to a solder/thick film failure mode was developed by examining failure modes as a function of the number of firing steps.   The failure mode percentages versus firing steps were plotted in Fig. 42. The failure mode percentages were the average for both joints #1 and #3. The three firing steps pertained to the 3x 4596 sample while the case of the four firing steps was populated primarily by the 1x 5742, 3x 4596 specimens. Overall, as the number of firing steps increased, there was an increase in the propensity for the both the solder/thick film and the LTCC divot failure modes. In the particular case under consideration here, there was only a very small increase in the percentage of LTCC divot failures; therefore, the increase of this failure mode likely contributed to a lesser extent to the pull strength loss. However, a significant increase was observed in the presence of the solder/thick film failures.
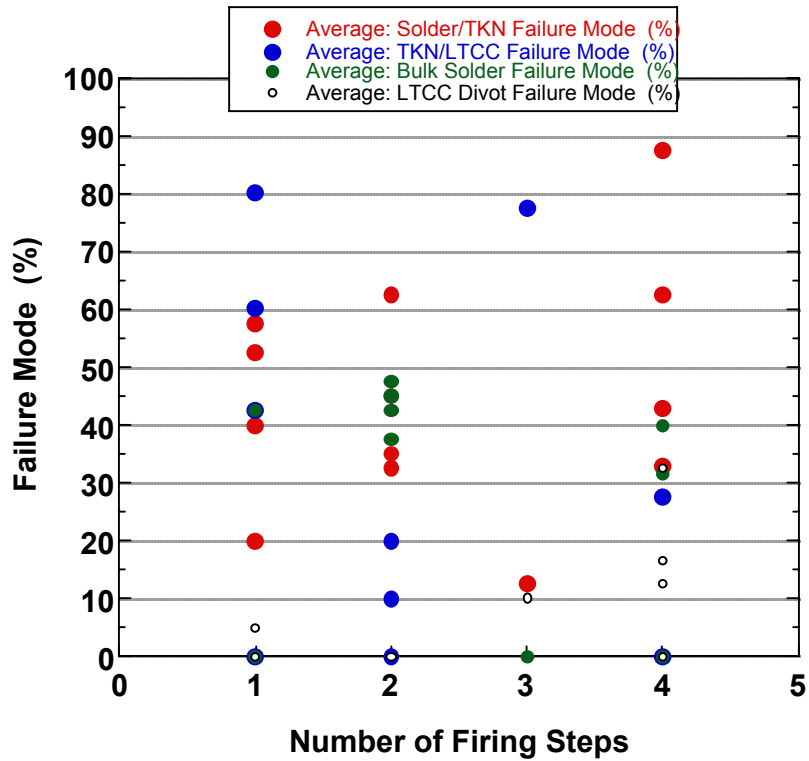
Fig. 42 Plot of the percentages of the five failure modes, as determined from the metallographic cross sections and averaged for both joints #1 and #3 versus the number of firing steps

Recall that the 5742 thick film served as a barrier layer that prevented the 4596 thick film's glassy phase from diffusing into the LTCC base material (with the exception of a few localized regions). It was construed that when the 1x 5742 layer blocked the diffusion of the glassy phase out of the thick film, large pores were eliminated from the latter. It was then argued that the added density improved the solder/thick film interface strength.

However, in the case of the 3x 4596 layer, it was hypothesized that *too much* of the 4596 glassy phase had "backed up" to the thick film surface. In fact, the oxygen potential above the thick film during the firing process may have actually driven the excess glassy phase to preferentially diffuse to the thick film surface. Thus, poor adhesion between the solder and greater degree of glassy phase caused the loss of pull strength.

The effect of the via on pull strength and failure mode was evaluated for the 3x 4596 layers by comparing the 1x 5742, 3x 4596, no via case to the 1x 5742, 3x 4596 (1.0:1.0), which had the vias. The data in Fig. 39 showed a small decrease in pull strength. Examining Fig. 41, the failure mode analysis showed a decrease in the solder/thick film mode and significant increase of LTCC divots when vias were added to the structure. With or without the vias, the thick film/LTCC failure mode was not observed at all. Therefore, it appeared that the loss of strength associated with the vias had its roots in the increased occurrence of the LTCC divot cracks. The same observation was drawn from the corresponding analysis of the effects of vias on the 1x 5742, 1x 4596 thick film case. In both cases, it can be surmised that the vias altered the stress state responsible for driving the fracture behavior, causing an increased tendency for the formation of LTCC divot cracks.

It was observed in Fig. 41 that, generally speaking, there was a greater prevalence for the LTCC divots to occur throughout the failure mode data associated with the 3x 4596 layers vis-à-vis the 1x 4596 structures, irrespective of the presence of the 1x 5742 thick film layer. Likely contributing factors were: (1) the increased amount of glassy phase associated with the three layers of 4596 thick film and greater probability of that glassy phase reaching the thick film/LTCC interface; (2) the additional firing steps associated with the multiple 4596 layers; and (3) the mechanical "stiffness" of the 3x 4596 layer. The larger amount of glassy phase (point 1) increased the likelihood of forming a more brittle interface between the thick film (metal layer) and the LTCC, which provided a preferred location for crack initiation and propagation. The added firing steps (point 2) enhanced the diffusion of 4596 glassy phase (past the 5742 layer when present) to the thick film/LTCC interface and into the LTCC bulk material. In the latter case, there was degradation to the mechanical strength of the near-interface LTCC material.

Lastly, the increased stiffness of the 3x 4596 layer (point 3) could contribute to an increased propensity for LTCC divots (point 3). The thicker layer would generate higher residual stresses in the underlying LTCC material due to the relatively high strength of the solid-solution Au-Pt-Pd alloy. The higher residual stresses provided the added driving force for divot crack initiation and propagation.

The microstructures associated with the LTCC divot failure mode were discussed earlier with the corresponding SEM photographs. The fractures initiated primarily at the rear location of the joint, where a combination of tensile and shear stresses was generated by the applied load. This stress combination, as opposed to the nearly

100% tensile stress at the front of the joint, initiated cracks in the 4596 thick film glassy phase where the 4596 thick film overlapped with the LTCC base material. The cracks then preferentially propagated in the LTCC, creating the divot. A finite element analysis would be necessary to quantitatively confirm the stress state created at the rear of the joint and the stresses within the LTCC base material.

The failure mode data in Fig. 41 were evaluated for the three 4596:5742 ratios. The strength data in Fig. 39 indicated a maximum pull strength at 1.0:0.5 for the 1x 5742, 3x 4596 thick film structure. The failure mode analysis indicated the following general trends when going from 1.0:1.0 to 1.0:0.2: (1) a decrease in the percentage of solder/thick film separation, (2) an increase in the thick film/LTCC failure mode percentage, and (3) a decrease in the LTCC divots. In the latter case (point 3), as the expanse of the 1x 5742 layer decreased when ratio changed from 1.0:1.0 to 1.0:0.2, the total layer thickness decreased at the outer extremes, thereby reducing the residual stresses imparted into the LTCC material. The result was a decrease of LTCC divots. The same behaviors were observed for the 1x 5742, 1x 4596 thick films for which, it was proposed that the competing mechanisms of decreasing LTCC divots (which caused a strength increase) and increasing thick film/LTCC failures (which resulted in a strength decrease) caused the strength maximum at the ratio of 1.0:0.5. In the present case of 3x 4596 layers (Fig. 41), similar scenarios were possibly in effect. However, it cannot be discounted that the strength increase from 1.0:1.0 to 1.0:0.5 was also made possible by an improvement in the solder/thick film interface strength because this failure mode dropped significantly between these two geometries.

Given the geometry of the pull test, it was surmised that the failure mode most relevant to the maximum strength was that which occurred at the front location of the joint, directly under the upright leg of the wire. Therefore, an analysis was performed that documented the failure modes for the "front portion" of the joint. The front portion was defined as the 60% of the bond line that extended from the front edge of the solder pad towards the rear location. Those failure mode data were plotted in Fig. 43.
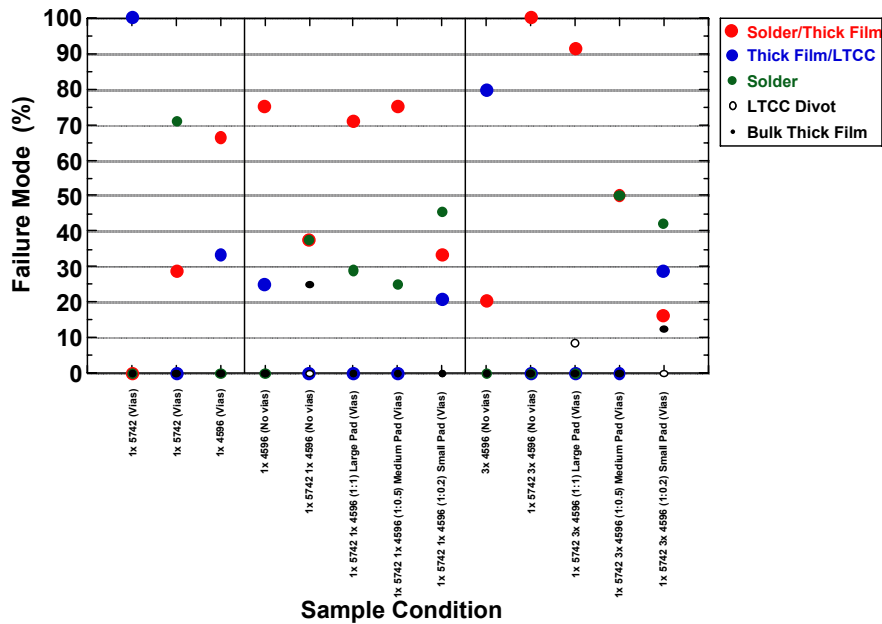
Fig. 43 Plot of the percentages of the five failure modes, as determined from the metallographic cross sections representing the *front portion* of the joint, versus solder joint structure. The failure mode percentages, came from cross section of the individual Joints #1 and #3 and were averaged together.

Overall, very similar trends were observed in Fig. 43 that were documented from the data in Fig. 41. Of course, the LTCC divot failure mode was almost entirely absent because it typically occurred at the rear location of the joint. Some specific trends were identified. There was an higher contribution by the solder/thick film failure mode at the front location of the solder joint structures for the 1x 4596 thick film layer (no via) than was observed for 3x 4596 layer (no via). When the 1x 5742 layer was added to either of these two 4596 layer thicknesses, the thick film/LTCC failure mode decreased, likely owing to the higher strength offered by the 5742 thick film/LTCC interface.

On the other hand, opposite trends were observed for the solder/thick film failure mode between the two thick film structures. (Again, there were no vias.) When the 1x 5742 layer was added to the 1x 4596 layer, the solder/thick film failure mode decreased, being replaced with failure in the solder, implying a strengthening of the solder/thick film interface. When the 1x 5742 layer was added to the 3x 4596 thick film, there was an increase of the solder/thick film failure mode that implied that the solder/thick film interface was weaker for the 1x 5742, 3x 4596 system versus the 1x 5742, 1x 4596 layer combination. Of course, this conclusion is based upon the premise that the solder failure mode was equally likely in both specimen types.

Regarding the data in Fig. 43 vis-à-vis the 5742 thick film foot print, different behaviors were noted for the 1x 5742, 1x 4596 and 1x 5742, 3x 4596 cases as the ratio of 4596:5742 went from 1.0:1.0 to 1.0:0.2. In the case of the 1x 5742, 1x 4596 thick film structure, nearly identical failure mode percentages were observed between 1.0:1.0 and 1.0:0.5. Between the same ratios, solder failures increased and solder/thick film failures decreased for the 1x 5742, 3x 4596 sample, which reflected an increased solder/thick film interface strength. On the other hand, both thick film structures reacted similarly from the 1.0:0.5 to 1.0:0.2 ratios as the solder/thick film failure mode decreased and thick film/LTCC failures increased. This similarity was a result of the dominating effect of the increased extent of the 4596 thick film/LTCC interface and its lower strength.

An analysis was performed to determine whether the cross section failure mode data would correlate with the pull strengths of the joints. Shown in Fig. 44 is a plot of the failure mode as a function of pull strength when these two data sets (Joints #1 and #3) were averaged together. First, the plot clearly illustrated that the pull strengths fell within the relatively narrow band of 3.2 – 4.5 lbs. A qualitative correlation was developed for the data in Fig. 44, based on the authors' best estimate of the data trends. The dotted lines represented that estimate and were not based upon a rigorous curve fit exercise. It appeared that the solder/thick film failure mode went through a maximum in the strength range of 3.5 – 4.0 lbs. This trend was represented by the red dotted line. In a similar regard, the trend of the thick film/LTCC failure mode was to decrease as a function of pull strength (blue dotted line). There was some indication that this failure mode increased again at the very high strength values.

The following scenario was developed from the analysis of Fig. 44. The lowest pull strengths were associated with failure at the thick film/LTCC interface and, in particular, the 4596 thick film/LTCC interface. Higher pull strengths were achieved through an improvement in the strength of the thick film/LTCC interface, in particular, by the addition of the 5742 thick film layer. The result was a preference for fracture to occur along the solder/thick film interface.
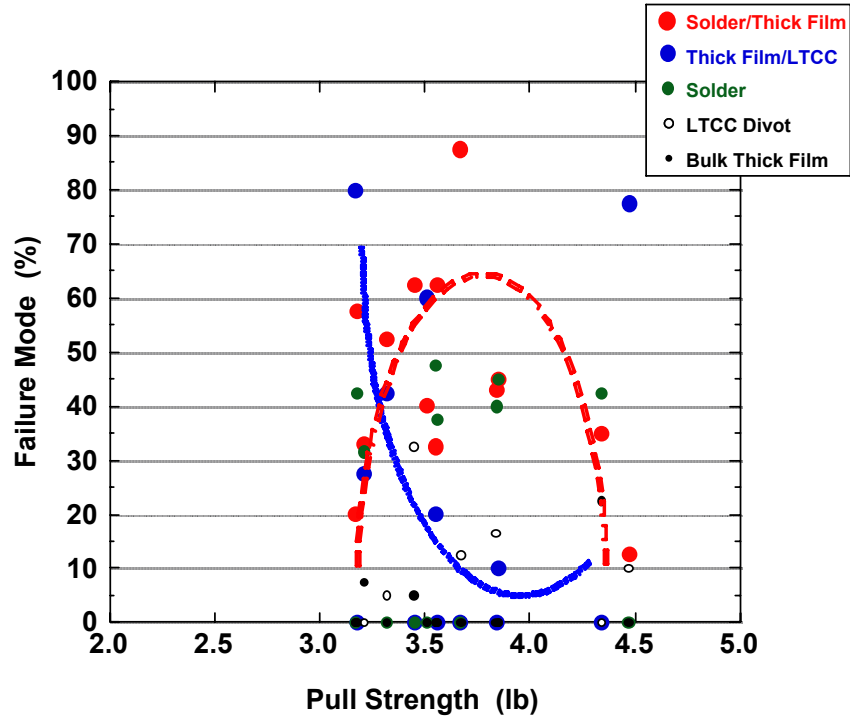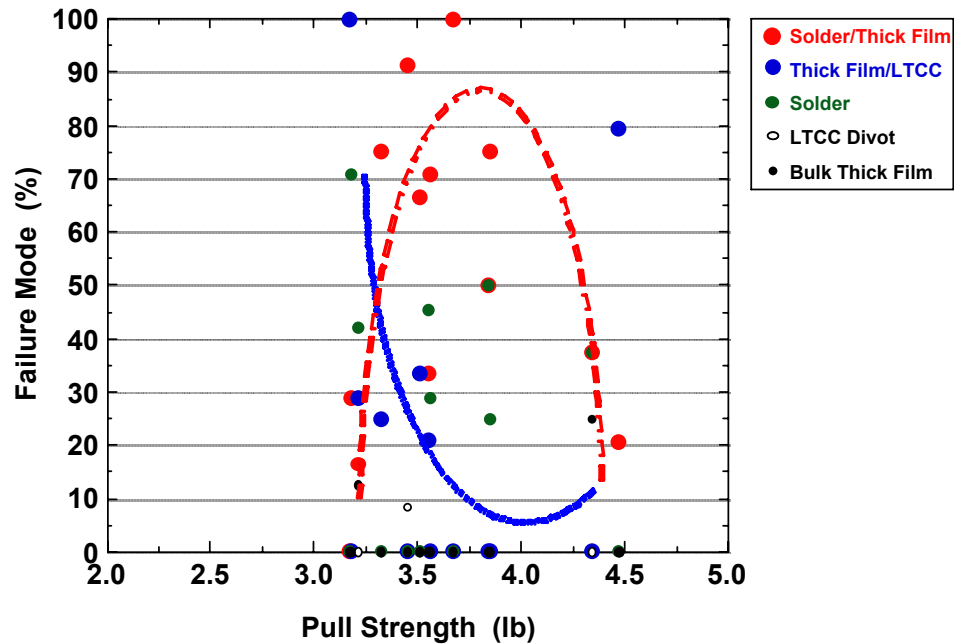
Fig. 44 Plot of the failure mode percentages (entire joint), as determined from the metallographic cross sections. The failure mode percentages and pull strengths, which came from cross section Joints #1 and #3, were averaged together. The red and blue dotted lines represented the trends in the solder/thick film and thick film/LTCC failure modes, respectively, as qualitatively estimated by the author.

The data in Fig. 44 also provided further insight into the performance of the solder/thick film interface. If this interface had maintained a largely constant strength, then it would not have been expected for pull strengths to exceed 3.7 lb, since this value represented the maximum strength associated with solder/thick film failure mode. However, higher pull strengths were, in fact, observed. The solder/thick film failure mode was replaced with the thick film/LTCC failure mode at those higher strengths. Therefore, it was concluded that strengths exceeding 3.7 lb became accessible because of higher solder/thick film interface strengths. The other three failure modes increased their presence at those higher strength, the magnitude of which, depended upon the specific interconnection construction.

Several other observations were documented from Fig. 44. First of all, there was the presence of the LTCC divot failure mode that rose sharply to a maximum at approximately 3.5 lb and then tailed-off at the higher strengths. The conclusion that was drawn here was that strengths higher than 3.5 lb were realized because a curtailment of the LTCC divots in those joints structures.

Another observation derived from Fig. 44, was that the bulk solder failure mode exhibited no particular trend across the pull strength range. In fact, either the failure mode was absent or it was present, but at percentages that did not exceed the relatively narrow range of approximately 37 – 47%. This upper limit on the bulk solder failure mode percentage arose from the work hardening property of the solder. Once the solder has begun to deform, its strength increased rapidly so that it became less likely to be the weakest structure in the joint. The pull strength and failure modes were then determined, either separately or in some combination, by the strengths of the solder/thick film interface, the thick film/LTCC interface, or the bulk strength of the combined 5742-4596 thick film.

The failure mode versus strength analysis was also performed, but with the failure mode limited to the front (60%) location of the solder joint. The data have been plotted in Fig. 45. Very similar trends were observed in Fig. 45, as were noted in the above evaluation of Fig. 44. The maximum in the solder/thick film failure mode, while changing very little in terms of position along the pull strength axis, was clearly more pronounced in Fig. 45. This corroborated the earlier analyses that indicated that there was an increased propensity for the solder/thick film failure at the front region of the solder joint. Also, the thick film/LTCC interface failures, which were due to primarily failure at the 4596 thick film on LTCC in the absence of the 5742 layer, predominated the low strength regime. Of course, there was very little presence of the LTCC divot failure mode because this behavior tended to occur at the rear location of the joint. The frequency of solder failures showed very little dependence on the pull strength.

Fig. 45 Plot of the failure mode percentages for the *front portion (60%)* of the solder joint (metallographic cross sections) versus pull strength. The pull strengths were the average values between Joints #1 and #3. The red and blue dotted lines represented approximate trends in the solder/thick film and thick film/LTCC failure modes, respectively, as determined by the author.

In summary, it was possible to draw several relationships between the cross section failure mode and pull strength for the solder joints examined in this study. It was apparent that the low strengths were generally due to a weakened thick film/LTCC interface. On the other hand, when that interface was strong – e.g., by the addition of the 5742 thick film layer – the failure mode transitioned to the solder/thick film interface and/or the bulk solder. However, it was possible to obtain further increases in pull strength only because of the additional strengthening of the solder/thick film interface that was observed for several thick film structures.

4. Summary

1. A study was performed that examined the microstructure and mechanical properties of 63Sn-37Pb (wt.%, Sn-Pb) solder joints made to thick film layers on low-temperature co-fired (LTCC) substrates. The thick film layers were combinations of the Dupont™ 4596 (Au-Pt-Pd) conductor and Dupont™ 5742 (Au) conductor, the latter having been deposited between the 4596 layer and

LTCC substrate. Single (1x) and triple (3x) thicknesses were evaluated for the 4596 layer. A 1x 5742 layer was used whenever indicated. Three footprint sizes were evaluated of the 5742 thick film. The maximum pull strength and failure modes provided quantitative metrics for assessing solder joint performance.

2. The 50In-50Pb (In-Pb) solder was used to evaluate the 5742 thick film by itself.

3. The Sn-Pb and In-Pb solder joints exhibited excellent solderability of the copper (Cu) leads and thick film surfaces. The extent of voids in the solder was as-expected and did not correlate with the presence or absence of any of the thick film or via structures.

4. In all test sample configurations, the 5742 thick film prevented side wall cracking in the vias.

5. The pull strengths were in the range of 3.4 – 4.0 lbs, including the 5742 (In-Pb) solder joints. These strengths were only slightly lower than historical data based upon traditional alumina (Al_2O_3) substrates.

6. In the absence of the 5742 layer, the 3x 4596 layer had a slightly higher strength than the 1x 4596 layer. The addition of vias did not affect these data.

7. The highest strength was obtained when the single 5742 layer was added to the single layer of 4596, using the 1.0:1.0 footprint diameter and no vias. Adding the 5742 layer to the 3x 4596 layer caused a lower pull strength for the same conditions. Generally, the presence of the via caused the pull strength to decrease slightly, yet maintaining acceptable levels.

8. Of the three footprint ratios, 4596:5742, the value 1.0:0.5 maximized the strength for both 1x or 3x 4596 layers. The strengths were slightly higher for the 1x 4596 series of test specimens. The competing factors were minimizing the amount of 4596/LTCC interface that was intrinsically weaker versus minimizing the overall thickness (stiffness) of the thick film layer, which generated residual stresses in the underlying LTCC substrate.

9. Pull strength was maximized at between two and three total firing steps. Too few firing steps resulted in a weaker solder/thick film interface. Excessive firing steps either explicitly damaged the thick film/LTCC interface and/or underlying LTCC substrate material or did so, implicitly, because of the additional layers and the residual stresses that they caused at the interface or in the LTCC material.

10. Failure analysis indicated that the pull test did not damage the via or surrounding LTCC structures, even when side wall cracks were present.

11. *Recommendations*: (a) In the presence of vias and the need for the 3x 4596 thick film, the preferred 4596:5742 ratio is 1.0:0.5. (b) For those LTCC components that require the 3x 4596 layer, but do not have vias, it would be preferred to refrain from using the 5742 layer in order to limit the number of layers to prevent damage caused, explicitly, by the increased number of firing steps, or generated indirectly by the overall thicker layer and associated residual stresses. Of course, it can be inferred that limiting the 4596 thick film to two layers (2x) would allow for the addition of a 5742 layer and there still be a higher thick film/LTCC interface strength.

12. *A cautionary note*: This study identified the role of residual stress in the failure of the soldered thick film pads on LTCC base material. Therefore, it is prudent that any proposed thick film structures be evaluated after exposure to a thermal cycling environment, particularly if cryogenic temperatures are to be used to assess next-assembly performance or are a part of the service requirements.

5. References

[1] F. Uribe, S. Garrett, S. Monroe, and S. Burchett (dec.), "Characterization of the Mechanical Properties of LTCC Green Tape for the MC4352 MET," *Sandia Report* SAND97-0497 (March 1997), Sandia National Laboratories, Albuquerque, NM.

[2] K. Ewsuk, S. Monroe, R. Uribe, H. Morgenstern, and L. Zawicki, "Design of a Barrier Layer to Eliminate Circumferential Cracking in LTCC Packaging," March 28, 2005.

[3] "Acceptance Requirements – Thick Film Fritted Conductor Paste", *SS309297 Issue J*, Appendix E. Sandia National Laboratories, Albuquerque, NM.

[4] W. Crossland and L. Hailes, "Thick Film Conductor Adhesion Reliability," *Solid State Technology* Feb. 1971, pp. 42 – 47.

[5] A. Milgram, "Influence of Metallic Diffusion on the Adhesion of Screen Printed Silver Films," *Metallurgical Transactions* 1 (1970), pp. 695 – 700.

[6] T. Hitch, " Adhesion, Phase Morphology, and bondability of Reactively-Bonded And Frit-Bonded Gold and Silver Thick-Film Conductors", *Journal of Electronic Materials* 3 (1974) pp. 553 – 577.

Copy to:

J. Williams	MS0487
D. Susan	MS0889
S. Monroe	MS0889
T. Garino	MS1411
K. Ewsuk	MS1349
R. Tandon	MS1349
R. Kilgo	MS0886
V. Chavez-Soto	MS0982
J. Custer	MS0889
P. Vianco	MS0889 (5 copies)
F. Uribe	MS0959 (3 copies)
Central Technical Files	MS9018 (2 copies)
Technical Library	MS0899 (2 copies)